HYDRODYNAMIC FORCE COEFFICIENTS OF A VERTICAL CIRCULAR CYLINDER

by

Carolin Susan Mihelcic

B.Sc. (Civil Engineering), Queen's University, 1987

A THESIS SUBMITTED IN PARTIAL FULFILLMENT OF

THE REQUIREMENTS FOR THE DEGREE OF

MASTER OF APPLIED SCIENCE

in

THE FACULTY OF GRADUATE STUDIES

Department of Civil Engineering

We accept this thesis as conforming

to the required standard

THE UNIVERSITY OF BRITISH COLUMBIA

March 1989

In presenting this thesis in partial fulfilment of the requirements for an advanced degree at the University of British Columbia, I agree that the Library shall make it freely available for reference and study. I further agree that permission for extensive copying of this thesis for scholarly purposes may be granted by the head of my department or by his or her representatives. It is understood that copying or publication of this thesis for financial gain shall not be allowed without my written permission.

Department of Civil Engineering

The University of British Columbia
Vancouver, Canada

Date March 18, 1989

DE-6 (2/88)

Abstract

The problem addressed in this thesis is that of the behaviour of large offshore structures subjected to ice and earthquake loading.

The theoretical formulation of the fluid force and associated added mass and damping coefficients acting on an isolated vertical surface-piercing rigid circular cylinder which is excited by sinusoidal unidirectional ground motions is presented. The closed-form solution is first developed on the basis of potential flow theory for arbitrary values of excitation frequency and, in addition, its asymptotic form for high frequencies is considered. The latter is found to be accurate in predicting the high-frequency added mass only for high structure radius-to-water depth ratios and the high-frequency damping for all radius-to-depth ratios. A computer method for numerical evaluation of the force coefficients is devised and theoretical results for different values of radius-to-depth ratios are thereby generated.

An experimental study has been conducted in the Earthquake Engineering Laboratory of the Department of Civil Engineering at the University of British Columbia to verify the theoretical results obtained for the vertical distribution of the force coefficients of a model cylinder which satisfies the large body regime of fluid-structure behaviour for which effects due to fluid viscosity are negligible. Owing to unanticipated technical problems, the current study is unsuccessful and data recorded in the sinusoidal tests are unrealistic, although the calculated coefficients appear to be independent of base displacement (an observation which indicates that viscous effects were insignificant during testing). Nevertheless, values of total force coefficients which were obtained experimentally for a similar model in a previous investigation are found to agree very well with the corresponding theoretical results for frequencies of up to 6 Hz.

It is concluded that the theoretical formulation provided for the hydrodynamic force coefficients of a vertical surface-piercing circular cylinder subjected to horizontal sinusoidal base motions of arbitrary frequency may be used to accurately predict the total added mass and damping of real structures satisfying the conditions imposed by the theory.

Table of Contents

List of Tables

List of Figures

List of Photographs

Acknowledgement

Although many people have contributed in one way or another to the preparation of this thesis, I feel that two certain people deserve to be acknowledged here. My sincere thanks must go to my supervisor Dr. M. Isaacson, who was an invaluable source of information and encouragement, and to Dr. A. Filiatrault, who helped me deal with the many frustrations that I had encountered during the experimental program. In addition to their academic guidance, their support on a personal level is very much appreciated.

Chapter One

INTRODUCTION

The more efficient design of coastal and offshore structures used in the development of coastal facilities and of domestic and international energy resources is now of considerable importance to Canada. Environmental load predictions are a critical component in such design and, of these, wave, earthquake, and ice loads are often of paramount importance. The forces exerted upon the structure can produce large and potentially damaging stresses. Considerable effort has been directed toward improving predictions of the behaviour of large offshore structures subjected to ice and earthquake loading.

1.1 Background

When an offshore structure is accelerated, for example by ground vibrations or ice loading, motions are imparted to the surrounding water, and net hydrodynamic forces act on the structure. These forces are related in part to the kinetic energy imparted to the water, which can be attributed to the moving structure having to accelerate a mass of fluid in addition to its own mass and in part to energy dissipation in the fluid due both to the generation of surface waves and to viscous effects at the fluid-structure boundary. The kinetic energy and energy dissipation may be regarded as inertial and damping effects, having components in phase and in quadrature, respectively, with the structural vibrations. Such hydrodynamic effects may be related to the concepts of "added mass" and "damping".

In the case of a body accelerating in a stationary inviscid fluid, the inertia force is often expressed in terms of the added mass m_a of the body, which is added to the body's own dry mass m when expressing the overall force F needed to accelerate the body:

$$F = (m + m_a)\frac{du}{dt} \qquad (1.1a)$$

where u is the velocity of the body and t is time.

A part of the resistance that a structure encounters in its oscillations in a fluid can be interpreted as the fluid-induced damping (or drag). In general, three types of resisting factors can be identified, which are more or less different in their mechanisms: friction effects which exist on all moving surfaces in contact with the fluid; vortex shedding and energy transfer to the flow field due to flow separation, an effect of fluid viscosity; and a wave-making process in free-surface flow which radiates energy to the far field. The concept of added damping is usually taken as linear in character, so that

$$F = \lambda u \tag{1.1b}$$

where u is the velocity of the body and λ is the damping coefficient. This acts in addition to structural damping and represents the latter type of resistance, namely the energy dissipated by surface waves generated by the vibrating structure. It is dependent on structural dimensions, total water depth, and frequency of excitation.

The determination of the hydrodynamic added mass and damping coefficients has been the object of considerable research in offshore engineering. Their values are obtained through the solution of the fluid-structure problem. Two separate regimes of fluid-structure interaction arise by which hydrodynamic force problems are treated:

(i) large body (or diffraction) regime; and
(ii) small body regime.

There are two corresponding approaches currently used for the solution of fluid-structure interaction associated with fixed or floating structures:

(i) the diffraction (or potential flow) theory; and
(ii) application of the so-called Morison equation.

With respect to the former approach, a given situation may be defined further in terms of one or both of two fundamental and somewhat related problems: the diffraction problem of

an incident wave train interacting with a fixed body; and the radiation problem of a body forced to oscillate in otherwise still water, the situation with which this thesis is concerned.

The selection of an appropriate regime depends primarily on the values of the Keulegan-Carpenter number K and structure diameter-to-wavelength ratio D/L. Keulegan and Carpenter (1958) showed that the ratio, $K=2\pi A/D$ (given here for two-dimensional sinusoidal flow), of water particle orbit amplitude A to characteristic structural horizontal dimension D (e.g. diameter of a cylinder) defines the relative importance of wave-induced drag and inertia effects.

When the parameter D/L is relatively small (i.e. structural elements are slender), flow separation rather than wave diffraction (or radiation, depending on the situation) becomes important, and a characteristic Keulegan-Carpenter number rather than D/L has more physical significance. On the other hand, when wave scattering is important (i.e. D/L is not too small), the fluid particle displacements relative to D may become sufficiently small for the effects of flow separation to be minimal or localized.

In the case of a vertical circular cylinder, linear wave theory gives the Keulegan-Carpenter number as

$$K = \frac{\pi\ H/L}{(D/L)\ \tanh(kd)} \tag{1.2}$$

at still water level, where H is the wave height, $k = 2\pi/L$ is the wave number; and the maximum wave steepness is approximated by

$$\frac{H}{L} = 0.14\ \tanh(kd) \tag{1.3}$$

for intermediate to deep water depths. The value of K is thus limited to about

$$K < \frac{0.44}{(D/L)}\ . \tag{1.4}$$

In the case of wave loading, when a body spans a significant fraction of a wavelength, the incident waves generally undergo significant scattering or diffraction and wave force

calculations should then take such scattering into account. Similarly, a vibrating structure produces surface waves which scatter away from itself. This situation characterizes the diffraction regime of wave-structure interaction, for which potential flow theory is the fundamental tool of analysis, and is generally considered to occur when the structure spans more than about a fifth of the wavelength. Under this condition, K will not exceed about 2.2 and will usually be less than about 1. Appreciable flow separation should then not occur, and the effects of viscosity will be confined to the boundary layers on the body surface. The flow may then be treated as irrotational and the problem solved on the basis of potential flow theory.

Figure 1.1 illustrates the conditions under which diffraction, flow separation, and nonlinear effects may be important for a vertical circular cylinder. However, in certain cases, such as resonant structural vibrations, viscous effects may be a significant consideration even though the flow is unseparated.

Historically, the Morison equation was introduced as a useful and somewhat intuitive formula for the estimation of wave-induced forces on structures belonging to the small body regime. Flow past the body is considered to have a velocity and acceleration such as would occur at the body's centre if it were not present in the flow, and the kinematics of the undisturbed flow in the region near the structure do not change in the direction of wave propagation. The form of the force equation which is commonly used in practice is based on the addition of an inertia force, associated with the fluid acceleration and analogous to the force due to an inviscid fluid, and a drag force having the form used in steady flow analyses. Since its introduction in 1950, the general validity of this expression, and in particular its validity in relation to wave-induced loads on circular cylinders, has been questioned. Nonetheless, during the four decades since 1950 a more appropriate formula has not been found.

The Morison equation is given as

$$F' = \frac{1}{2}\rho C_d D |U| U + \rho C_m \frac{\pi D^2}{4} \frac{dU}{dt} \qquad (1.5)$$

where F' is the fluid force per unit length, U and dU/dt represent the undisturbed velocity and acceleration of the fluid or body respectively, ρ is the fluid density, and D is the

structure diameter. The Morison equation can be reconciled with a general dimensional analysis of the problem only if a drag coefficient C_d and an inertia coefficient C_m are considered to be functions of the Reynolds number $Re = U_m D/\nu$, the Keulegan-Carpenter number $K = 2\pi A/D$, the phase angle of the periodic motion $2\pi t/T$, and the relative roughness of the cylinder ε/D, where U_m is the maximum velocity and ν is the kinematic fluid viscosity. Consequently, these coefficients are not fundamental constants and must be obtained experimentally.

As a point of interest, it can be demonstrated that the acceleration of a body in an otherwise stationary fluid is kinematically identical to an accelerating flow of the fluid past the body when fixed. The forces acting on the body in the two situations are closely related, such that the drag force is unaltered. The only difference is that the inertia coefficient C_m applies to the case of an oscillatory flow past a fixed cylinder and is instead $C_a = C_m - 1$ for the case of oscillation of a cylinder in still fluid. C_a is termed the "added mass coefficient".

Large offshore structures are now an established aspect of offshore technology, and an alternate approach valid over a wide range of D/L has become necessary. In response to this need, formulations using potential flow theory have been established. In this theory, the velocity of any point is specified as the gradient of a scalar potential function, the velocity potential, which satisfies the Laplace equation and appropriate boundary conditions. Once the velocity potential has been determined, the pressure may be obtained using the unsteady Bernoulli equation, and the hydrodynamic loads and associated force coefficients may then be calculated from an integration of the pressure around the body surface. Local flow separation due to sharp configurations can occur on large structures and lead to inaccuracies in solutions obtained from the potential flow assumptions. The significance of these errors should be given consideration in such cases.

There exists a variety of numerical schemes for tackling various structural configurations. A closed-form solution to the linear wave diffraction problem for an isolated vertical surface-piercing circular cylinder is available. Bodies of more general shape have been treated by various numerical techniques such as the traditional wave source distribution method whereby wave interaction with a stationary body of arbitrary geometry is computed by representing the body as a distribution of point wave sources

over its immersed surface. The method's applicability, however, is limited; loads due to high-frequency excitation (e.g. short waves) on a large structure may not be reliably computed as any accurate prediction would involve an impracticably large number of facets or wave sources. There is a need, therefore, to improve predictions of the behaviour of large offshore structures subjected to a wide range of excitation frequency. A first step in this thesis has been to develop a closed-form solution for a vertical surface-piercing circular cylinder valid for the entire range of frequencies, followed by consideration of a high-frequency asymptotic approximation to this.

1.2 Literature Review

The concept of "added mass" was recognized as early as 1779, when Chevalier DuBuat experimented with spheres oscillating in water. Subsequently, in 1828 Bessel conducted experiments on spherical pendulums in air and in water. Noting that the object's period of motion in water differed from that in air, both DuBuat and Bessel concluded that it is necessary to attribute to the test object a virtual mass greater than its ordinary mass. The concept of "added mass" was thus introduced.

Since the time of DuBuat, the added mass due to submergence of an object in a fluid has been the subject of many analytical and experimental investigations. Determination of added mass by experiment, however, has often been inconsistent and unreasonable. Measured values for added mass have usually been larger than can be explained by theory and analysis. Luneau (1949), for example, reported on tests of circular disks in which he found added mass values ranging from 3 to 9 times the theoretical values. One reason for the discrepancy is that classical explanations for the phenomenon did not account for the effect of wake or cavity-induced mass. Moreover, for an accelerating or decelerating body (or ambient fluid), the induced mass varies with the instantaneous shape and volume of wake or cavity as well as with rates of change. The instantaneous magnitude of added mass in transient conditions depends on the time history of motion. Indeed, Iverson and Balent (1951) concluded that added mass is a variable which depends on the state of motion and is not a constant as had been shown by studies of potential flow.

Added mass may be expressed in many ways. Sarpkaya and Isaacson (1981) examine in detail the various forms for two- and three-dimensional bodies. In classical formulations, the hydrodynamic force and moment acting on a rigid body in an irrotational flow of an unbounded inviscid fluid are expressed in terms of the added mass coefficients of the body and the components of its velocity and acceleration. Special cases exist for which the added mass coefficients that are obtained through use of the velocity potential may be used. One such case is of particular concern in this thesis: that of a body subjected to relatively small-amplitude oscillations (so as to preclude effects of separation) at a relatively high frequency.

Experimental Studies

Measurements on a body undergoing small-amplitude harmonic oscillations in water have commonly been used to determine added mass coefficients and to compare them with those obtained from potential flow theory.

Stelson and Mavis (1955) determined the added masses for the first mode frequencies of cylinders, spheres, and rectangles suspended in air and in water from a flexible support and set into free vibration. With the assumption that the support stiffness remained constant, the two frequency values were compared and the added mass taken as the difference in the mass values calculated from the measured frequencies. There was good agreement between their results and those obtained from a potential flow solution.

Similar experiments were performed by Clough (1970) on horizontally-oriented cylinders, plates, and rectangles. In addition to measuring added mass, Clough determined the damping values and found that submerged models experienced increased damping. He concluded, as well, that it is unlikely that structural vibrations due to seismic excitation would be large enough to induce flow separation, thus allowing one to use potential flow theory in obtaining a solution.

The dependence of added mass and damping on the actual base excitation, which may vary in amplitude and frequency, had not been considered in the preceding free vibration experiments. Application of a linearized potential flow solution requires that the added mass and damping be independent of base amplitude. However, because the amount of

energy needed to generate surface waves through structural motion varies with wave (and hence excitation) frequency, the added mass and damping do depend on excitation frequency, as evident in experiments conducted by Liaw and Chopra (1973) and Eatock-Taylor and Duncan (1980). A dimensional analysis by Sarpkaya and Isaacson (1981), as well as by McConnell and Young (1965), clearly illustrates the frequency dependence of the hydrodynamic force.

McConnell and Young (1965) investigated the dependence of added mass and damping on Stokes number, $\omega a^2/\nu$, for a sphere in a bounded fluid, where ω is the excitation frequency, a is the sphere radius, and ν is the kinematic fluid viscosity. Based on the general agreement between theoretical and experimental results, McConnell and Young concluded that the Stokes viscous flow solution will accurately predict the added mass and fluid damping coefficients for spheres. They showed that for a given fluid at a given excitation frequency, the problem can be resolved into a second-order differential equation with constant added mass and damping coefficients for a constant Stokes number. It should also be mentioned that provided that all free surface boundary conditions are included in the analysis the dependence on excitation frequency is part of the solution. McConnell and Young argue further that, because the hydrodynamic coefficients actually depend on the Stokes number, the potential flow solutions are valid only for large values of this parameter and, consequently, good agreement between experimental results and potential flow analysis is reported when the experiment is conducted in water or other low viscosity fluids.

Byrd (1978) conducted an extensive experimental study of the forces resulting from seismic loading on submerged structures. A well-instrumented model of a cylindrical underwater storage tank was attached to a shaking table such that the floor of the water tank and the model underwent identical motions. Hydrodynamic forces arising from horizontal, vertical, and rotational motions were measured. The natural frequency of the model in air and in water was determined by free vibration tests, and added mass and damping terms, as well as the total hydrodynamic force, were established from sinusoidal tests as a function of excitation frequency above 3 Hz. The results were then compared with those determined from potential flow theory excluding the free surface boundary conditions. As noted earlier, the added mass and damping coefficients become independent of excitation frequency when these boundary conditions are omitted from the analysis (i.e. they have

constant values for a given structure). Furthermore, Dong (1978) and Byrd discovered that for certain structure dimensions this frequency dependence can be relatively insignificant above 3 Hz. Pegg (1983) confirmed their observations.

The experimental study carried out by Pegg (1983) played an important role in the current research, particularly where the development of an appropriate testing facility and model was concerned. Pegg investigated the dynamic characteristics of submerged and surface-piercing vertical cylinders satisfying the large body regime of fluid-structure behaviour, for a low frequency range of 0.1 to 6.0 Hz of seismic activity; whereas, in this thesis, a much larger range of excitation frequency is considered, and for this reason an entirely new closed-form solution which is valid over this range is developed, on the basis of potential flow theory with appropriately-imposed boundary conditions. In structural dynamics, the transfer function relating base shear with input base acceleration is a useful design parameter. Pegg had derived such a transfer function from the solution of Laplace's equation based on the traditional boundary element method involving an axisymmetric Green's function. Pegg verified the parameter's validity by comparing it with the transfer function developed from experimentally-obtained values for the added mass and damping coefficients. In addition, Pegg examined the variation of the coefficients with excitation frequency and found that their frequency dependence is significant for surface-piercing cylinders, owing to the production of surface waves.

Although most experimental studies have been restricted to the laboratory environment, full-scale investigations of dynamic characteristics of offshore structures had been conducted by Ruhl and Berdahl (1979). Forced vibration tests on a deepwater platform were performed, during which the first few mode shapes and periods and damping characteristics were measured. Such information is useful in the detection of member failures occurring after severe earthquake, ice, or wave loading events.

Theoretical Studies

The details of the analytical procedures used in obtaining the hydrodynamic forces will not be discussed in this thesis, but it is appropriate that some consideration be given to the techniques which are generally used in engineering applications and to the types of problems which they solve.

The classical treatment of the hydrodynamics of a moving body in a fluid can be found in the works of Lamb (1945), Kochin *et al.* (1964), and in recent reviews presented by Newman (1977) and Sarpkaya and Isaacson (1981). Special attention and a variety of experimental and theoretical studies have been devoted to flow around circular cylinders.

Hogben (1974) outlined the relative importance of drag and inertial effects and the diffraction phenomenon's role in the determination of fluid loading on large bodies. The advent of large gravity structures in the North Sea created a demand for a general analysis method which would permit calculation of diffraction effects and associated fluid loadings on arbitrarily-shaped bodies. As a result, various procedures were developed to provide a solution to three-dimensional potential flow problems; they can now be grouped into three broad categories:

a. closed-form solutions;
b. source distribution methods; and
c. variational methods (finite elements and boundary elements).

Closed-form solutions are unique to the configuration for which they were developed. Source distribution methods are ideally suited for modelling the conditions at the boundaries when the fluid medium is homogenous. A common numerical approach is the wave source or integral equation method, involving development of a surface integral equation and its solution by a discretization procedure. Finite element methods, on the other hand, cope with continuum problems which may involve inhomogenities in the medium properties. A detailed description of the boundary element method, which involves dividing the fluid-structure interface into equal facets, is provided by Garrison (1978).

The assumptions that are generally common to these and other methods are:

a. small amplitude displacement such that linear boundary conditions may be assumed;
b. inviscid fluid (irrotational flow); and
c. incompressible fluid.

Solutions to the fluid problem under these circumstances can be considered as "linear potential flow" solutions, and it can be shown by comparison of the results under similar conditions that the solutions by any of these methods are comparable, as expected. All methods are not, however, available under all circumstances.

The wave source method using a Green's function has been applied successfully to problems of the diffraction type. John (1950) developed the Green's function satisfying the Laplace equation, the bottom and linearized free surface boundary conditions, together with the radiation condition. Garrison (1978), Isaacson (1978), Eatock-Taylor and Waite (1978), Chakrabarti (1979), and Kioka (1980) used this technique to study the effect of waves on submerged bodies of various configurations. Wehausen and Laitone (1960) presented variations of the technique and discussed the solutions of a general boundary-value problem. The appeal of this method may be attributed to the fact that it can accommodate various geometries and approximations. However, as discussed by Murphy (1978), there exist critical frequencies that lead to the failure of the integral equation used in connection with the Green's function method.

The radiation problem of forced waves on the water surface induced by oscillations of an object has been investigated. Havelock (1929) derived a solution for the symmetric wave field created by the vibrations of a circular cylinder in water of infinite depth. A useful set of relations concerning wave-making of oscillating bodies has been developed by Haskind (1957). He showed that the exciting force on a fixed body due to waves is directly related to the waves generated by the forced oscillations of the body. The result is a fundamental relationship between the damping coefficients associated with the radiation problem and the exciting forces associated with the diffraction problem. Black *et al.* (1971) applied the Haskind's theorem, along with a variational formulation, to the radiation and scattering of surface waves by rigid bodies. Potash (1971) presented a second order theory for oscillating cylinders in water.

For bodies of simple geometry, such as a submerged or surface-piercing vertical circular cylinder seated on a horizontal sea floor, solution to the equations of fluid motion may be successfully achieved by the method of separation of variables and expressed in terms of the eigenfunctions of the resulting equations. MacCamy and Fuchs (1954) used this

technique to present the exact mathematical solution for the symmetric diffraction of linear waves by a circular cylinder. This semi-analytical method was treated by Garrett (1971) for a floating vertical circular cylinder. Since the method applies in much the same way to radiation problems (such as that considered in this thesis), only brief mention was made of these cases by the authors. Titchmarsh (1946) and Levinson *et al.* (1949) have investigated the technique of separation of variables and eigenfunction expansion in potential flow problems and the subtleties involved.

Scattering and radiation problems for various obstacles, including the vertical circular cylinder, have also been treated by a variational formulation. The complex amplitude of the scattered wave in the far field is obtained accurately without striving for equal accuracy for the near field. Black *et al.* (1971) show that, by formulating simultaneously the integral equations for the radiation and scattering problems, the far-field amplitude of the radiated wave can also be calculated variationally; by means of a theorem of Haskind, the information obtained is then used to calculate the force and moment on a fixed body in a plane incident wave. Bai (1975) used the finite element technique to represent the velocity potential in the problem of wave diffraction. A finite-element formulation of the response of a submerged tower structure in an earthquake is discussed in Liaw and Chopra (1973). Nilrat (1980) used this method with a transmitting boundary to investigate the hydrodynamic effects of axisymmetric bodies.

In the design of offshore structures, particularly in deep waters, dynamic response of the entire structure to various environmental loadings must be considered. The first essential step in such an analysis is the formulation of an appropriate mathematical model representing the structure and its foundation by suitably-defined mass, damping, and stiffness matrices and the hydrodynamic force by a suitable expression developed according to any one of the methods mentioned above. In this way, the added mass and damping coefficients for the structure under consideration can be determined.

Penzien and Kaul (1972) performed regular modal and spectral analyses on offshore towers, simplified by the assumption that the added mass and damping were constant. Their approach, which gives results suitable for design approximations for a small number of structure types, involved the simple addition of the added mass and damping to the structure's own dry mass and damping values.

A comprehensive analytical study of the response of elastic structures surrounded by a fluid using potential flow theory was presented by Liaw and Chopra (1973). The authors utilized a modal analysis technique in combination with a finite element method to predict structural response. No experimental verifications were given in this study.

Eatock-Taylor and Duncan (1980) developed a design method which employs added mass and damping matrices dependent on frequency, derived from Laplace's equation and used in design with regular modal analysis. They also reported experimental verification.

The dynamic response of vertical circular cylinders to earthquake excitation in compressible water of finite depth was presented by Tanaka and Hudspeth (1986). Analytical solutions were developed by eigenfunction expansions, which included the effects of structure-fluid interaction, and provided the added mass and hydrodynamic radiation damping coefficients. Verification involved comparison between the numerical results and experimental data for both a rigid and a flexible circular cylinder.

Of considerable relevance to this thesis is the work done by Garrison and Berklite (1973), who generated theoretical and experimental values of added mass coefficients for a number of rigid objects of arbitrary shape. A simple yet practical numerical analysis was developed using three-dimensional sources and image sources to represent the flow produced during impulsive motion of a large arbitrarily-shaped rigid structure immersed in the sea. Garrison and Berklite found that the proximity of the free surface has a considerable effect on the added mass coefficient, tending to reduce it in comparison to the rigid boundary case. The results are directly applicable in the determination of earthquake loading of rigid submerged and surface-piercing bottom-mounted structures.

1.3 Research Objectives

The evaluation of the added mass and damping of bodies oscillating in a free surface has been a subject of considerable research interest. Notably absent in the published literature is a comprehensive set of hydrodynamic force coefficients for the relatively simple but practical case of a vertical circular cylinder oscillating horizontally in a finite-depth fluid.

The primary purpose of this investigation is to present theoretical and experimental results for hydrodynamic added mass and damping coefficients for an isolated vertical surface-piercing circular cylinder oscillating horizontally in still water for a wide range of excitation frequency. Apart from the total added mass and damping coefficients, attention is focussed on their vertical distribution.

A segmented circular cylinder, belonging to the large body regime of fluid-structure behaviour, was constructed and tested under conditions of unidirectional, horizontal, sinusoidal base motion in the Earthquake Engineering Laboratory at the University of British Columbia. For each segment, experiments were performed to determine the sectional hydrodynamic force and associated added mass and damping coefficients for a wide range of excitation frequency. Comparisons were then to be made between the experimental results and the numerical predictions based on potential flow theory. In this way, the distribution of hydrodynamic force and coefficients on the cylinder surface was to be established.

Chapter Two

THEORETICAL FORMULATION

2.1 Introduction

When a structure is large compared to the wave length, Morison's equation is no longer applicable. Incident waves undergo significant scattering or diffraction; similarly, a vibrating structure generates surface waves which radiate out to the far field. In both cases, diffraction and/or radiation of waves from the surface of the structure should be considered in wave-force calculations.

Unfortunately, the behaviour of large offshore structures subjected to ice and earthquake loading, expressed in terms of the added mass and damping coefficients of the structure, cannot be accurately predicted by traditional methods of solution because of the relatively high frequency range of such environmental loading. The current chapter will present a closed-form solution for a vertical surface-piercing circular cylinder which is valid for a wide range of excitation frequency.

2.2 Assumptions of Fluid State

The dynamics of a physical fluid-structure system subjected to various excitations may be mathematically modelled as an initial boundary value problem with specified fluid conditions. Prior to setting up the boundary value problem for a circular cylinder undergoing horizontal oscillations in otherwise still water, it is appropriate initially to list and comment on the various assumptions that are made. These are the following:

(i) incompressible fluid;
(ii) no flow separation;
(iii) irrotational flow;

(iv) small amplitude oscillations; and
(v) otherwise stationary fluid.

These are discussed in turn.

Incompressibility

The assumption of incompressibility is valid for most studies of fluid-structure interaction. The frequency of wave and earthquake excitations is generally such that the effects of compressibility in water may be neglected. The fluid velocity, u, is of the order [ωA], where ω is the excitation frequency and A is the oscillation amplitude. Water compressibility becomes unimportant when the fluid velocity is very much less than the speed of sound in water. It can be seen that for a frequency of 15 Hz and an oscillation amplitude of about 2 cm, the resulting fluid velocity amplitude is 1.9 m/s, which is indeed much smaller than the speed of sound in fresh water at room temperature.

No Flow Separation

For the reference two-dimensional case of a circular section oscillating in still fluid, flow separation does not occur for K less than about 1.6. Chapter One indicated the relationship between K and D/L. On this basis, $K < 1.6$ corresponds to $D/L > 0.28$ and to $\omega^2 a/g > 0.86$. Therefore, for the structure considered in the current study, cylinder radius a = 0.162 m, the assumption of no flow separation is valid for excitation frequencies greater than about 7.3 rad/s (i.e. 1.2 Hz). The above examination neglects the case of bodies with sharp corners, such as square sections, for which flow separation could occur at lower values of K.

Irrotational Fluid Motion

The assumption of irrotationality allows one to solve the fluid-structure problem by Laplace's equation for potential flow. In fact, if the fluid is assumed to be inviscid, then the flow will in general be irrotational (although not necessarily so).

Nonlinearities

An additional limitation of linear diffraction theory is that which rises from the assumption of small amplitude motion as implied by the application of the linearized free-surface boundary conditions. Upon consideration of the results obtained from extensions of the diffraction theory to the second-order, one can generally assess that nonlinear effects, such as the velocity-squared term occurring in Bernoulli's equation, become significant only in the case of shallow-water, large-amplitude waves. Inasmuch as typical values of oscillatory ground displacement produced in earthquakes are only a few inches, the assumption of small values of the relative amplitude of the fluid motion is well satisfied for most large structures.

Still Fluid

It is assumed that water disturbances are due only to the horizontal motion of the structure. No steady or unsteady cross flow is present in the fluid domain. Currents and other effects are not considered. The fluid is of constant density, and the effects of internal waves are also not considered.

2.3 Closed-Form Solution

A vertical circular cylinder of radius a extends from the seabed and pierces the free surface. The structure is located in initially still water of uniform depth d and is subjected to a sinusoidal, unidirectional base motion X(t) which is given by the real part of the expression below:

$$X(t) = \xi\, e^{-i\omega t} \tag{2.1}$$

where ξ is a complex displacement amplitude and ω is the excitation frequency. The fixed Cartesian coordinate system (x,y,z) used is shown in Figure 2.1: the vertical coordinates z and s are positive upward, measured from the still water level (SWL) and seabed respectively, and x is measured in the direction of base motion. The cylinder is specified

by the cylindrical polar coordinate system (r, θ, z) with r = 0 lying along the cylinder axis when in the equilibrium position and θ = 0 corresponding to the positive x-axis.

In the usual manner, the fluid is assumed to be incompressible and inviscid and the fluid motion irrotational so that the flow can be described by a velocity potential ϕ. The height of surface waves produced by the vibrating structure is assumed to be sufficiently small such that linear wave theory is applicable. The excitation frequency ω (and hence wave frequency) and wave number of the surface waves are thus related by the linear dispersion relation, given by

$$\omega^2 = gk \tanh(kd) \tag{2.2}$$

where g is the gravitational acceleration, k is the wave number defined as $2\pi/L$, L is the wavelength, and d is the water depth. This equation governs the propagation of surface waves from the near field to the far field. There are two real roots to Equation (2.2), and only one of them is positive [see Figure 2.2].

The irrotational fluid motion is governed by the Laplace equation, expressed in the cylindrical coordinate system as

$$\frac{\partial^2\phi}{\partial r^2} + \frac{1}{r}\frac{\partial\phi}{\partial\theta} + \frac{1}{r^2}\frac{\partial^2\phi}{\partial\theta^2} + \frac{\partial^2\phi}{\partial z^2} = 0 \tag{2.3}$$

within the fluid region. The velocity potential ϕ is subject to the linearized free surface boundary conditions as well as kinematic conditions at the seabed and the body's surface:

$$\frac{\partial^2\phi}{\partial t^2} + g\frac{\partial\phi}{\partial z} = 0 \quad \text{at } z = 0 \tag{2.4a}$$

$$\eta = -\frac{1}{g}\left(\frac{\partial\phi}{\partial t}\right)_{z=0} \tag{2.4b}$$

$$\frac{\partial\phi}{\partial z} = 0 \qquad \text{at } z = -d \tag{2.4c}$$

$$\frac{\partial \phi}{\partial r} = V_n \qquad \text{at } r = a \tag{2.4d}$$

where η is the free surface elevation above the still water level and V_n is the normal velocity of any point on the structure surface, which may be written as

$$V_n\,(\theta, r=a, z, t) = -i\omega\xi \cos\theta\, e^{-i\omega t} \,. \tag{2.5}$$

An additional condition, known as the Sommerfeld radiation condition, must be satisfied in the far field:

$$\text{limit } \sqrt{r}\left(\frac{\partial \phi}{\partial r} - ik\phi\right) = 0 \quad \text{for } r \to \infty \tag{2.6}$$

where r is radial distance.

Following the approach used by Garrett (1971), and on the basis of Bernoulli's method of separation of variables, the velocity potential ϕ may be given by an expression which satisfies the Laplace equation and all the boundary conditions except that on the structure surface. This expression is given as

$$\phi = \left\{\sum_{m=1}^{\infty} \phi_m \cos(m\theta)\right\} e^{-i\omega t} \tag{2.7}$$

where

$$\phi_m = \alpha_{om} H_m^{(1)}(kr)\, f_o(ks) + \sum_{n=1}^{\infty} \alpha_{nm} K_m(k_n r)\, f_n(k_n s) \tag{2.8}$$

and

$$f_o(ks) = \frac{1}{N_o} \cosh(ks) \tag{2.9a}$$

$$f_n(k_n s) = \frac{1}{N_n} \cos(k_n s) \tag{2.9b}$$

$$N_o = \left[\frac{d}{2} \left(1 + \frac{1}{2kd} \sinh(2kd) \right) \right]^{\frac{1}{2}} \tag{2.9c}$$

$$N_n = \left[\frac{d}{2} \left(1 + \frac{1}{2k_n d} \sinh(2k_n d) \right) \right]^{\frac{1}{2}} \qquad n = 1, 2, 3, \ldots \tag{2.9d}$$

$H_m^{(1)}$ is the Hankel function of the first kind and order m; K_m is the modified Bessel function of the second kind and order m; and α_{om} and α_{nm} are initially unknown complex coefficients which will depend on the application of the body surface boundary condition. The variables f_o and f_n are eigenfunctions in the vertical direction, and k and k_n are eigenvalues which satisfy respectively the following equations:

$$kd \cdot \tanh(kd) = \frac{\omega^2 d}{g} \tag{2.10}$$

and

$$k_n d \cdot \tan(k_n d) = \frac{\omega^2 d}{g} \tag{2.11}$$

There are an infinite number of solutions to Equation (2.11); the graphical solutions for high values of $\omega^2 d/g$ are shown in Figure 2.3. The Hankel and Bessel functions are components of eigenfunctions in the horizontal direction such that the radiation condition is satisfied.

On the basis of Equation (2.7), the partial derivative of ϕ with respect to r is given as

$$\frac{\partial \phi}{\partial r} = \left\{ \sum_{m=1}^{\infty} \left[k\, \alpha_{om}\, H_m^{(1)\prime}(kr)\, f_o(ks) + \sum_{n=1}^{\infty} \alpha_{nm}\, K_m'(k_n r)\, f_n(k_n s) \right] \cos(m\theta) \right\} e^{-i\omega t} \qquad (2.12)$$

where the prime denotes differentiation with respect to the argument. Applying Equations (2.12) and (2.5) to the body surface boundary condition given by Equation (2.4d), one obtains

$$\left\{ \sum_{m=1}^{\infty} \left[k\, \alpha_{om}\, H_m^{(1)\prime}(ka)\, f_o(ks) + \sum_{n=1}^{\infty} \alpha_{nm}\, K_m'(k_n a)\, f_n(k_n s) \right] \cos(m\theta) \right\} = -i\omega\xi \cos\theta \ . \qquad (2.13)$$

Only the terms m = 1 will be needed in evaluating the hydrodynamic forces. These give the following:

$$k\, \alpha_{o1}\, H_1^{(1)\prime}(ka)\, f_o(ks) + \sum_{n=1}^{\infty} \alpha_{n1}\, K_1'(k_n a)\, f_n(k_n s) = -i\omega\xi = U \qquad (2.14)$$

at any depth, where $U = -i\omega\xi$ is defined as the velocity amplitude.

The orthogonality properties of the functions f_o and f_n can now be utilized to determine the unknown coefficients α_{o1} and α_{n1}. The eigenfunctions cosh(ks) and cos(k_ns) are orthogonal with respect to a weight function equal to unity on the interval (-d,0) for the depth variable z; that is,

$$\int_0^d \cosh(ks)\cdot\cos(k_n s)\, ds = 0 \quad . \tag{2.15}$$

Both sides of Equation (2.14) are multiplied by $f_b(k_b s)$, b=0,1,2,3, ... in turn, and integrated with respect to s over (0,d):

$$\int_0^d \left\{ k\,\alpha_{o1}\, H_1^{(1)'}(ka)\, f_o(ks) + \sum_{n=1}^{\infty} \alpha_{n1}\, K_1'(k_n a)\, f_n(k_n s) \right\} f_b(k_b s)\, ds = \int_0^d U\cdot f_b(k_b s)\, ds \quad . \tag{2.16}$$

Thus for b = 0,

$$k\,\alpha_{o1}\, H_1^{(1)'}(ka) = U \int_0^d f_o(ks)\, ds \tag{2.17a}$$

and for b = n,

$$k_n\,\alpha_{n1}\, K_1'(k_n a) = U \int_0^d f_n(k_n s)\, ds \quad . \tag{2.17b}$$

Substituting the expressions for f_o and f_n and carrying out the integrations, explicit expressions for the complex coefficients α are finally obtained:

$$\alpha_{o1} = \frac{U}{k\, H_1^{(1)'}(ka)} \cdot \frac{\sinh(kd)}{k\, N_o} \tag{2.18a}$$

$$\alpha_{n1} = \frac{U}{k\, K_1'(k_n a)} \cdot \frac{\sin(k_n d)}{k_n\, N_n} \tag{2.18b}$$

where U, N_n, and N_o have been defined previously. One should note that the α coefficients have dimensions associated with them.

2.3.1 Hydrodynamic Force and Coefficients

The hydrodynamic pressure at any point in the fluid may be expressed by a linearization of the unsteady Bernoulli equation:

$$p(r,\theta,z) = -\rho \frac{\partial \phi}{\partial t} = i\omega\rho \cdot \phi(r,\theta,z) \ . \tag{2.19}$$

The amplitude of the sectional force F_z acting in the positive x-direction is obtained by an appropriate integration of the hydrodynamic pressure over the body surface:

$$F_z = -\int_0^{2\pi} p(r,\theta,z)\, a \cos\theta \, d\theta \tag{2.20a}$$

$$= -i\omega\rho a \int_0^{2\pi} \phi(r,\theta,z) \cos\theta \, d\theta \ . \tag{2.20b}$$

Using the Fourier representation of ϕ given in Equation (2.7), it is seen that only the ϕ_1 term is included:

$$F_z = -i\omega\rho a\pi \cdot \phi_1 \cdot e^{-i\omega t} \tag{2.20c}$$

where, for r=a,

$$\phi_1 = \alpha_{o1} H_1^{(1)}(ka) f_o(ks) + \sum_{n=1}^{\infty} \alpha_{n1} K_1(k_n a) f_n(k_n s) \ . \tag{2.21}$$

The total hydrodynamic force on the cylinder is obtained when Equation (2.20c) is integrated over depth:

$$F_T = \int_0^d F_z \, ds \tag{2.22}$$

and in final form

$$F_T = - i\omega\rho a\pi \left\{ \alpha_{o1} H_1^{(1)}(ka) \frac{\sinh(kd)}{k N_o} + \sum_{n=1}^{\infty} \alpha_{n1} K_1(k_n a) \frac{\sin(k_n d)}{k_n N_n} \right\} e^{-i\omega t} \qquad (2.23)$$

where

$$\alpha_{o1} = \frac{U}{k H_1^{(1)'}(ka)} \cdot \frac{\sinh(kd)}{k N_o} = U \cdot \alpha'_{o1} \qquad (2.24a)$$

$$\alpha_{n1} = \frac{U}{k K_1'(k_n a)} \cdot \frac{\sin(k_n d)}{k_n N_n} = U \cdot \alpha'_{n1} \qquad (2.24b)$$

$$N_o = \left[\frac{d}{2} \left(1 + \frac{1}{2kd} \sinh(2kd) \right) \right]^{\frac{1}{2}} \qquad (2.9c)$$

$$N_n = \left[\frac{d}{2} \left(1 + \frac{1}{2k_n d} \sinh(2k_n d) \right) \right]^{\frac{1}{2}} \qquad n = 1, 2, 3, \ldots . \qquad (2.9d)$$

The fluid force F_T can be conveniently decomposed into components in phase with the velocity and the acceleration; so that

$$F_T = - \left(\mu \frac{\partial^2 X(t)}{\partial t^2} + \lambda \frac{\partial X(t)}{\partial t} \right) \qquad (2.25a)$$

or

$$F_T = \left[\omega^2 \mu + i\omega \lambda \right] \xi e^{-i\omega t} \qquad (2.25b)$$

where μ and λ are the total added mass and damping coefficients and taken as real. Equation (2.23) may now be substituted for F_T in the above equation; after some manipulation of the resulting expression, one obtains the following:

$$\omega\mu + i\lambda = -i\omega\rho\pi a \cdot \{\Omega\} \tag{2.26}$$

where

$$\Omega = \alpha'_{o1} \cdot H_1^{(1)}(ka) \cdot \frac{\sinh(kd)}{k\, N_o} + \sum_{n=1}^{\infty} \alpha'_{n1} \cdot K_1(k_n a) \cdot \frac{\sin(k_n d)}{k_n\, N_n} \quad . \tag{2.27}$$

Substitution of the appropriate expressions for the coefficients in Equation (2.27) yields

$$\Omega = \frac{1}{k} \cdot \frac{H_1^{(1)}(ka)}{H_1^{(1)\prime}(ka)} \cdot \frac{\sinh^2(kd)}{(kN_o)^2} + \sum_{n=1}^{\infty} \frac{1}{k_n} \cdot \frac{K_1(k_n a)}{K'_1(k_n a)} \cdot \frac{\sin^2(k_n d)}{(k_n N_n)^2} \tag{2.28}$$

which can be further simplified by expanding N_o and N_n and applying the appropriate trigonometric identities:

$$\Omega = \frac{1}{k^2} \cdot \frac{H_1^{(1)}(ka)}{H_1^{(1)\prime}(ka)} \cdot h_o(kd) + \sum_{n=1}^{\infty} \frac{1}{k_n^2} \cdot \frac{K_1(k_n a)}{K'_1(k_n a)} \cdot h_n(k_n d) \tag{2.29a}$$

$$h_o(kd) = \frac{2 \cdot \tanh(kd)}{\left[1 + \frac{2kd}{\sinh(2kd)}\right]} \tag{2.29b}$$

$$h_n(k_n d) = \frac{4 \cdot \sin^2(k_n d)}{[\, 2k_n d + \sin(2k_n d)\,]} \quad . \tag{2.29c}$$

The total added mass and damping coefficients may now be defined explicitly as

$$\mu = -\rho\pi a^3 \cdot \mathrm{Re}\{\Omega'\} \tag{2.30a}$$

$$\lambda = -\omega\rho\pi a^3 \cdot \mathrm{Im}\{\Omega'\} \tag{2.30b}$$

where

$$\Omega' = \frac{\Omega}{a^2} \; ; \tag{2.30c}$$

Ω is given in Equation (2.29a); and Re{ } and Im{ } denote real and imaginary parts respectively. One should note that, in accordance with Equation (2.4d), $\partial\phi/\partial r$ is always imaginary over the structure surface and so μ and λ are indeed real. The units of μ and λ are kg and kg/s respectively.

2.3.2 Vertical Distribution of the Coefficients

On the basis of Equations (2.20c) and (2.21), the sectional fluid force is already known and is given as

$$F_z = - i\omega\rho\pi a \left[\alpha_{o1} H_1^{(1)}(ka) f_o(ks) + \sum_{n=1}^{\infty} \alpha_{n1} K_1(ka) f_n(ks) \right] e^{-i\omega t} \tag{2.31a}$$

where

$$\alpha_{o1} = - i\omega\xi \left(\frac{\sinh(kd)}{k \cdot N_o} \right) \left(\frac{1}{k \cdot H_1^{(1)\prime}(ka)} \right) \tag{2.31b}$$

$$\alpha_{n1} = - i\omega\xi \left(\frac{\sin(k_n d)}{k_n \cdot N_n} \right) \left(\frac{1}{k_n \cdot K_1'(ka)} \right) . \tag{2.31c}$$

As with the total force F_T, the sectional fluid force F_z is decomposed into components in phase with the velocity and acceleration, so that

$$F_z = \left(\omega^2 \mu' + i\omega \lambda' \right) \xi \, e^{-i\omega t} \tag{2.32}$$

where μ' and λ' are respectively the sectional added mass and damping coefficients. Equating Equation (2.32) to Equation (2.31a) and simplifying the resulting expression by using various trigonometric identities, one finds that the added mass and damping coefficients per unit length of cylinder may be calculated using the following expressions:

$$\mu' = -\rho\pi ad \cdot \mathrm{Re}\{\emptyset\} \tag{2.33a}$$

$$\lambda' = -\rho\omega\pi ad \cdot \mathrm{Im}\{\emptyset\} \tag{2.33b}$$

where

$$\emptyset = \frac{H_1^{(1)}(ka)}{H_1^{(1)\prime}(ka)} \cdot \frac{1}{kd}\left[\frac{2}{1 + \frac{2kd}{\sinh(2kd)}}\right] \cdot \frac{\cosh(ks)}{\cosh(kd)} + \sum_{n=1}^{\infty} \frac{K_1(ka)}{K_1'(ka)} \cdot \frac{1}{k_n d}\left[\frac{2\sin(2k_n d)}{2k_n d + \sin(2k_n d)}\right] \cdot \frac{\cos(k_n s)}{\cos(k_n d)} \quad . \tag{2.33c}$$

The S.I. units of the sectional added mass and damping coefficients are kg/m and kg/m/s respectively. Their dimensionless forms are given below:

$$\frac{\mu'}{\rho a^2} = -\pi\frac{d}{a} \cdot \mathrm{Re}\{\emptyset\} \tag{2.34a}$$

$$\frac{\lambda'}{\rho\omega a^2} = -\pi\frac{d}{a} \cdot \mathrm{Im}\{\emptyset\} \tag{2.34b}$$

where $\emptyset$ is defined in Equation (2.33c).

2.4 Summary of Expressions for the Coefficients

The aim of the theoretical formulation presented above was to derive both total and sectional added mass and damping coefficients, with and without dimensions attached to them. It would be worthwhile now to list their final expressions, valid for all frequencies.

First, the total hydrodynamic coefficients are obtained through the following:

$$\frac{\mu}{\rho a^3} = -\pi \, \mathrm{Re}\{\Omega'\} \tag{2.35a}$$

$$\frac{\lambda}{\rho a^3 \omega} = -\pi \, \mathrm{Im}\{\Omega'\} \tag{2.35b}$$

where

$$\Omega' = \frac{1}{(ka)^2} \cdot \frac{H_1^{(1)}(ka)}{H_1^{(1)\prime}(ka)} \cdot h_o(kd) + \sum_{n=1}^{\infty} \frac{1}{(k_n a)^2} \cdot \frac{K_1(k_n a)}{K_1'(k_n a)} \cdot h_n(k_n d) \tag{2.36a}$$

$$h_o(kd) = \frac{2 \cdot \tanh(kd)}{\left[1 + \frac{2kd}{\sinh(2kd)}\right]} \tag{2.36b}$$

$$h_n(k_n d) = \frac{4 \cdot \sin^2(k_n d)}{[\, 2k_n d + \sin(2k_n d) \,]} \qquad n = 1, 2, 3, \ldots \; . \tag{2.36c}$$

Second, the variation of the hydrodynamic coefficients with s, elevation above the seabed, can be determined from the following:

$$\frac{\mu'}{\rho a^2} = -\pi \frac{d}{a} \cdot \mathrm{Re}\{\emptyset\} \tag{2.34a}$$

$$\frac{\lambda'}{\rho a^2 \omega} = -\pi \frac{d}{a} \cdot \mathrm{Im}\{\emptyset\} \tag{2.34b}$$

where

$$\emptyset = \frac{H_1^{(1)}(ka)}{H_1^{(1)\prime}(ka)} \cdot \frac{1}{kd}\left[\frac{2}{1 + \frac{2kd}{\sinh(2kd)}}\right] \cdot \frac{\cosh(ks)}{\cosh(kd)} + \sum_{n=1}^{\infty} \frac{K_1(ka)}{K_1'(ka)} \cdot \frac{1}{k_n d}\left[\frac{2\sin(2k_n d)}{2k_n d + \sin(2k_n d)}\right] \cdot \frac{\cos(k_n s)}{\cos(k_n d)}$$

$$n = 1, 2, 3, \ldots . \tag{2.33c}$$

2.5 High-Frequency Approximation

At high frequencies, the dimensionless parameters ka and kd become large and simplified expressions for the hydrodynamic coefficients may then be developed by using asymptotic approximations to the hyperbolic, Hankel, and Bessel functions which are present.

The asymptotic expansion for the Hankel function $H_1^{(1)}(x)$ is given as

$$H_1^{(1)}(x) \approx \sqrt{\frac{2}{\pi x}} \cdot \exp\left[i\left(x - \frac{3\pi}{4}\right)\right] \tag{2.37}$$

when x is large. The associated derivative with respect to x is then found to be

$$H_1^{(1)\prime}(x) \approx -\sqrt{\frac{2}{\pi x}}\left\{\frac{1}{2x} - i\right\} \exp\left[i\left(x - \frac{3\pi}{4}\right)\right] . \tag{2.38}$$

The ratio of the Hankel function to its derivative is required and is given as

$$\frac{H_1^{(1)}(x)}{H_1^{(1)'}(x)} \approx -\frac{1}{2x} - i \ . \tag{2.39}$$

Similarly, in seeking an asymptotic expression for the ratio of the Bessel function $K_1(x)$ and its derivative for large x, one finds the following:

$$K_1(x) \approx \sqrt{\frac{\pi}{2x}} \cdot e^{-x} \tag{2.40}$$

$$K_1'(x) \approx -\left\{1 + \frac{1}{x}\right\} \cdot \sqrt{\frac{\pi}{2x}} \cdot e^{-x} \tag{2.41}$$

so that

$$\frac{K_1(x)}{K_1'(x)} \approx -1 \ . \tag{2.42}$$

In the present context, the argument x used in Equation (2.39) is equal to the parameter ka; whereas, in Equation (2.42) x is equal to $k_n a$. Equations (2.39) and (2.42) can then be substituted into Equation (2.36a) when the high-frequency approximations for both hydrodynamic coefficients are being determined. Because kd is also large, the hyperbolic functions in Equation (2.36a) take on the following asymptotic approximations:

$$\tanh(kd) \approx 1 \tag{2.43a}$$

and

$$\frac{2kd}{\sinh(2kd)} \approx 0 \ . \tag{2.43b}$$

The high-frequency approximation for the damping coefficient can thus be determined quite easily by substituting the asymptotic approximations given by Equations (2.39) and (2.43) into Equation (2.35b):

$$\frac{\lambda}{\rho a^3 \omega} \approx \frac{2\pi}{(ka)^2} \ . \tag{2.44}$$

The terms involving the modified Bessel functions are real and hence do not influence the above approximation.

It remains to find a corresponding expression for the added mass coefficient. When ka is large, the solutions for $k_n d$ in Equation (2.11) are given as

$$\begin{aligned} k_1 d &= \frac{\pi}{2} \\ k_2 d &= \frac{3\pi}{2} \\ k_n d &= \frac{\pi}{2}(2n-1) \ . \end{aligned} \tag{2.45}$$

Consequently, the expression for $h_n(k_n d)$ which appears in Equation (2.36a) is simplified:

$$h_n(k_n d) = \frac{4}{(2n-1)\pi} \qquad n = 1, 2, 3, \ldots \ . \tag{2.46}$$

The argument $k_n a$ of the modified Bessel function K_1 appearing in Equation (2.36a) is given as

$$\begin{aligned} k_1 a &= \frac{\pi}{2} \cdot \frac{a}{d} \\ k_2 a &= \frac{3\pi}{2} \cdot \frac{a}{d} \\ k_n a &= k_n d \cdot \frac{a}{d} = \frac{\pi}{2}(2n-1) \cdot \frac{a}{d} \end{aligned} \tag{2.47}$$

and thus the argument for the lowest values of n will not be large. When there is no restriction on the ratio a/d, the high-frequency approximation to the total added mass coefficient becomes (ignoring the $\pi/(ka)^3$ contribution to the approximation)

$$\frac{\mu}{\rho a^3} \approx - \frac{16}{\pi^2} \left(\frac{d}{a}\right)^2 \sum_{n=1}^{\infty} \frac{1}{(2n-1)^3} \cdot \frac{K_1(x_n)}{K_1'(x_n)} \tag{2.48a}$$

where

$$x_n = (2n-1)\frac{\pi}{2}\cdot\frac{a}{d} \quad . \tag{2.48b}$$

When d/a is sufficiently small, specifically when d/a is smaller than about 0.1 (for only a 3 percent error), the summation in Equation (2.36a) becomes

$$\sum_{n=1}^{\infty} \equiv \left(\frac{d}{a}\right)^2 \cdot \left[\frac{2}{(2n-1)\pi}\right]^2 \cdot (-1) \cdot \frac{4}{(2n-1)\pi} \tag{2.49a}$$

$$\equiv -\left(\frac{d}{a}\right)^2 \cdot \frac{16}{\pi^3}\left\{1 + \frac{1}{3^3} + \frac{1}{5^3} + \frac{1}{7^3} + \ldots\right\} \tag{2.49b}$$

$$\equiv -0.54266\left(\frac{d}{a}\right)^2 \quad . \tag{2.49c}$$

Substituting Equations (2.39), (2.42), (2.43), and (2.49c) into the exact expression for the total dimensionless added mass coefficient, given by Equation (2.35a), one finds that the first term in the resultant equation is negligible, making no significant contribution to the numerical result. The high-frequency approximation to the total added mass coefficient can therefore be expressed as

$$\frac{\mu}{\rho a^3} \approx 0.5427\,\pi\left(\frac{d}{a}\right)^2 \qquad \text{for } \frac{d}{a} < 0.1 \quad . \tag{2.50}$$

2.6 Derivation of Added Mass and Damping from Experiment

The experimental setup and instrumentation depend primarily on the parameters which need to be measured and recorded for subsequent evaluation of the hydrodynamic force coefficients as a function of excitation frequency. This section identifies the required data for such an evaluation.

In each frequency test, the forces acting on a section of the model cylinder are to be determined from measurements of the base shear V(t) resulting from a known sinusoidal input acceleration a(t). These may be expressed as

$$a(t) = \mathbf{a} \cos(\omega t) \tag{2.51}$$

$$V_B(t) = \mathbf{V} \cos(\omega t - \beta) \tag{2.52}$$

where **a** is the acceleration amplitude, ω is the excitation frequency, **V** is the base shear amplitude, and β is the phase shift. For a given sinusoidal base displacement

$$X(t) = \mathbf{X} \cos(\omega t) \ , \tag{2.53}$$

where **X** is the displacement amplitude; the velocity is

$$\dot{X}(t) = - \omega \mathbf{X} \sin(\omega t) \tag{2.54}$$

and the acceleration is

$$a(t) = \ddot{X}_g(t) = - \omega^2 \mathbf{X} \cos(\omega t) \ . \tag{2.55}$$

Figure 2.4 shows a free body diagram of the forces acting on the cylinder section. The sectional fluid force is represented by $F_z(t)$, ma(t) is the inertia force of the active part of the cylinder system (of which m is the dry mass), $V_B(t)$ is the base shear reacting to the sectional fluid force, and M(t) is the base moment. Dynamic equilibrium of the forces shown gives

$$ma(t) = F_z(t) + V_B(t) \tag{2.56}$$

and introduction of Equations (2.52) to (2.55) into Equation (2.56) results in

$$-m\omega^2 \mathbf{X} \cos(\omega t) = \mathbf{V} \cos(\omega t - \beta) + F_z(t) \ . \tag{2.57}$$

The expression for base shear [Equation (2.52)] can be expanded, giving

$$V_B(t) = \mathbf{V} \cos\beta \cos(\omega t) + \mathbf{V} \sin\beta \sin(\omega t) \ . \tag{2.58}$$

Moreover, for sinusoidal input the fluid force is also sinusoidal and can consequently be resolved into its components and written in terms of added mass and damping (as discussed previously):

$$F_z(t) = -[\mu' \ddot{X}(t) + \lambda' \dot{X}(t)] \ . \tag{2.59}$$

Substituting Equations (2.58) and (2.59) into Equation (2.57) and rearranging the resulting expression, one can solve for the added mass and damping coefficients:

$$-(m + \mu')\omega^2 \mathbf{X} \cos(\omega t) - \lambda' \omega \mathbf{X} \sin(\omega t) = \mathbf{V} \cos\beta \cos(\omega t) + \mathbf{V} \sin\beta \sin(\omega t) \tag{2.60}$$

so that

$$\mu' = -\frac{\mathbf{V} \cos\beta}{\omega^2 \mathbf{X}} - m = \frac{\mathbf{V} \cos\beta}{\mathbf{a}} - m \tag{2.61}$$

and

$$\lambda' = -\frac{\mathbf{V} \sin\beta}{\omega \mathbf{X}} = \frac{\mathbf{V} \sin\beta}{\mathbf{a}} \omega \ . \tag{2.62}$$

It would appear, therefore, that the required test data are the base shear, the base acceleration, and the phase shift between these two variables. The aluminum shaft of the cylinder is thus instrumented with strain gauges, and equations in which the strain data are incorporated are derived to calculate the shear force.

In evaluating **V** from the acquired strain data, one must consider bending moments in the analysis. The moment developed due to the eccentricity of the fluid force (see Figure 2.4) is eliminated when the difference in the top and bottom strains is taken. The moment due to the inertia of the active component, on the other hand, does not enter the analysis if the strains recorded in air tests are subtracted from those recorded in the corresponding water tests. The details of the data analysis are given in Appendix B.

Chapter Three

FACILITIES, INSTRUMENTATION, AND MODEL DESIGN

One of the primary objectives of the present study is to measure the sectional added mass and damping coefficients of an isolated vertical surface-piercing circular cylinder to horizontal base excitation. The existing facilities at the University of British Columbia Earthquake Laboratory used for this purpose include a shaking table, water tank, and data acquisition system. In this chapter, a suitable model, instrumentation system, and test program are chosen such that they are compatible with these facilities.

3.1 Development of Testing Apparatus

3.1.1 Earthquake Simulator

The seismic tests reported in this thesis were carried out on the Earthquake Simulator in the Earthquake Engineering Laboratory of the Civil Engineering Department at the University of British Columbia. The advanced, closed-loop, servo-controlled electro-hydraulic shaking table is a high-performance seismic simulator which can accurately reproduce earthquake ground motions and a variety of other input wave forms. The shaking table is 3 m x 3 m in plan and is fabricated as a cellular box from welded aluminum plate. It is mounted on four pedestal legs with universal joints at each end to ensure linear horizontal motion. Three hydrostatic bearings restrain lateral movement (or yaw). Test specimens are attached to the table by steel bolts which thread into steel inserts arranged in a grid. Figure 3.1 shows the general arrangement of the table.

The shaking table is operated by an MTS Systems Corporation electronic feedback control system for simulation of single axis horizontal ground motion (SDOF) and is driven by a 155-kN hydraulic actuator. The table is capable of a maximum peak-to-peak

displacement of 15 cm at low frequencies. The system has a resonant frequency of 16 Hz and operates in the frequency range of 0 to 30 Hz, with very limited motion capability at the higher frequencies. Additional system specifications include the following: maximum specimen weight is 16,000 kg; maximum horizontal acceleration is 2.5 g; and mass of the empty table is 2090 kg.

3.1.2 Data Acquisition

The shaking table and data acquisition system are controlled by a PDP-11/04 minicomputer with 32K word memory and a processing capability of 16 channels in any one test. Five channels were used in these tests. The PDP-11/04 uses an AR-11 real time module to perform Analog-Digital conversion and support real time clock functions. Data is stored digitally on floppy disks and can be transferred to the U.B.C. mainframe Amdahl computer or the Earthquake Laboratory AST 286 Premium microcomputer. Photo 3.1 shows the physical arrangement of the data acquisition system.

3.1.3 Water Tank

Figure 3.2 shows a schematic of the water tank, and Figure 3.3 shows the sealing arrangement used. A 3.96m x 3.66m x 1.22m water tank, comprised of a steel frame with plywood sheathing, had originally been constructed to accommodate the experimental study conducted by Pegg (1983), with the intent of incorporating future testing of a variety of models, etc. The water tank straddles the shaking table so as not to be influenced by the table's motion. A plastic pool liner seals the tank, and horsehair matting around the perimeter minimizes the effects of wave reflection on the model response.

The model to be tested is attached to the table through a hole in the floor of the water tank, sealed with a natural rubber diaphragm. This watertight seal at the assembly base effectively allows uninhibited motion of the model. An aluminum plate is fastened to a rigid steel cross-frame which is itself mounted onto the table. The model base is attached to this plate. Another aluminum plate is sealed into the bottom of the tank at its centre through which an 18-inch hole is bored. A round 1/16-inch thick rubber membrane is then fastened between the base plate on the table and the plate on the tank floor by means of a stainless steel sealing ring. This forms a seal between the tank and table, allowing full transfer of

table motion to the model. So that this mounting apparatus does not disturb the surrounding water, an aluminum sealing ring, which reduces the hole diameter to 9 inches, is used to seal the rubber to the tank floor. Over this aluminum ring, a smaller 18-inch diameter plexiglass disc is attached to the model support. In this way, the water which is set into motion by the mounting apparatus does not interfere with that water surrounding the model.

Photographs of the shaking table, model cylinder, and its base support are provided (Photos 3.2, 3.3, and 3.4 respectively).

3.2 Design of Model

The theoretical formulation presented in the previous chapter is applicable only for rigid circular bodies belonging to the large body regime of fluid-structure interaction; a cylindrical model was thus required. In addition to being the simplest shape for representing the large body regime, the circular cylinder is quite common in offshore construction. Moreover, relevant experimental investigations, which could be used for purposes of comparison, have concentrated on this configuration.

The dimensions of the cylinder were carefully chosen so as to meet the requirements of no flow separation, corresponding to a Keulegan-Carpenter number less than 2.2, that is, a maximum allowable displacement-to-diameter ratio of A/D less than 0.35 (the reader is referred to Chapter Two). A reasonable estimate of the maximum base amplitude allowed during the tests appeared to be 1.5 inches. To a minor extent, the availability of materials required that the cylinder diameter be 12.75 inches, so that the maximum value of A/D is 0.12, which is less than the limiting value of 0.35. The use of the potential flow (or large body) regime could, therefore, be justified.

The objectives of the current research further required that the model be designed to allow measurement of sectional fluid forces at predetermined levels along the length of the cylinder. The variation of the hydrodynamic coefficients with water depth could therefore be determined. Unlike the cylinders constructed by Pegg (1983) and Vernon (1984) to accommodate total force measurement, the model used in this study can be identified as

having two components, aptly named the "active" and "passive" parts. The overall mechanics of the design comprises the "active part" of the model, which utilizes the cantilever-beam configuration for force calculations. The "passive part", on the other hand, physically represents the vertical surface-piercing circular cylinder, which in accordance with the research objectives is segmented. The interaction of the ambient fluid with only one of the segments was actually measured during the tests. This particular segment, therefore, belongs to the active part of the model design. The remaining cylindrical segments are interchangeable so that the level of the active segment can be adjusted.

The details of the model design, including materials and dimensions, are clearly illustrated in Figures 3.4 and 3.5. The basic circular cylinder is made of a rigid 12.75-inch diameter polyvinyl chloride (PVC) shell, 1/2 inches thick and almost 32 inches high. Both top and bottom ends are capped by 1/4-inch thick, 13.75-inch diameter PVC plates. The PVC shell consists of nine segments. Seven of these are 4 inches high and completely interchangeable; whereas, the remaining two are only about 2 inches wide and permanently connected to the PVC plates. The male and female ends of each segment are not threaded; hence the connection between adjacent segments is not accomplished by screwing the ends together. Instead, the male end of one segment is pushed snugly onto the female end of the other until their inside edges make contact. As intended, their outside edges do not meet; this creates a thin, shallow groove which runs along the circumference of the connection and inside which an O-ring is placed to seal this connection. As identified in the previous paragraph, one of the 4-inch segments is active; it consists of a 2-inch central section, on which the measured fluid force acts, and upper and lower pieces of segment bridged together by a 3/4-inch thick PVC tube and used to connect adjacent segments. The small space between the section and pieces is covered by a durable latex seal which is secured to the solid surfaces by O-rings and maintains a dry model interior. It is important to note that the overall surface of the model is smooth; the sharp edges of the grooves which circle the cylinder between the segments, however, may induce some flow separation.

The construction of the model effectively prevents transfer of fluid forces between the active and passive parts, so that only the force acting on the 2-inch section is measured by means of the cantilever-beam setup, as shown in Figure 3.4(a). The force acting on the section is transferred to the top of a 24-inch aluminum shaft at the centre of the model through two 1.25-inch diameter steel rods aligned in the direction of base motion and a 1/8-

inch thick, 6-inch diameter aluminum can encircling the shaft. As a result, the shaft acts as an end-loaded cantilever, with appropriate expressions for the calculation of the sectional force. Adjustment of the vertical elevation of the section involves removing the segments above and/or below the current level, loosening a metal ring which circles the aluminum can and to which the steel rods are attached, moving this ring and accompanying segment up or down to the next level after replacing the segments up to this new level (if necessary), tightening the metal ring, and replacing the remaining segment(s) on top of the active one.

3.2.1 Model Parameters

In the design of the model, both theoretical and physical factors had to be dealt with; that is, the cylinder had to meet the requirements imposed by the large body regime of fluid-structure behaviour as well as those presented by the instrumentation (particularly the strain gauges) mounted on key parts of the cylinder. It was relatively simple to simulate conditions for the large body regime. Difficulty was encountered when attempts were made to meet the latter criteria, namely:

(i) the central shaft (material initially unknown) had to be flexible enough so that strains could be recorded at all load levels; and
(ii) the natural frequency of the cantilever system (i.e. active part) had to be well-separated from the test frequencies or else resonant interference had to be considered and accounted for in data reduction.

Preliminary calculations to establish the upper and lower limits of the diameter and length of the central shaft utilized various concepts in structural dynamics. For the design which was finally decided upon, the fundamental natural frequency in air of the active part of the structure system was calculated to be approximately 13 Hz. Experimental estimation of this and other structural characteristics, the details of which can be found in Chapter Four, proved to be the next necessary step in providing an accurate description of the structure-fluid properties needed for subsequent dynamic analysis.

3.3 Instrumentation

A variety of sensors were mounted on the model cylinder and on the shaking table and water tank for the purpose of measuring certain response values of the model due to ground motion excitations. The final section in Chapter Two identified the amplitude of the sectional base shear V(t) and of the base acceleration a(t) and the phase shift β between these variables as the data required for evaluation of the hydrodynamic coefficients.

The absolute displacement of the table was measured by a Linear Variable Displacement Transformer (LVDT) permanently mounted inside the shaking table actuator. The LVDT was excited by a D.C. power supply having an excitation voltage of 6 volts. A Kistler accelerometer is permanently clamped to the shaking table in order to monitor the table acceleration. The analog signals from the accelerometer were fed into a servo-amplifier then to the multi-plexed Analog-Digital (A-D) converter. Because discrepancies between the input command motion and the actual recorded table motion were possible, the measured acceleration record was used in the data analysis in lieu of the known input excitation record.

Two linear potentiometers were connected to the wall of the stationary water tank, one above the other and separated by 10 inches; they were used to measure the absolute displacement of the cylinder's shaft tip and also the angle through which the shaft itself rotated, from which the fluid force acting on the section could be calculated using a different analytical procedure. Each potentiometer was excited by a D.C. power supply with an excitation voltage of 9 volts. The analog signals from the instrument were fed directly into the multi-plexed Analog-Digital converter. The relative displacement of the shaft tip with respect to its moving base (i.e. the table) could be obtained by subtraction of the digitized record of the table displacement from the corresponding potentiometer record.

In order that resonant effects could be detected and appropriately accounted for, a Stratham 20g accelerometer was mounted on the aluminum flange at the shaft tip. Any amplification in the acceleration of the shaft tip relative to the base value, presumably as a result of the active part of the cylinder approaching a resonant condition, could thus be noted and a correction be made for this anticipated effect. In addition, the natural frequency

of the cylinder was obtained through a spectral analysis of the data obtained by this accelerometer in a free vibration test.

Horizontal motion of the aluminum shaft tip induces flexure in the shaft which can be measured by strain gauges. Two sets of 350-ohm strain gauges were mounted on the aluminum shaft in Wheatstone bridge arrangements. Half bridge circuits were utilized so that only bending strains in the direction of loading were recorded. The analog signals from the gauges were fed through Daytronic amplifiers to the multi-plexed Analog-Digital converter. All strain gauges were calibrated by static load tests to.correlate a given applied load value with the voltage output from each Wheatstone bridge.

Appendix B describes in greater detail the measurement and analysis of the experimental data.

Chapter Four

EXPERIMENTAL STUDY

The purpose of the experimental study was to verify the theoretically-derived values of the sectional added mass and damping coefficients for the given model cylinder. This chapter outlines the test program which was adopted. The results which are important to this thesis are given in the following chapter, accompanied by a detailed discussion.

As was shown in Chapter Two, the fluid force can be calculated from the subtraction of the average strain in air from that in water, multiplied by the appropriate constant. Consequently, the test program could be divided into two distinct parts, each of which would include the appropriate equipment calibration and parameter estimation of the test specimen:

(1) sinusoidal excitation tests in water; and
(2) sinusoidal excitation tests in air.

Furthermore, the conditions imposed in a given combination of water and air frequency tests (e.g. base displacement) would have to be duplicated for each of the four cylinder section levels (represented by the dimensionless parameter s/d) so that the vertical distribution of the hydrodynamic coefficients could be accurately obtained.

4.1 Model Characterisitics and Damping Tests

The first step in the parameter estimation of a test structure is to measure the natural frequencies of the system. One standard method of exhibiting the frequency content of a time-history record uses the Fourier Amplitude Spectrum.

The natural frequencies of a structure are determined experimentally by first exciting the structure with harmonic base motions having frequencies which differ significantly from the calculated natural frequencies of the structure and then suddenly stopping the base excitations. At this point, the horizontal acceleration-time decay is recorded for a sufficient period of time by an accelerometer positioned at the highest point on the structure, and a standard Fast Fourier Transform program is used to convert this record into a Fourier Amplitude Spectrum. The natural frequencies of the structure correspond to the frequencies defining the maximum spectral values (the "spikes") of the Fourier Amplitude Spectrum. A typical acceleration-time decay record and Fourier Amplitude Spectrum are illustrated in Figures 4.1(a) and 4.1(b) respectively. The Fourier Amplitude Spectrum of the recorded motion is calculated using the Earthquake Laboratory software program "EDSPEC", which allows the user to plot the spectrum from formatted data files. Generated spectral values may be Hanned (Kanasewich, 1975) and can be stored in a print file for later hard copy printout.

Structural damping ratios for a single-degree-of-freedom system, ζ, may be determined experimentally by one of two methods which are based on linear system theory:

(i) Half-Power (Bandwidth) Method; and
(ii) Logarithmic Decrement Method.

The second method was utilized in this study. The structure under consideration is excited at the desired resonant frequency and, a short time later, the excitation is suddenly stopped. The acceleration-time decay is recorded from this point. If the acceleration response at time $t = t_i$ is denoted by $\ddot{x}_i$ and the response at $t = t_i + 2\pi r/\omega_d$ is denoted by $\ddot{x}_{i+r}$ where r is the cycle increment and ω_d is the damped natural frequency equal to $\omega\sqrt{1-\zeta^2}$, then it can be shown that

$$\frac{\ddot{x}_{i+r}}{\ddot{x}_i} = \exp\left[-\zeta \cdot \frac{\omega}{\omega_d} \cdot 2\pi r\right] . \qquad (4.1)$$

If $\ddot{x}_i$ corresponds to a peak point on the acceleration decay record with magnitude A_i, then $\ddot{x}_{i+r}$ corresponds to the peak point r cycles later in the acceleration-time history and its magnitude is denoted by A_{i+r}. It follows that

$$\frac{A_{i+r}}{A_i} = \exp\left[- \zeta \cdot \frac{\omega}{\omega_d} \cdot 2\pi r \right] . \tag{4.2}$$

Expanding ω_d and eliminating the exponential leads to

$$\ln\left[\frac{A_{i+r}}{A_i}\right] = - \frac{\zeta}{\sqrt{1-\zeta^2}} \cdot 2\pi r . \tag{4.3}$$

For a lightly damped system (i.e. $\zeta < 0.20$)

$$\ln\left[\frac{A_{i+r}}{A_i}\right] = - \zeta \cdot 2\pi r \tag{4.4}$$

from which

$$\zeta = \frac{1}{2\pi r} \cdot \ln\left[\frac{A_{i+r}}{A_i}\right] . \tag{4.5}$$

Figure 4.2 illustrates the application of the Logarithmic Decrement Method. The structural damping coefficient c for each test frequency is then determined from

$$c = 2m \cdot \zeta_1 \cdot \omega . \tag{4.6}$$

4.2 Sinusoidal Tests

Originally, the entire test program was to consist of four major experiments, one for each cylinder section level. For every major experiment, various frequency tests were to be conducted with the model cylinder immersed in water; these same frequency tests, namely the conditions imposed in each (e.g. base displacement), were then to be repeated for the model sitting in air. In this way, the position and alignment of the cylinder section would be identical for both the water and air tests. Therefore, for each combination of water and air tests at a given frequency, the strain data from one test may be subtracted from the other because the conditions in each situation are essentially the same. In addition, by conducting

the water tests first, one could set the table's SPAN control (hence the table displacement) such that the surface waves produced would be of sufficiently small amplitude and non-breaking, as required by potential flow theory.

Resonance and table limitations governed the selection of test frequencies used in the experimental study. From preliminary water and air free vibration tests for the top and bottom section levels, the corresponding approximate natural frequencies of the active model were determined. It was then decided to conduct tests at excitation frequencies of 1.0, 3.0, 5.0, 11.0, and 15.0 Hz, with varying displacement amplitudes for the 1.0- and 5.0-Hz frequency tests (to explore the dependence of the added mass and damping coefficients on the oscillation amplitude). However, tests carried out at 5.0 and 11.0 Hz appeared to display resonant effects. Unfortunately, owing to unforseen technical problems (which will be discussed in the succeeding chapter), additional testing could not be done at different frequencies. In the early stages as well, trial tests revealed that the potentiometers were unable to perform accurately at the higher frequencies (i.e. the wheels simply did not move); therefore, data was not acquired from these instruments in future testing.

The strain gauges were to be calibrated three times: once at the beginning of the test program; once again half-way through; and a final time at the end. This was to ensure that the correct calibration factor would be used in data formatting by the PDP-11/04 minicomputer.

Because of the unanticipated experimental-setup difficulties which had arisen over the course of the study, the adopted test program was not completely executed; testing was limited to the top two section levels, corresponding to s/d = 0.9048 (Level 1) and s/d = 0.6482 (Level 2) respectively. For each level, before a group of tests was carried out in either air or water, a free vibration test was performed. Only the shaft tip acceleration, table displacement, and table acceleration signals were recorded at this time. A free vibration test at the measured natural frequency to determine the structural damping ratio was not done because this information was not crucial to the study and speed in testing was of the essence now. For each of the tests which followed, ten seconds of steady state motion were recorded and the five channels were each monitored at a time interval of 0.01 seconds when f = 1.0, 3.0, 5.0 Hz and 0.005 seconds when f = 11.0, 15.0 Hz. After each

successful run, the acquired data from every channel were formatted and stored in files on 8.5" floppy disks. Following the final frequency test for a given medium (i.e. air, water), the formatted files were then transferred to the AST-286 microcomputer from the PDP-11/04 minicomputer.

Chapter Five

RESULTS AND DISCUSSION

Theoretical and experimental values of the added mass and damping coefficients have been generated for an isolated vertical surface-piercing circular cylinder. They are presented and discussed in this chapter.

5.1 Discussion of Theoretical Results

5.1.1 Total Hydrodynamic Force Coefficients

The dimensionless total hydrodynamic coefficients are functions of the parameter ka and the radius-to-depth ratio a/d only. They are graphically presented for a/d values of 0.5, 1.0, 1.5, 2.0, and 5.0 in Figures 5.1(a) and 5.1(b).

The velocity potential ϕ is known to be frequency-dependent, as a consequence of the free surface and radiation boundary conditions. Hence the added mass and damping are also frequency-dependent. Physically, this is associated with the generation of surface waves by the oscillating body, which is classified as a dispersive type of energy propagation. That is, the velocity of the radiating wave depends directly on the structure's oscillation frequency. It is the phase shift between the oscillation velocity of the structure and the propagation velocity of the surface waves that causes the large variation in added mass and damping at the lower frequency range. The extent of this fluctuation depends on the ratio a/d, as is clearly evident in Figures 5.1. The fluctuation becomes more pronounced as a/d becomes smaller, illustrating the importance of free surface effects for thinner but deeper structures (of the large body regime).

For all values of a/d, the dimensionless hydrodynamic damping is zero at zero frequency, attains its extreme value in the region of ka = 1.0, and then becomes less

significant as the frequency increases further.

5.1.2 Vertical Distribution of Force Coefficients

The vertical distribution of the added mass and damping coefficients of the circular cylinder as a function of excitation frequency is of particular interest. Each of Figures 5.2 to 5.4 illustrates the changing distributions of these with depth as ka increases for a given a/d value (note that the ka values correspond to f = 1.0, 3.0, 5.0, 11.0, 15.0 Hz respectively). Because the total hydrodynamic force is obtained by an integration of the sectional forces over depth, it is not surprising then that as the frequency increases the top and bottom endpoints (i.e. s/d = 1 and s/d = 0) of the vertical distribution increase and decrease in a pattern similar to that followed by their total coefficient counterpart.

The vertical distribution of the added mass coefficient for the model cylinder, as presented in Figure 5.2(a), is first examined. The added mass at s/d = 0 (i.e. the seabed) does not vary significantly and converges to a constant value when ka is greater than about 42. At the free surface, however, the variation of added mass is much more dramatic. For $ka \leq 0.16$ added mass is positive and constant with depth. At $ka \approx 0.37$ the dimensionless coefficient reaches its maximum of 4.9, after which it drops drastically in value, becoming negative at $ka \approx 2.6$ and reaching its minimum of -0.1 at $ka \approx 5.9$. From ka of 5.9 to 110, the added mass coefficient becomes larger and eventually equals zero for $ka \geq 110$. Between the free surface and seabed, the variation of the dimensionless added mass coefficient is greater in the top half than in the bottom, as should be expected considering how the top and bottom ends of the distribution fluctuate. The vertical distribution of the added mass is constant for diffraction parameter ka greater than about 110.

Finally, further examination of the figures for added mass reveals that for low values of a/d, corresponding to shallow waves, the high frequency limit of $\mu/\rho a^2$ approaches π, which corresponds to the theoretical value for two-dimensional flow. However, a somewhat surprising result is that at higher values of a/d the high frequency limit of $\mu/\rho a^2$ tends to a lower value.

Although similar, the changing vertical distribution of the damping coefficient is less considerable, as illustrated in Figure 5.2(b) for the model cylinder. Damping at the seabed

does not vary to such a degree as the damping at the free surface, not unlike the pattern followed by the added mass. When ka $\geq$ 16 damping is essentially zero at all elevations below s/d of 0.90. The distribution is constant at zero for all s/d when ka $\geq$ 147. As expected, at no point does damping take on a negative value.

Examination of Figures 5.3 and 5.4, which show the coefficients' vertical distributions for a/d of 5 and 10 respectively, reveals that the numerical values of these hydrodynamic coefficients are essentially constant with depth. Moreover, they do not fluctuate significantly but remain near zero as ka increases. This would indicate that the importance of excitation frequency to the vertical distribution of the added mass and damping coefficients diminishes for relatively larger a/d ratios, such as 5.

5.1.3 High Frequency Approximation

The asymptotic form of the theoretical solutions for the added mass and damping coefficients has also been considered in this thesis (Chapter Two). For the radius-to-depth ratio of 10, the exact and approximate solutions of the total added mass and damping coefficients are compared in Figures 5.6(a) and 5.6(b). The high-frequency approximation (i.e. large ka and kd values) for damping follows the exact solution very closely at the high end of the frequency range. In fact, this is the case for all radius-to-depth ratios. On the other hand, the high-frequency approximation for added mass is given by Equation (2.48) for all values of a/d; and may be further simplified, as in Equation (2.50) for a/d greater than about 10. [The reason for this is that the ratio of the modified Bessel function and its derivative cannot be written in its asymptotic form because, as the ratio appears in the summation in Equation (2.36a), its argument $k_n a$ is not large for small values of n.] The appeal of the latter equation is of course its simplicity. Figure 5.5 compares the high-frequency added mass coefficient given by either equation, illustrating the point beyond which either approximation equation may be used, namely a/d $\approx$ 10 if a 3 percent error in the added mass value is acceptable.

The question is now posed: for what values of the depth parameter kd can the high-frequency approximations be used? The high-frequency approximation for the damping coefficient of a vertical circular cylinder, as given by Equation (2.44), can be used when kd is greater than or equal to about 5. This is valid for all a/d ratios. Equation (2.48) can be

used to predict the added mass coefficient of a vertical circular cylinder when kd is greater than about 967 and the radius-to-depth ratio is arbitrary. This unique value of kd corresponds to the point at which the added mass coefficient achieves a constant value or, in other words, becomes independent of ka.

Although it was not addressed in Chapter Two, the low-frequency approximation of the theoretical formulation for the added mass and damping coefficients can be shown to correspond to the expected theoretical two-dimensional results. Specifically, for small ka and kd, Equation (2.36a) reduces to the following:

$$\Omega' = \frac{1}{(ka)^2} \cdot (-ka) \cdot (kd) \ . \tag{5.1}$$

The summation which appears in the original equation does not enter the expression above because $\sin(k_n d)$ is zero for $k_n d = n\pi$. Moreover, the hyperbolic functions tend to kd for small kd, and the ratio of the Hankel function to its derivative approaches (-ka) for small ka. Consequently, the low-frequency approximations for the hydrodynamic coefficients are given as

$$\frac{\mu}{\rho a^3} \approx \pi \left[\frac{d}{a}\right] \tag{5.2}$$

and

$$\frac{\lambda}{\rho a^3 \omega} \approx 0 \ . \tag{5.3}$$

5.2 Discussion of Experimental Results

5.2.1 Present Study

It was noted in the previous chapter that unforseen problems with the testing facility and instrumentation forced the test program to a premature conclusion. Testing was completed for only the top two section levels, corresponding to s/d = 0.9048 (Level 1) and s/d = 0.6482 (Level 2) respectively. An analysis of the data acquired for these levels produced the results in Tables 5.1 and 5.2. An initial comparison of these values for added mass and

damping with those that were derived theoretically for the same physical conditions indicates that the experimental results are unrealistic; therefore, an attempt at any further comparison is futile.

Nevertheless, the results determined from tests run at 1.0 Hz for both section levels seem to show that added mass is independent of base displacement amplitude (as required by potential flow theory); that is, viscous effects did not influence the magnitude of the experimental data. Furthermore, one can also speculate on the reasons why the results for Level 1 appear to be much worse than those for Level 2. It is known that non-linearity of damping has a greater effect near or at the free surface and the significance of this effect decreases with depth. The theoretical formulation assumes linear theory. Perhaps if second-order terms are considered, the experimental results would appear more reasonable. Further examination of the available data, namely the amplitude values of the strain, base acceleration, and shaft tip acceleration signals, revealed that the model may have approached a resonant condition near the frequency of 5.0 Hz in water and 11.0 Hz in air. Modification of the acceleration to account for resonance and subsequent recalculation of the coefficients are not attempted; it seems pointless to try to improve the experimental results when no top strain data had entered the analysis in the first place, as described later.

It is believed that the large discrepancies between the theoretical and experimental values of added mass and damping can be attributed primarily to faulty instrumentation and model construction. An attempt will be made to explain the reasons why the study was unsuccessful and why the results cannot be relied upon as being accurate.

When the actual test program was conducted, following a series of trial water and air tests, reasonable data could not be obtained from the top strain gauges. Nevertheless, the final data analysis was done in spite of this lack of crucial information. It was hoped that the strain signal at the top of the aluminum shaft would be close to zero, as seemed apparent during early testing and analysis, and therefore have a negligible effect in calculations of the force coefficients (the details for which are given in Appendix B). In the initial stages of instrumentation preparation for data acquisition, particularly during calibration, it became evident that the strain gauge Daytronic amplifiers which were available for use in this study performed at an unacceptable level. Because the measured strains, as well as the difference between successive values in a signal, were expected to be small, it was especially

important that the minute changes in strain could be accurately measured and recorded. It was observed, however, that when a load was applied the output voltages which were recorded by both the top and bottom strain gauges did not remain constant, but rather they fluctuated to such an extent as to make accurate readings difficult. Calibration tests were repeated so that reasonably representative calibration factors could be obtained and used with some degree of confidence.

The situation concerning the strain gauges and amplifiers seemed to get worse, particularly when the cylinder itself leaked. As previously mentioned, trial experiments were conducted in air and water for the purpose of testing the adequacy of the facility and of becoming familiar with the testing procedure as defined by the data acquisition system. During the one and only trial water test, the model cylinder had developed a slow leak which had gone undetected until the next day, although the status of the top quarter of the model interior had been periodically monitored (the model did not accommodate full interior visual inspection). As a result, the strain gauges, which were not specially prepared for such a situation, were submerged in water for several hours as the tank was slowly draining. It was immediately believed that the gauges were irreparably damaged. But a frequency test demonstrated that they were still functioning, if not accurately. A noticeable period of time had passed before the section seal could be replaced with an alternate special-order material and its ability to keep the model dry inside checked. Recalibration of the strain gauges indicated that they had "degenerated". Although the voltage output from the bottom gauges was reasonably consistent in its response to the change in applied load, the new slope of the calibration curve was dramatically different from ones originally obtained. Moreover, calibration of the top strain gauges was impossible; their signal was erratic and could not be balanced. Because time was now so limited at this stage of the experimental study, instrumenting the aluminum shaft with new gauges and locating amplifiers which worked properly were inconceivable remedies.

Just before the water tests of the second major experiment (for Level 2) began, the tank itself developed a very bad leak, the only solution for which would have been to replace the pool liner. Again, the lack of time did not permit this. Instead, tests were hastily done and the water depth regularly monitored and adjusted. The opportunity to investigate the behaviour of the section at the other two levels to sinusoidal excitation no longer existed.

In addition to the problems encountered in data acquisition, it is quite probable that the physical model itself contributed to the overall failure of the experimental investigation. Although the model cylinder was designed such that only the fluid force acting on the 2-inch section is measured, it is possible that forces outside the section had also been transferred to the aluminum shaft. Furthermore, the original model design specifications required that the sealing material cover the gaps between the active section and the adjacent segments around the inner cylinder circumference. However, for ease of construction, the latex seal had to be wrapped around the cylinder on the outer surface. Undoubtedly, concerns arose with respect to flow separation caused by the O-rings holding the material in place and to the slight bulkiness of the material possibly interfering with the free movement of the section. Finally, the holes in the 3/8-inch PVC tube through which the steel rods passed may not have been big enough; the rods might have rubbed against the surrounding PVC tube. Another point which should be mentioned is that the flexibility of the model may have contributed to the erroneous results, particularly at the higher frequencies when the aluminum shaft may have taken on a rocking mode of motion rather than a pure translational one. To account for this, one can assume first mode of vibration and take some sort of average of the accelerations at all points on the shaft, using this numerical value in the analysis for the hydrodynamic coefficients.

5.2.2 Comparison with Other Experimental Results

Certainly, the current experimental study was not successful in fulfilling one of the objectives of this thesis, specifically the verification of the theoretically-derived vertical distribution of the added mass and damping coefficients for a vertical surface-piercing circular cylinder. Despite this misfortune, however, the applicability of the theory for prediction of total hydrodynamic coefficients for the same structure configuration undergoing horizontal sinusoidal excitation at frequencies ranging from 0.5 to 6.0 Hz has been confirmed. Table 5.3 presents the results obtained by the current theoretical formulation and those acquired experimentally by Pegg (1983) for a model cylinder of height 22 inches and diameter 11 inches in water of depth 21 inches, a value which could only be assumed because Pegg did not specify the actual number he had used in his calculations. For a complete discussion of Pegg's experimental investigation, the reader is referred to Pegg (1983). The theoretical and experimental results for the dimensionless added mass and damping coefficients are graphically compared in Figures 5.7.

The results derived from the present theoretical formulation agree very well with those obtained experimentally by Pegg. Further examination of both sets of results indicates that the present theory tends to slightly overestimate the added mass coefficient where the dependence on frequency is strongest, yet underestimate to some extent the damping coefficient, particularly in the peak region. Nevertheless, in all practicality, the validity of the current theoretical formulation for total hydrodynamic coefficients is confirmed.

Chapter Six

CONCLUSIONS AND RECOMMENDATIONS

Because frequencies encountered in earthquake excitation correspond to rather large values of the diffraction parameter ka in the case of large structures, standard numerical techniques may be inefficient in predicting the high-frequency fluid loading. As a result, an alternate method which includes the free surface and seabed effects on the hydrodynamic force and is valid for arbitrary values of excitation frequency is necessary.

The theoretical formulation of the added mass and damping coefficients acting on an isolated vertical surface-piercing rigid circular cylinder which is excited in initially still water by horizontal sinusoidal ground motions has been developed. The vertical distribution of the coefficients is also considered. The total hydrodynamic force coefficients are functions of the parameter ka and the ratio a/d only; the vertical distribution of either coefficient is a function of s/d, a/d, and ka but is notably less dependent on ka as a/d becomes substantially large. A somewhat surprising result is that the high-frequency limit of the added mass coefficient near the seabed tends to a low value (near zero) for large a/d, yet approaches the expected two-dimensional value of π when a/d is small.

The frequency dependence of added mass and damping is significant in the low frequency range and can be attributed to the generation of surface waves by the moving structure.

The high-frequency approximation of the theoretical solution is found to be accurate in predicting the damping coefficient [i.e. Equation (2.44)] for all structure radius-to-water depth ratios a/d for kd greater than about 5. The added mass high-frequency approximation which utilizes the asymptotic form of the modified Bessel function [i.e. Equation (2.50)] converges to the exact solution only when a/d is greater than about 10. An alternate high-frequency approximation which does not use this asymptotic expression [i.e. Equation

(2.48)] can be used without any restriction on a/d and is entirely valid for kd greater than about 967.

With the purpose of verifying the theoretically-derived vertical distribution of the hydrodynamic coefficients for a model cylinder satisfying the large body regime of fluid-structure behaviour, an experimental study was attempted. Unanticipated technical problems caused the test program to terminate prematurely and the experimental results to appear unrealistic.

Although the theory's applicability in predicting the vertical distribution could not be validated, comparisons between total hydrodynamic coefficients derived theoretically and those obtained in a previous experimental investigation for the same structure configuration and fluid assumptions were excellent, confirming that the theoretical solution can be used with confidence to predict the total added mass and damping of a large surface-piercing circular cylinder subjected to sinusoidal excitation of arbitrary frequency.

Recommendations for further study include the following:

— Experimental verification of numerical predictions of total high-frequency hydrodynamic force coefficients of large bodies of arbitrary geometry

— Experimental verification of the theoretically-derived vertical distribution of the coefficients for a vertical circular cylinder and other large bodies of arbitrary configuration, with particular attention paid to the behaviour of the added mass near the seabed

BIBLIOGRAPHY

Ansari, G.R. (1983), "A Laboratory Study of Submerged Multi-Body Systems in Earthquakes", *Earthquake Engineering Research Center Report*, No. UCB/EERC-78/08, University of California, Berkeley, CA.

Bai, K.J. (1975), "Diffraction of Oblique Waves by an Infinite Cylinder", *Jour. Fluid Mech.*, Vol. 68, Part 3, pp. 513-535.

Black, J.L., Mei, C.C., and Bray, M.C.G. (1971), "Radiation and Scattering of Water Waves by Rigid Bodies", *Jour. Fluid Mech.*, Vol. 46, Part 1, pp. 151-164.

Bowes, W.H., Russell, L.T., and Suter, G.T. (1984), *Mechanics of Engineering Materials*, John Wiley & Sons, New York.

Byrd, R. (1978), "A Study of the Fluid Structure Interaction of Submerged Tanks and Caissons in Earthquakes", *Earthquake Engineering Research Center Report,* No. UCB/EERC-78/08, University of California, Berkeley, CA.

Chakrabarti, S.K. (1979), "Wave Interaction with Multiple Horizontal Cylinders", *Applied Ocean Research* , Vol. 1, No. 4, pp. 213-216.

Chakrabarti, S.K. (1981), "Hydrodynamic Coefficients for a Vertical Tube in an Array", *Applied Ocean Research* , Vol. 3, No. 1, pp. 2-12.

Chakrabarti, S.K. (1987), *Hydrodynamics of Offshore Structures*, Springer-Verlag, Berlin.

Clough, R.W. (1970), "Effects of Earthquakes on Underwater Structures", *Proc. 2nd World Conf. on Earthquake Engineering* , Roorkee, India, pp. 161-171.

Clough, R.W. and Penzien, J. (1975), *Dynamics of Structures* , McGraw-Hill Inc., New York.

Cornett, A.M. (1987), "Short-Crested Wave Forces on a Rigid Segmented Vertical Cylinder", M.A.Sc. Thesis, University of British Columbia, Vancouver, Canada.

Dong, R.G. (1978), "Effective Mass and Damping of Submerged Structures", Report No. UCRL-52342, *U.S. Department of Commerce, Lawrence Livermore Laboratory*, Livermore, California.

Eatock-Taylor, R. and Waite, J.B. (1978), "The Dynamics of Offshore Structures Evaluated by Boundary Integral Technique", *Jour. Numerical Methods in Engineering*, Vol. 13, No. 2.

Eatock-Taylor, R. and Duncan, P.E. (1980), "Fluid-induced Inertia and Damping in Vibrating Offshore Structures", *Applied Ocean Research*, Vol. 2, No. 1, pp. 2-12.

Ewins, D.J. (1984), *Modal Testing* , John Wiley & Sons, Inc., New York.

Filiatrault, A. (1985), "Performance Evaluation of Friction Damped Braced Steel Frames Under Simulated Earthquake Loads", M.A.Sc. Thesis, University of British Columbia, Vancouver, Canada.

Garrett, C.J.R. (1971), "Wave Forces on a Circular Dock", *Jour. Fluid Mech.*, Vol. 46, Part 1, pp. 129-139.

Garrison, C.J. (1978), "Hydrodynamic Loading of Large Offshore Structures: Three Dimensional Source Distribution Methods", *Numerical Methods in Offshore Engineering*, (Ed. O.C. Zienkiewicz, R.W. Lewis, K.G. Stagg) John Wiley & Sons, Inc., New York, pp. 87-140.

Garrison, C.J. (1980), "A Review of Drag and Inertia Forces on Circular Cylinders", *Proc. Offshore Tech. Conf.*, Houston, Paper No. OTC 3760, pp. 205-212.

Garrison, C.J. and Berklite, Ronald B. (1973), "Impulsive Hydrodynamics of Submerged Rigid Bodies", *Jour. Eng. Mech.*, ASCE, Vol. 99, No. EM1, pp. 99-120.

Haskind, M.D. (1957), "The Exciting Forces and Wetting of Ships in Waves", *Izvestia Akademii Nauk S.S.S.R., Otdelenie Technicheskikh Nauk*, No. 7, pp. 65-79 (*David Taylor Model Basin Translation*, No. 307, 1962).

Havelock, T.H. (1929), "Forced Surface-Waves on Water", *Philosophical Magazine*, Series 7, Vol. 8, No. 51, pp. 569-576.

Havelock, T.H. (1940), "The Pressure of Water Waves Upon A Fixed Obstacle", *Proc. Royal Soc.*, London, Ser. A, Vol. 963, pp. 175-190.

Hogben, N. (1974), "Fluid Loading on Offshore Structures, A State-of-the-Art Appraisal: Wave Loads", *Maritime Tech. Monograph*, No. 1, RINA.

Isaacson, M. (1978), "Vertical Cylinders of Arbitrary Section in Waves", *Jour. Waterway, Port , Coastal , and Ocean Div.*, ASCE, Vol. 104, No. WW4, pp. 309-324.

Iverson, H.W. and Balent, R. (1951), "A Correlating Modulus for Fluid Resistance in Accelerated Motion", *Jour. of Applied Physics*, Vol. 22, pp. 324-328.

John, F. (1950), "On the Motion of Floating Bodies, II", *Committee on Pure and Applied Math.*, Vol. 3, pp. 45-101.

Kanasewich, E.R. (1975), *Time Sequence Analysis in Geophysics*, The University of Alberta Press, Calgary, Canada.

Keulegan, G.H. and Carpenter, L.H. (1958), "Forces on Cylinders and Plates in an Oscillatory Fluid", *Journal of Research of the National Bureau of Standards*, Vol. 60, No. 5, pp. 423-440.

Kioka, W. (1980), "A Green-Function Method for Wave Interaction with a Submerged Body", *Earthquake Engineering Research Center Report*, No. UCB/EERC-80/11, University of California, Berkeley, CA.

Kochin, N.E. *et al* . (1964), *Theoretical Hydrodynamics*, English Translation of 5th Russian ed., John Wiley & Sons, Inc., New York.

Lamb, H., (1945), *Hydrodynamics*, 6th ed., Dover, New York; also Cambridge University Press, 1932.

Levinson, N. *et al*.. (1949), "Separation of Laplace's Equation", *Quarterly of Applied Math*., Vol. VII, No. 3.

Liaw, C.Y. and Chopra, A.K. (1973), "Dynamics of Towers surrounded by Water", *Earthquake Engineering Research Center Report*, No. UCB/EERC-73/25, University of California, Berkeley, CA.

Lou, Y.K. (1973), "Perturbation Method for Low-Frequency Fluid-Structure Interaction Problems", *Jour. Applied Mech* ., ASME, Vol. 40, pp. 388-394.

Luneau, J. (1949), "Sur l'effet d'inerti des sillages de disque circulaires se deplacant dans l'eau d'un mouvement uniformement accelere", *Comptes rendus de l'academic des Sciences*, Paris, Vol. 229, pp. 927-928.

MacCamy, R.C. and Fuchs, R.A. (1954), "Wave Forces on Piles: A Diffraction Theory", U.S. Army Corps of Engineers, *Beach Erosion Board, Corps of Engineers*, Tech. Memo No. 69.

McConnell, K.G. and Young, D.F. (1965), "Added Mass of a Sphere in a Bounded Viscous Fluid", *Jour. of Engineering Mechanics Div*., ASCE, Vol. 91, No. EM4, pp. 147-163.

Murphy, J.E. (1978), "Integral Equation Failure in Wave Calculations", *Jour. Waterway Port Coastal and Ocean Div*., ASCE, Vol. 104, No. WW4, pp. 330-334.

Newman, J.N. (1962), "The Exciting Forces on Fixed Bodies in Waves", *Jour. of Ship Research*, Vol. 6, No. 3, pp. 10-17.

Newman, J.N. (1977), *Marine Hydrodynamics*, MIT Press, Cambridge, Mass.

Nilrat, F. (1980), "Hydrodynamic Pressure and Added Mass for Axisymmetric Bodies", *Earthquake Engineering Research Center Report,* No. UCB/EERC-80/12, University of California, Berkeley, CA.

Pegg, N.G. (1983), "An Experimental Study of the Seismic Forces on Submerged Structures", M.A.Sc. Thesis, University of British Columbia, Vancouver, Canada.

Penzien, J. and Kaul, M. (1972), "Response of Ofshore Towers to Strong Motion Earthquakes", *Earthquake Engineering and Structural Dynamics*, Vol. 1, pp. 55-68.

Potash, R.L. (1971), "Second-Order Theory of Oscillating Cylinders", *Jour. of Ship Research*, Vol. 15, No. 4, pp. 295-324.

Raman, H. *et al.* (1977), "Nonlinear Wave Interaction with Vertical Cylinder of Large Diameter", *Jour. of Ship Research*, Vol. 21, No. 2, pp. 120-124.

Ruhl, J.A. and Berdahl, R.M. (1979), "Forced Vibration Tests of a Deepwater Platform", *Proc. Offshore Tech. Conf.*, Houston, Paper No. OTC 3514, pp. 1341-1354.

Sarpkaya, T. and Isaacson, M. (1981), *Mechanics of Wave Forces on Offshore Structures*, Van Nostrand Reinhold Co., New York.

Stelson, T.E. and Mavis, F.T. (1955), "Virtual Mass and Acceleration in Fluids", *ASCE* , Vol. 81, No. 670, pp. 1-9.

Tanaka, Y. and Hudspeth, R.T. (1986), "Earthquake Response of Circular Cylindrical Structures in Water", *OMAE*, Tokyo, pp. 655-662.

Titchmarsh, E.C. (1946), *Eigenfunction Expansion* , The Clarendon Press, Oxford.

Tung, Chi C. (1979), "Hydrodynamic Forces on Submerged Vertical Circular Cylindrical Tanks under Ground Excitation", *Applied Ocean Research*, Vol. 1, No. 2, pp. 75-78.

Vernon, T.A. (1984), "Response of a Flexible Marine Column to Base Excitation", M.A.Sc. Thesis, University of British Columbia, Vancouver, Canada.

Wehausen, J.V. and Laitone, E.V. (1960), "Surface Waves", *Handbuch der Physik,* (ed. S. Flugge) Springer-Verlag, Berlin, Vol. IX, pp. 446-778.

Yeung, R.W. (1981), "Added Mass and Damping of a Vertical Cylinder in Finite-depth Waters", *Applied Ocean Research*, Vol. 3, No. 3, pp. 119-133.

FIGURES

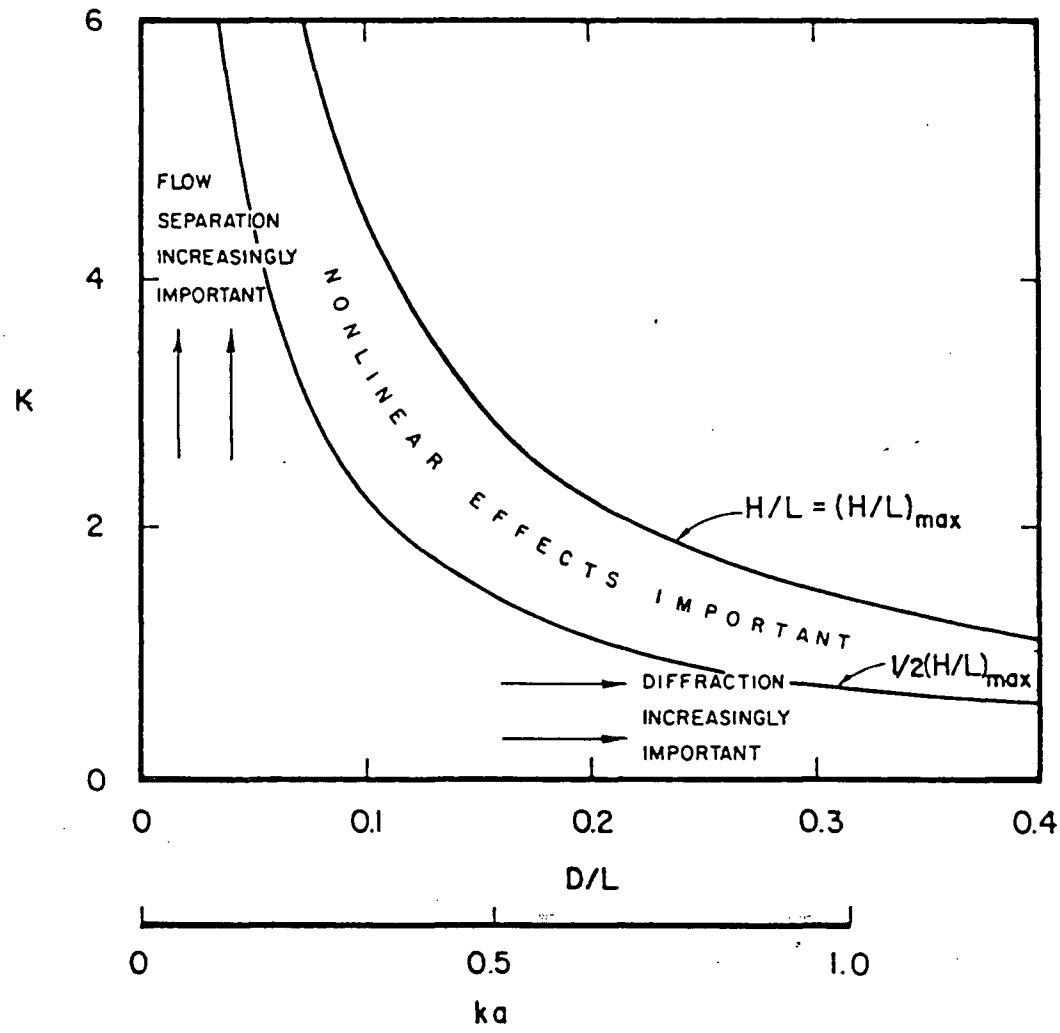

Figure 1.1 Regions of Validity for Wave Interaction with Pile (taken from Sarpkaya and Isaacson, 1981)

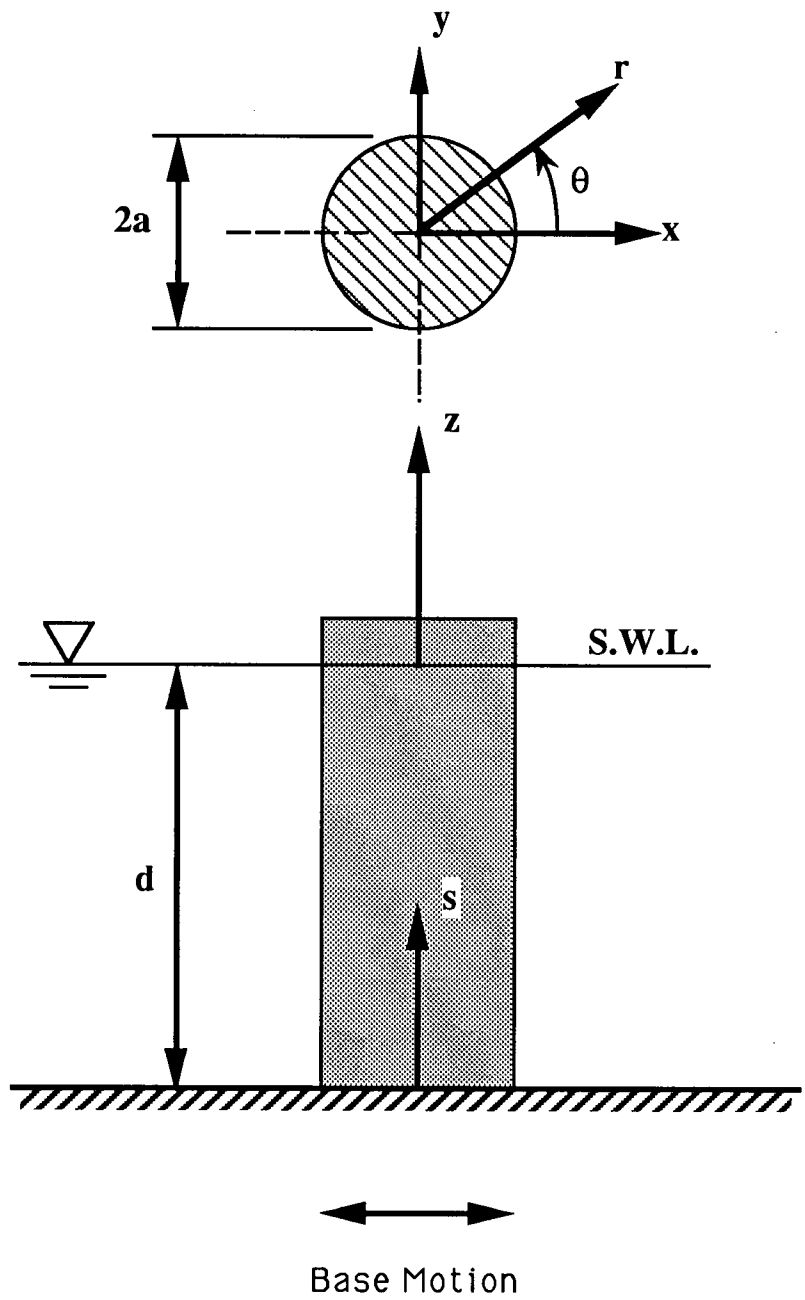

Figure 2.1 Definition Sketch for a Circular Cylinder subjected to Horizontal Unidirectional Ground Motion

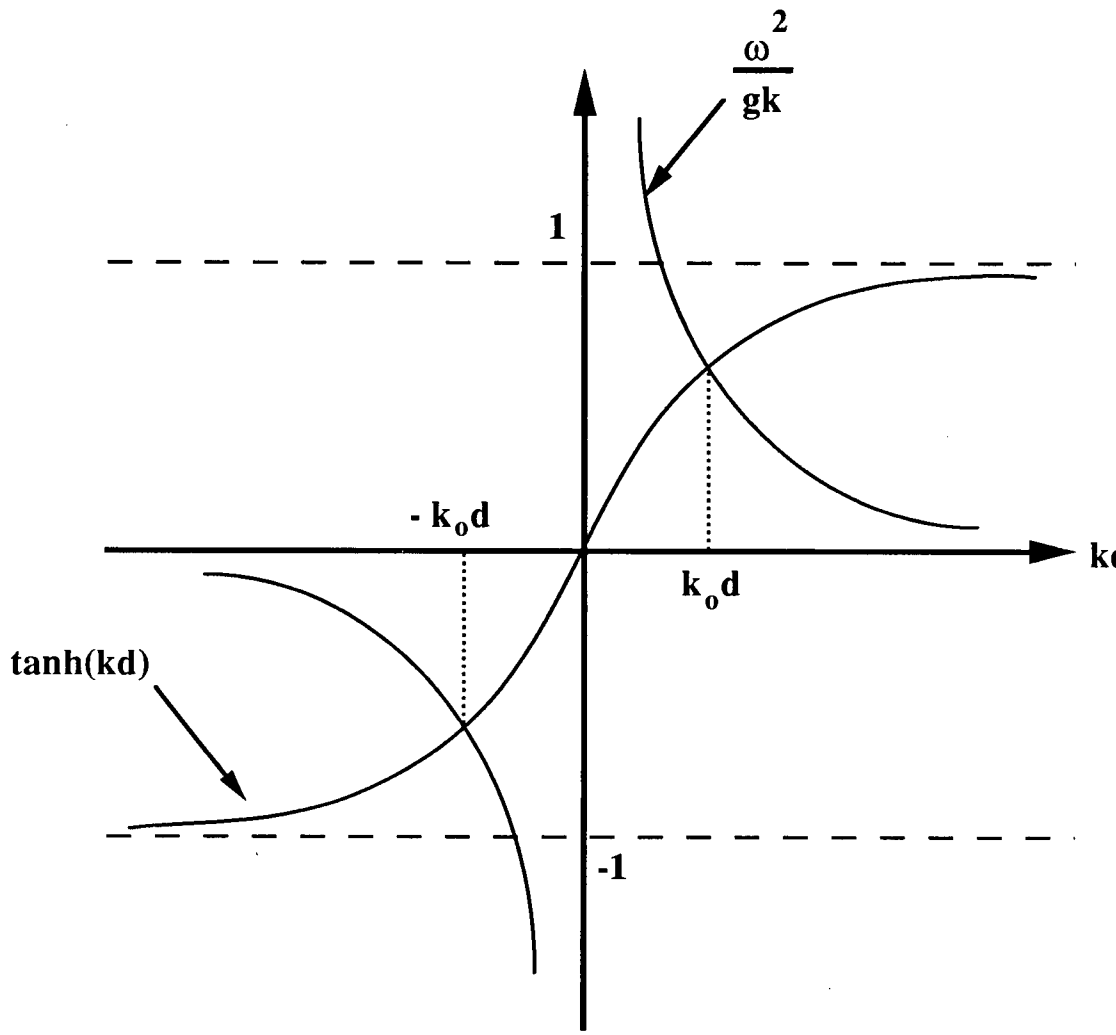

Figure 2.2 Graphical Solution of Dispersion Relation

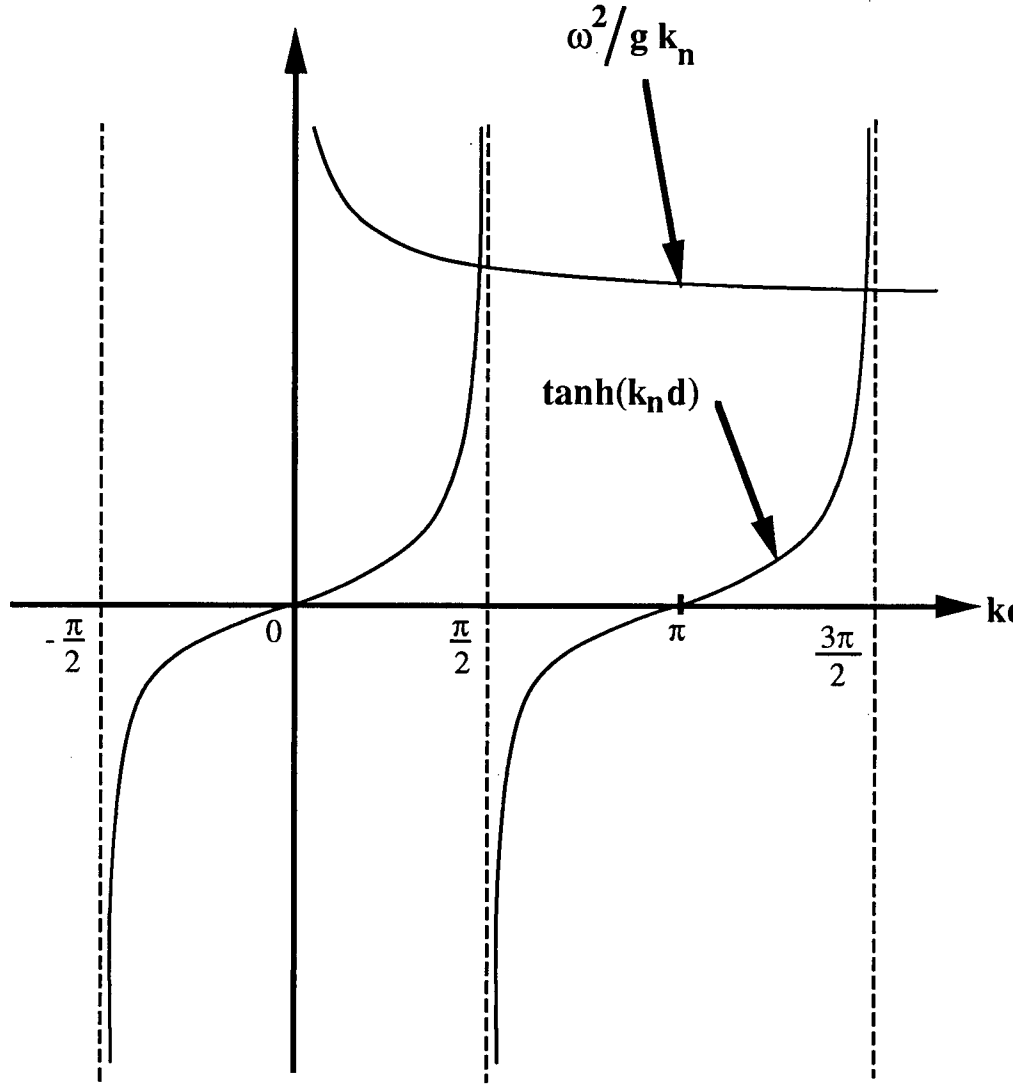

Figure 2.3 Graphical Solution of $\tan(k_n d) = \omega^2 / k_n d$

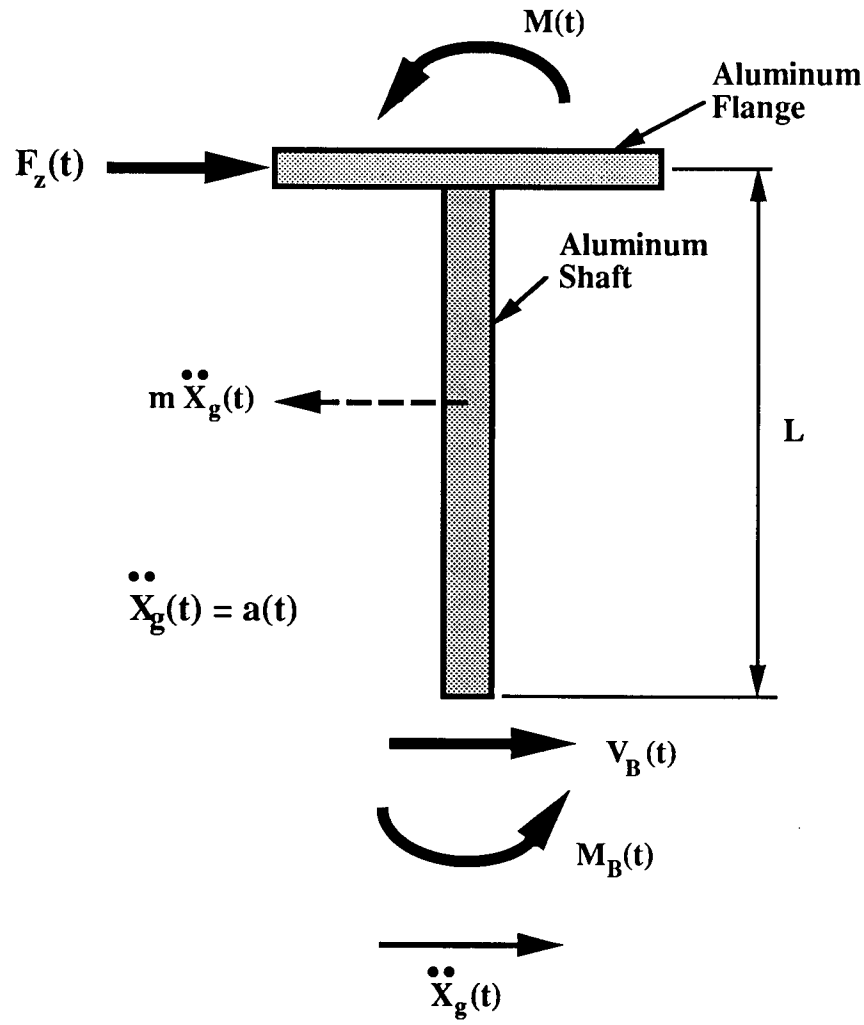

Figure 2.4 Free Body Diagram of Forces Acting on the Model Cylinder Section

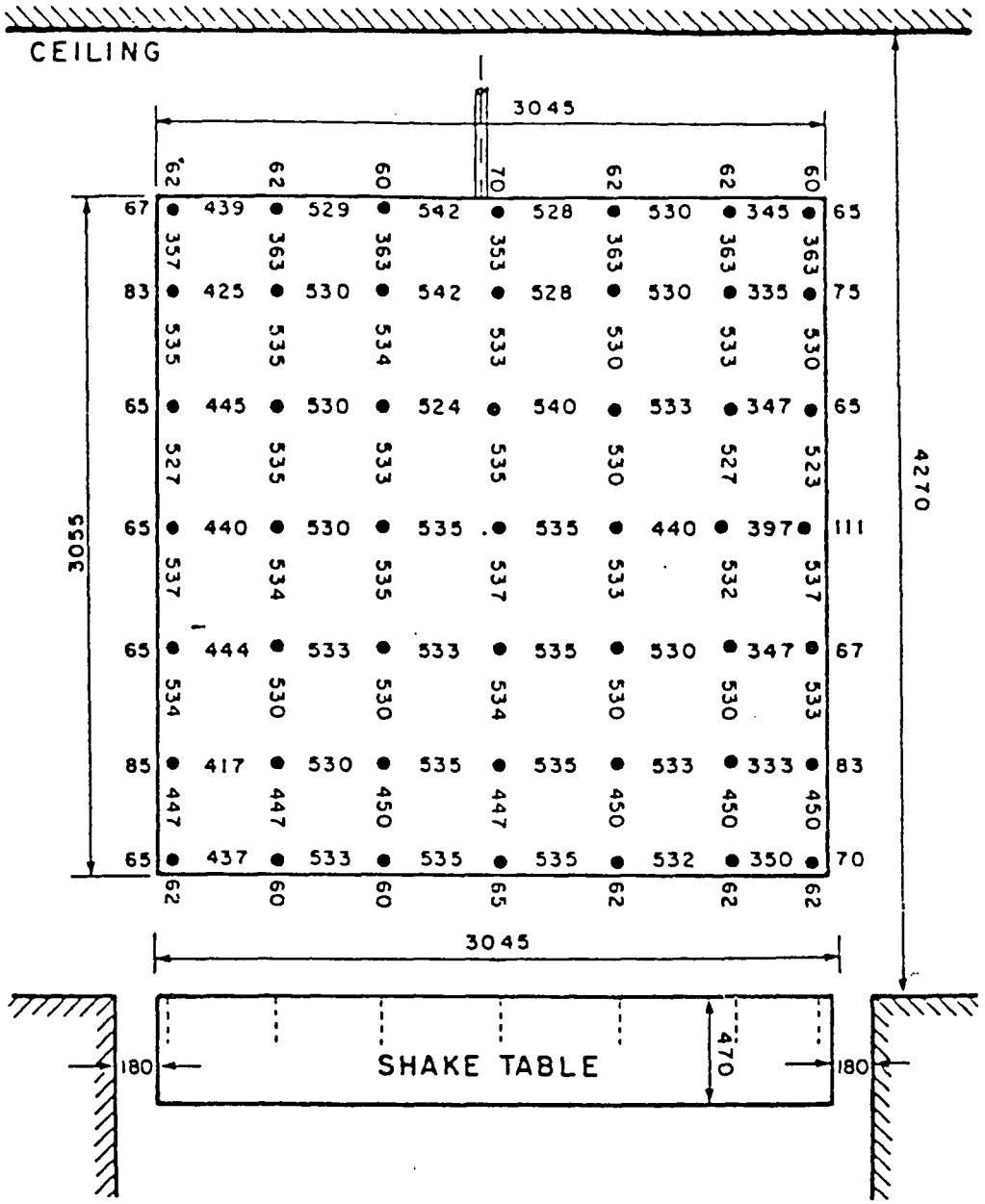

NOTE :

ALL MEASUREMENTS ARE IN mm

Figure 3.1 General Arrangement of Earthquake Simulator Table (taken from Filiatrault, 1985)

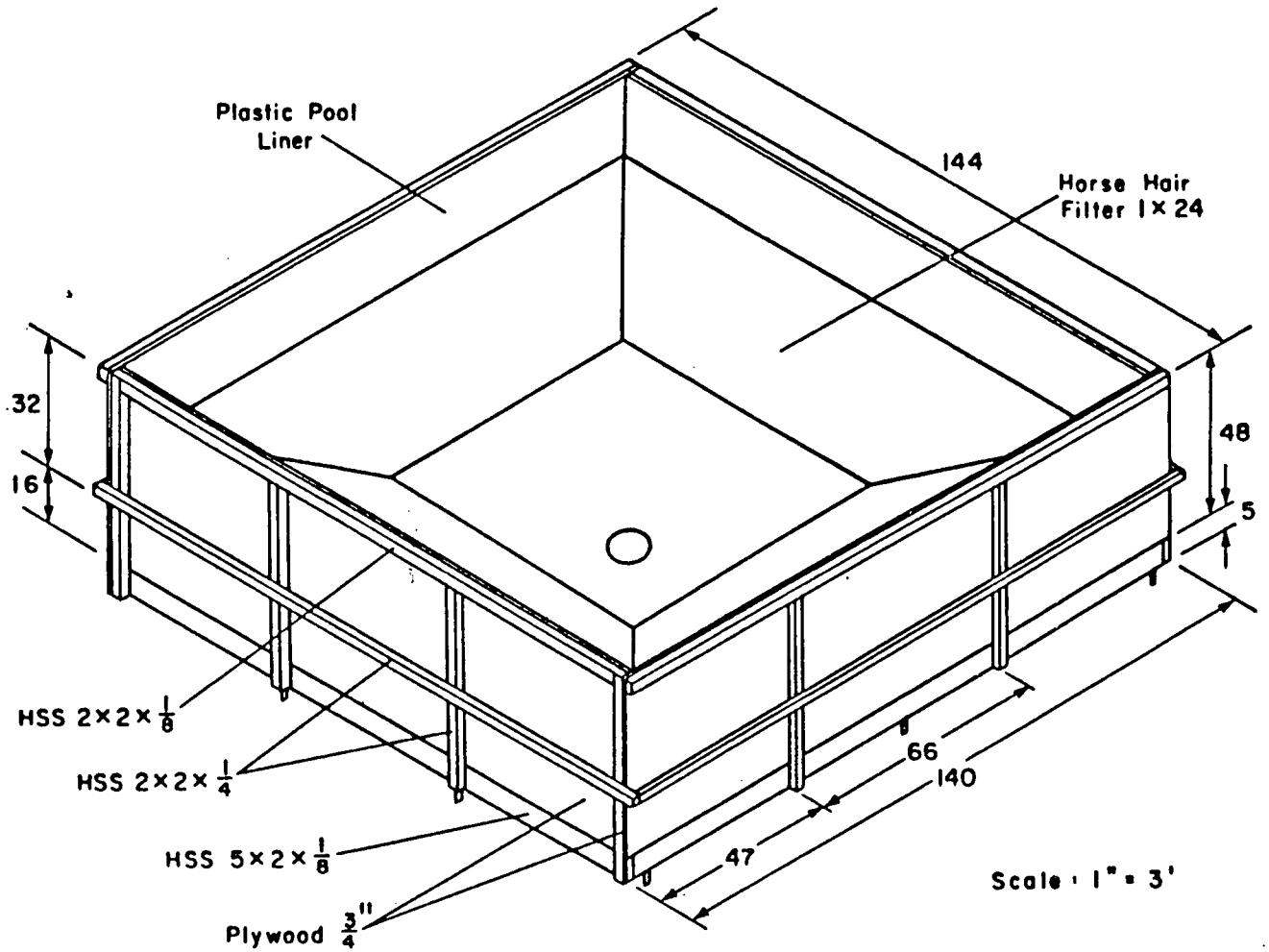

Figure 3.2 Schematic of Water Tank
(taken from Pegg, 1983)

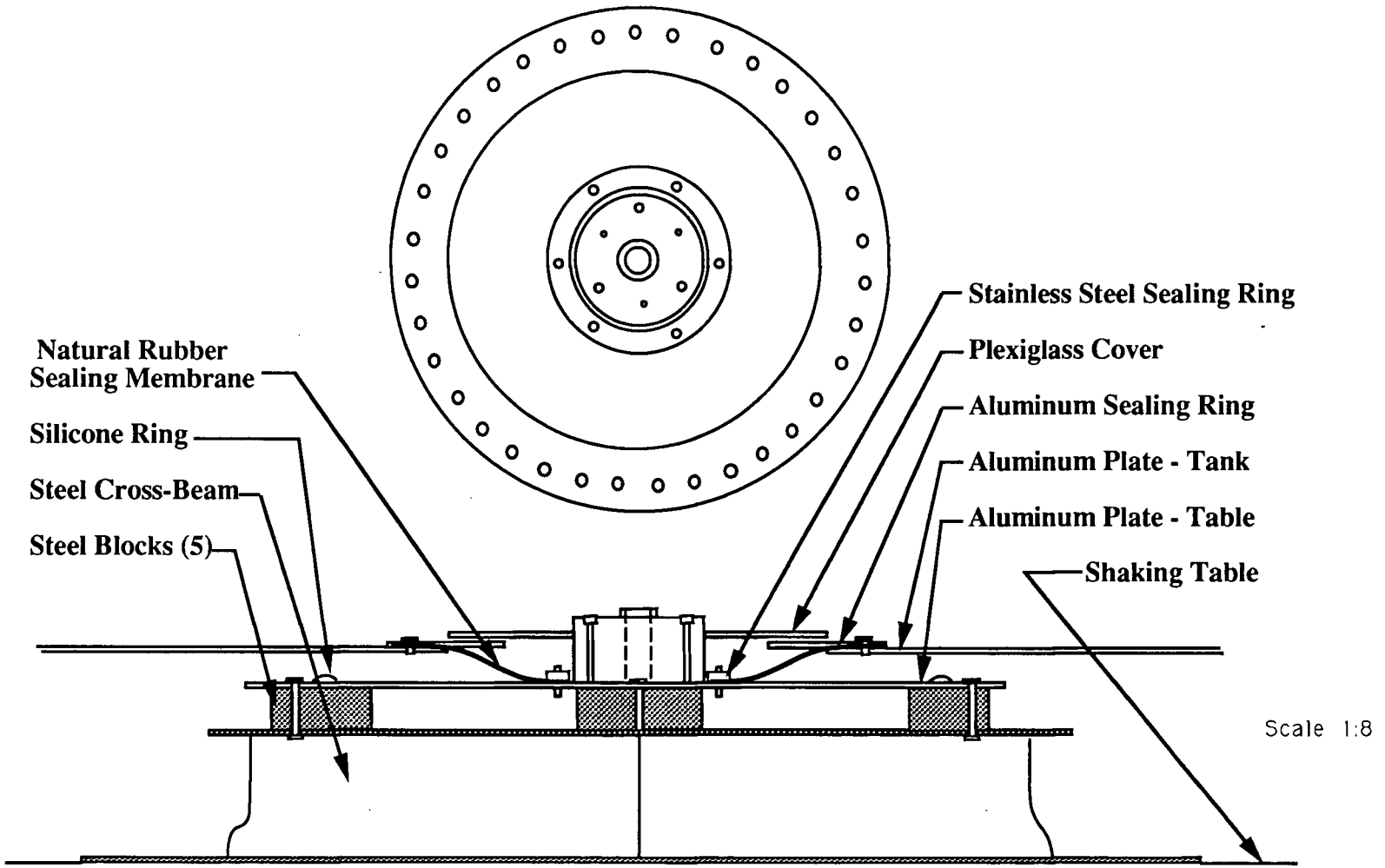

Figure 3.3 Schematic of Base Support and Seal

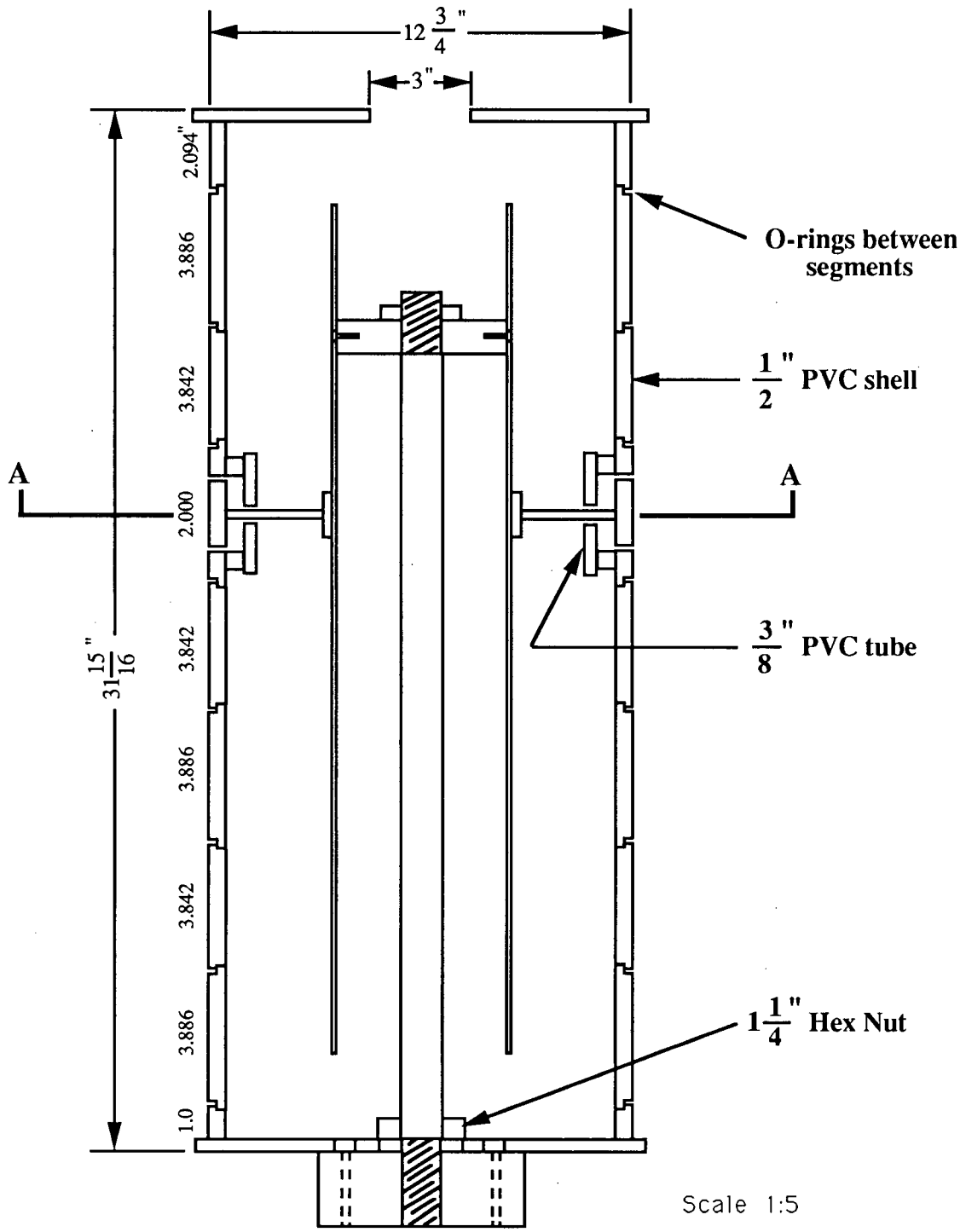

Figure 3.4(a) Vertical Section of Model showing Active and Passive Components

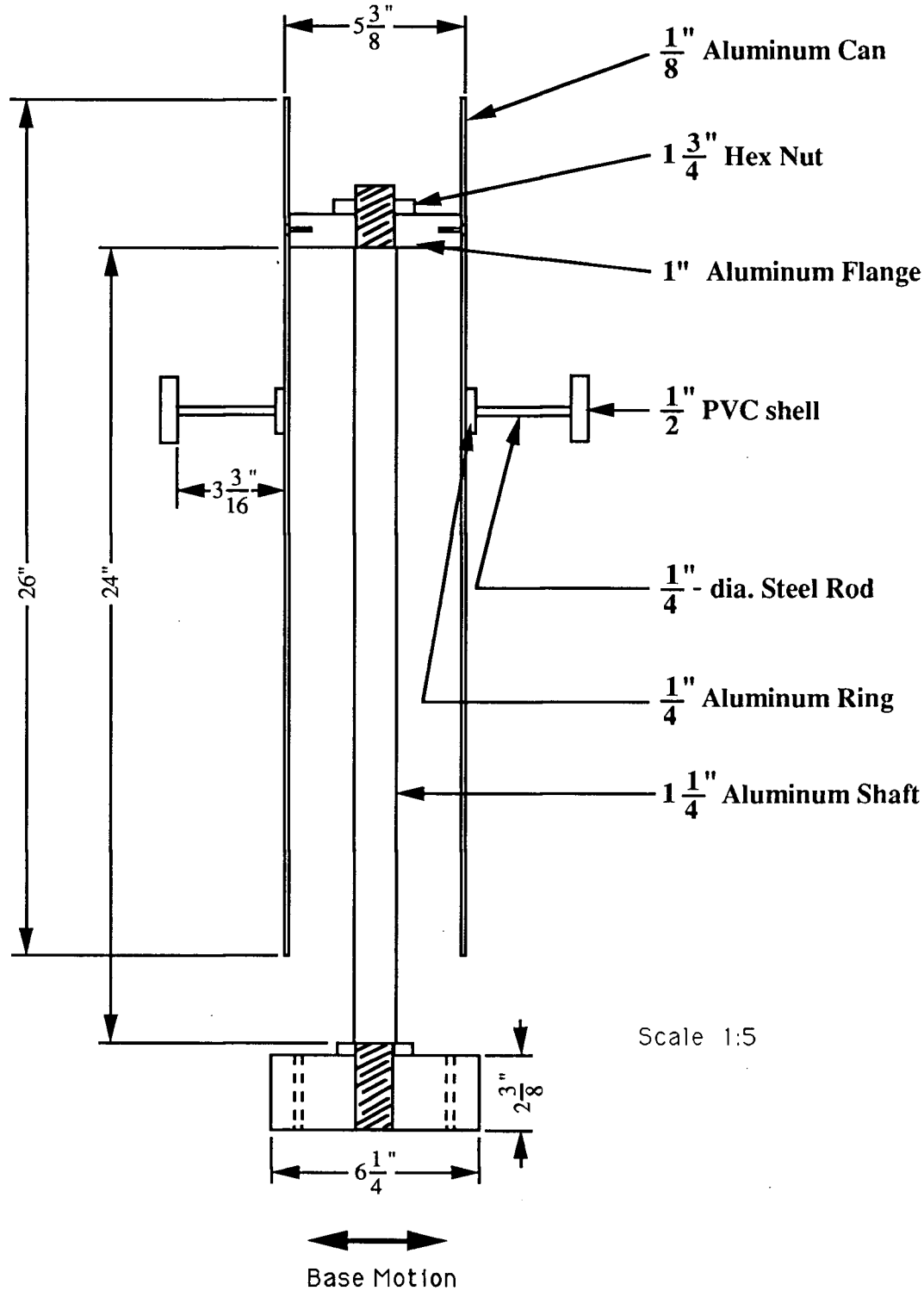

Figure 3.4(b) Details of Active Component of Model Design

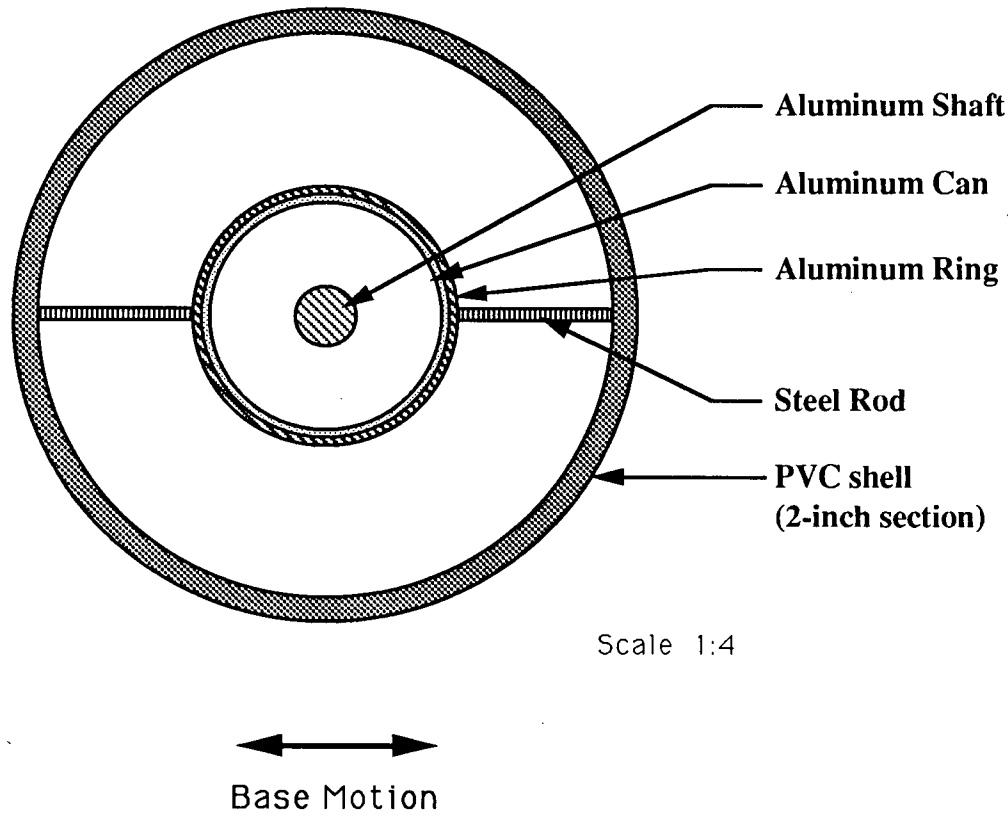

Figure 3.5 Horizontal Cross-Section A/A of Model

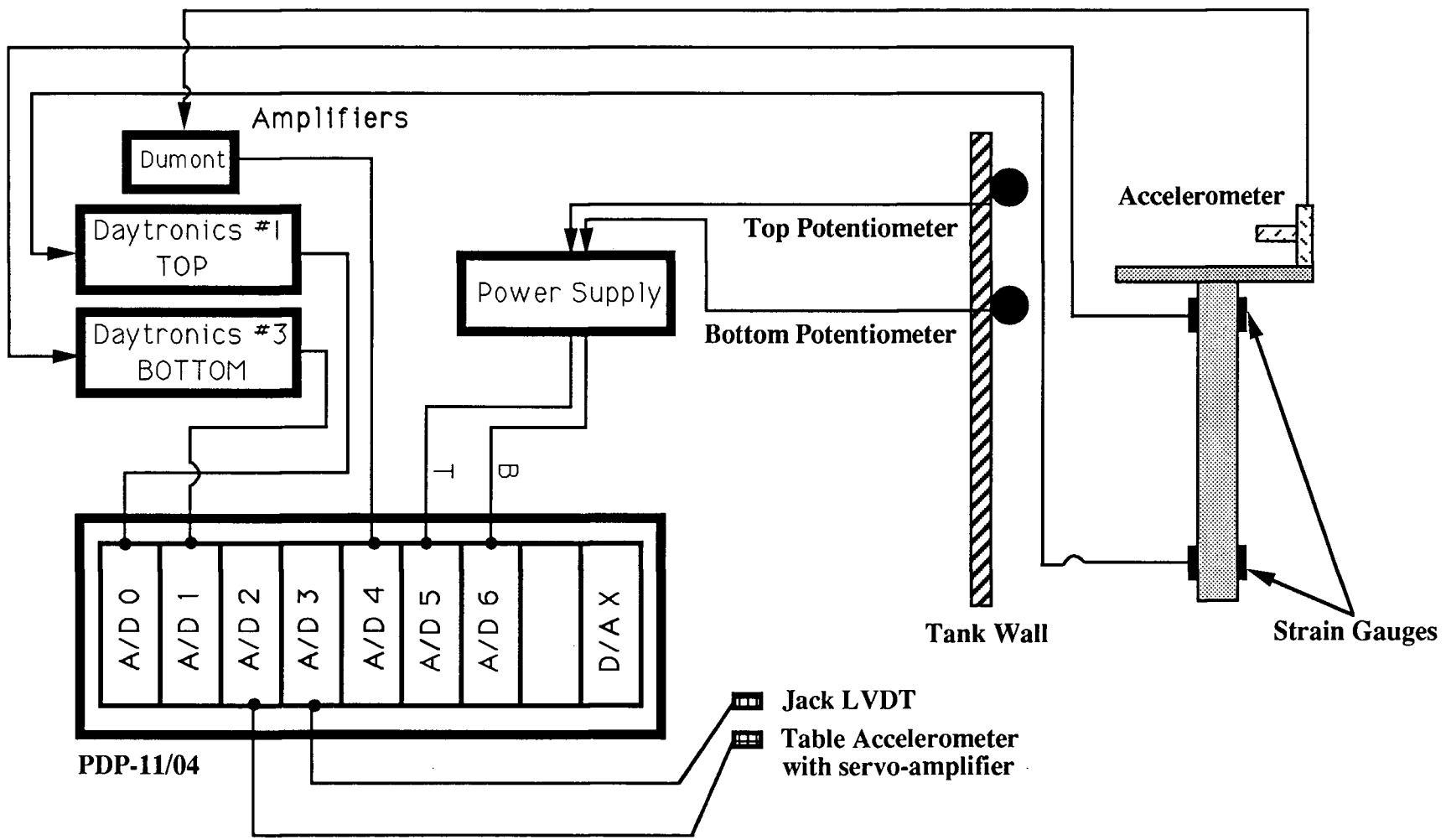

Figure 3.6 Schematic of Instrumentation Layout

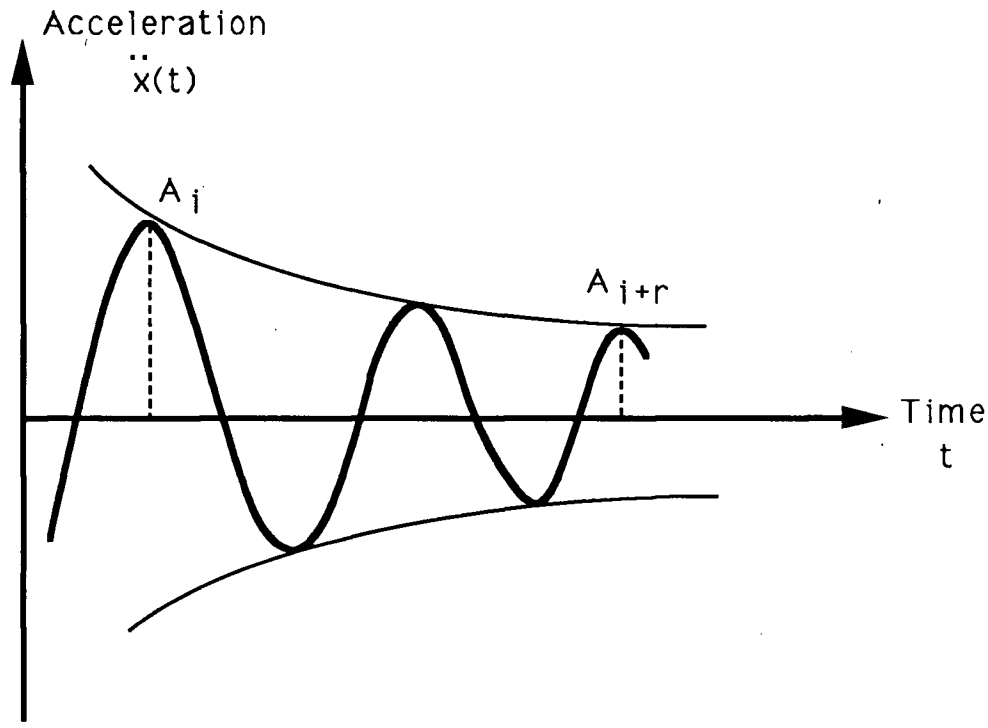

Figure 4.1(a) Typical Acceleration-Time Decay Record

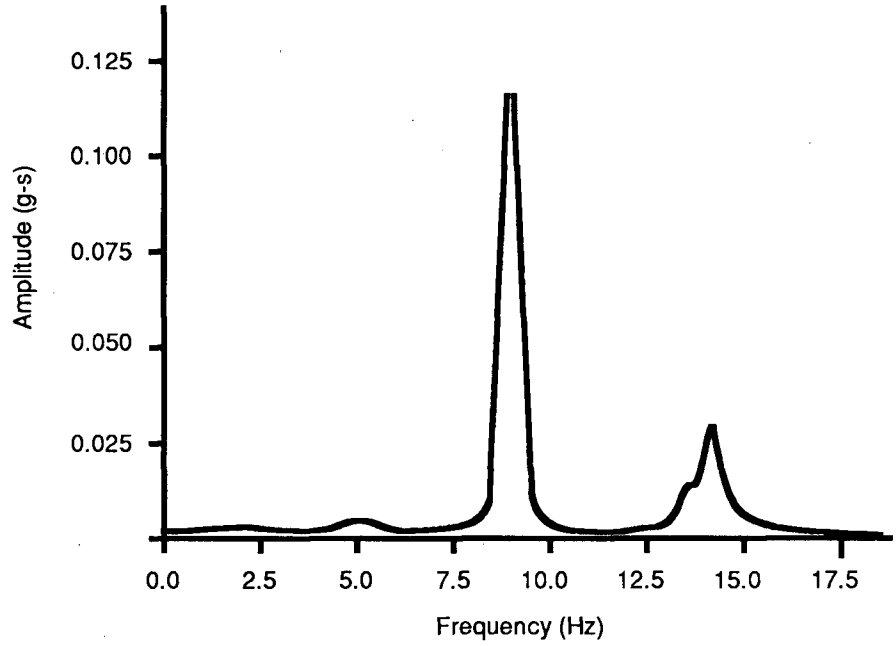

Figure 4.1(b) Typical Fourier Amplitude Spectrum
(taken from Filiatrault, 1985)

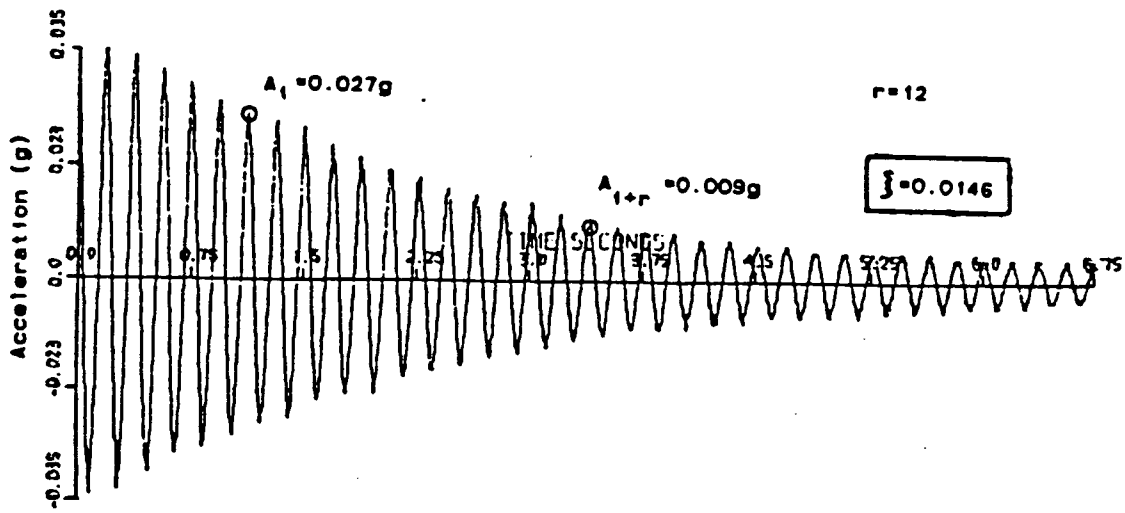

Figure 4.2 Logarithmic Decrement Method Applied to Sample Acceleration-Time Decay Record (taken from Filiatrault, 1985)

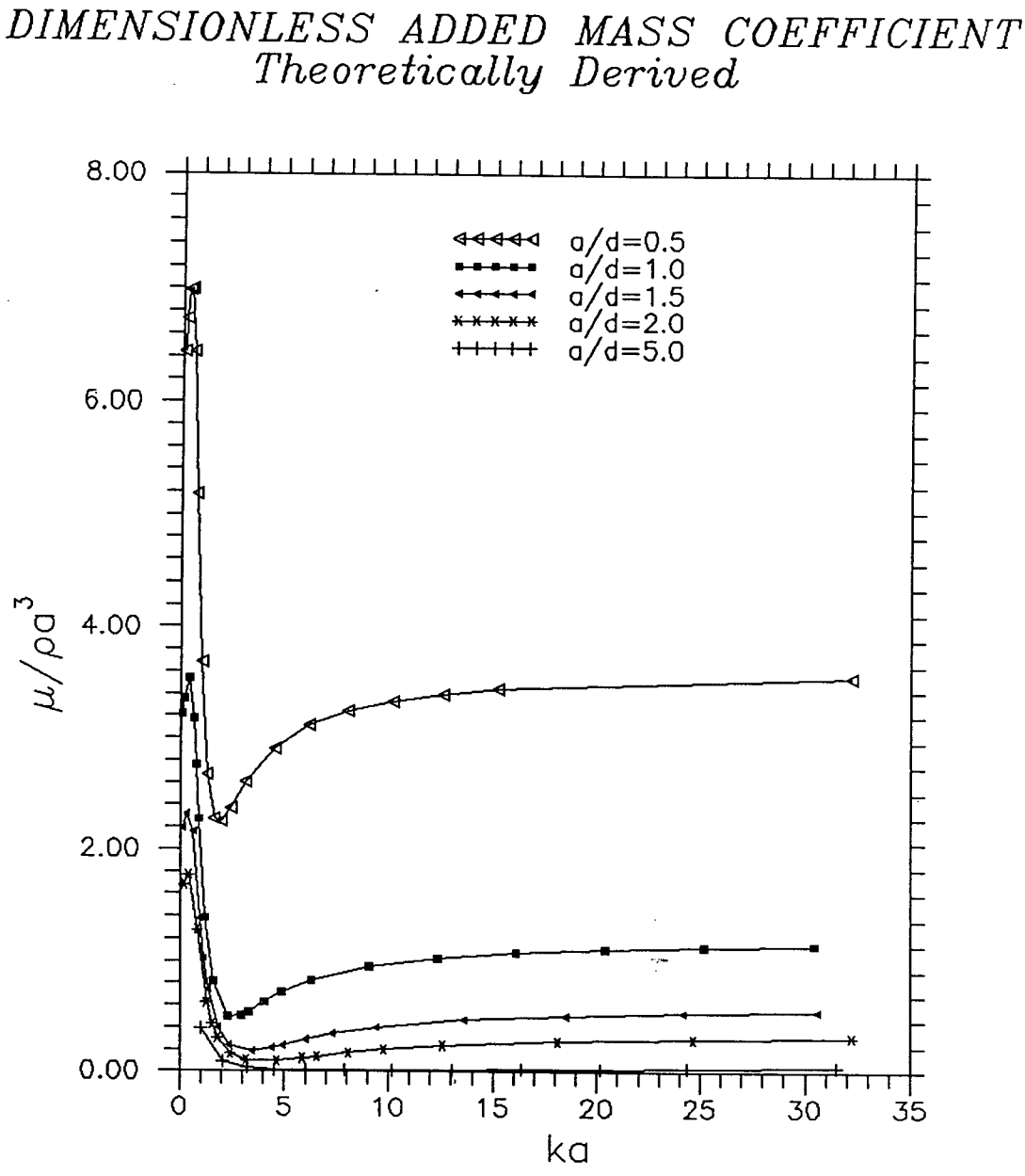

Figure 5.1(a) Theoretical Added Mass Coefficient for Various a/d

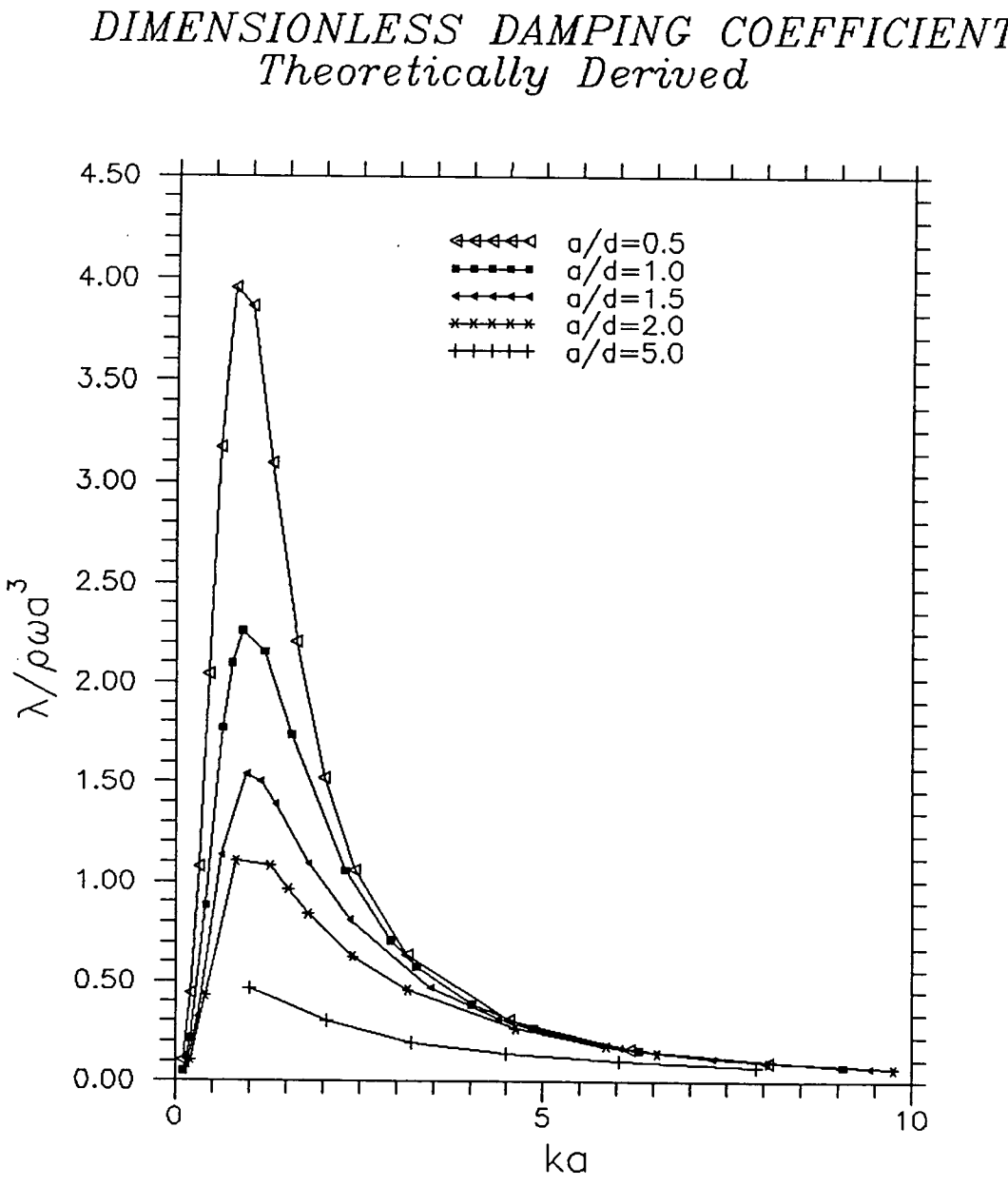

Figure 5.1(b) Theoretical Damping Coefficient for Various a/d

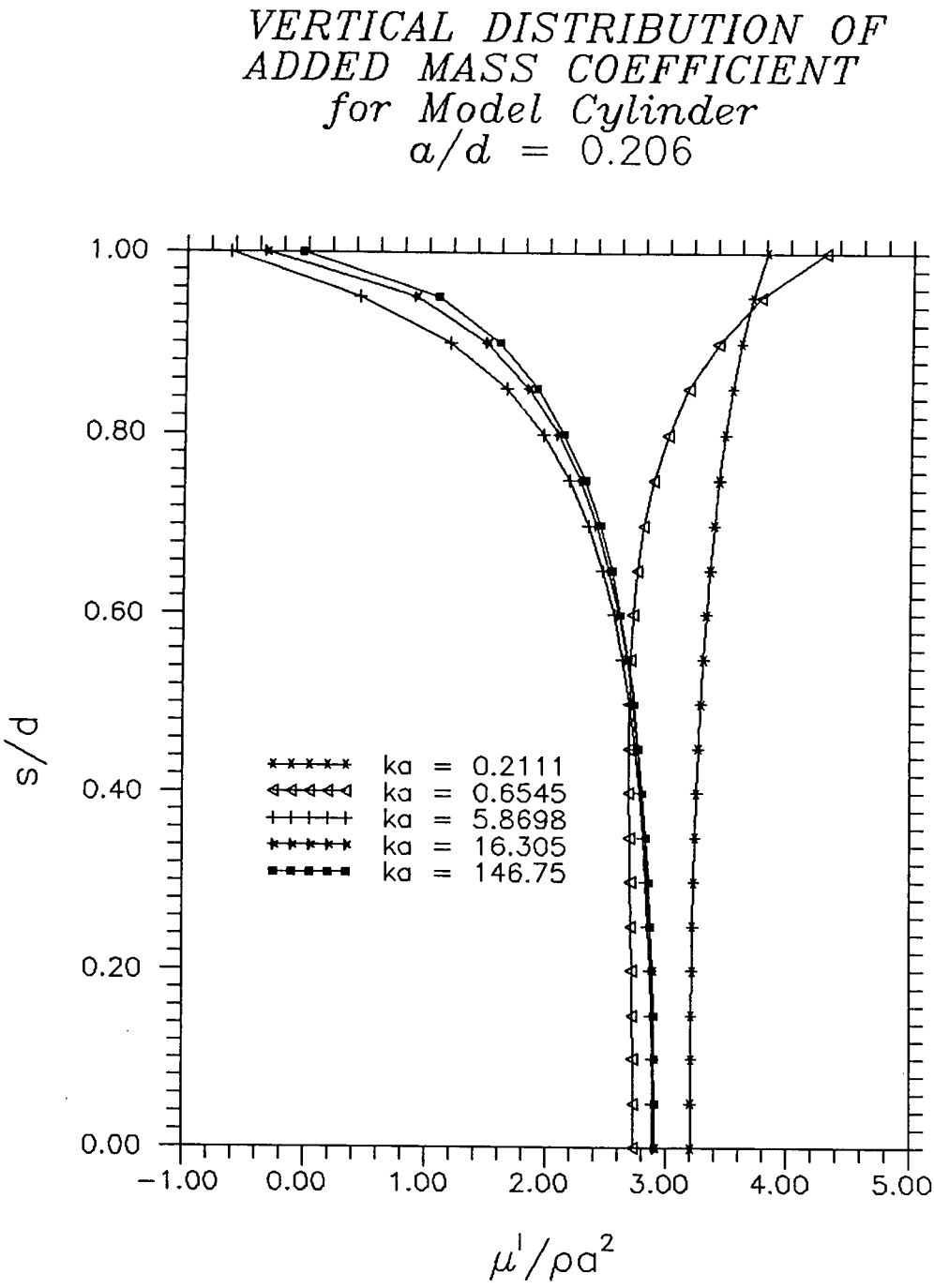

Figure 5.2(a) Vertical Distribution of Added Mass for Model

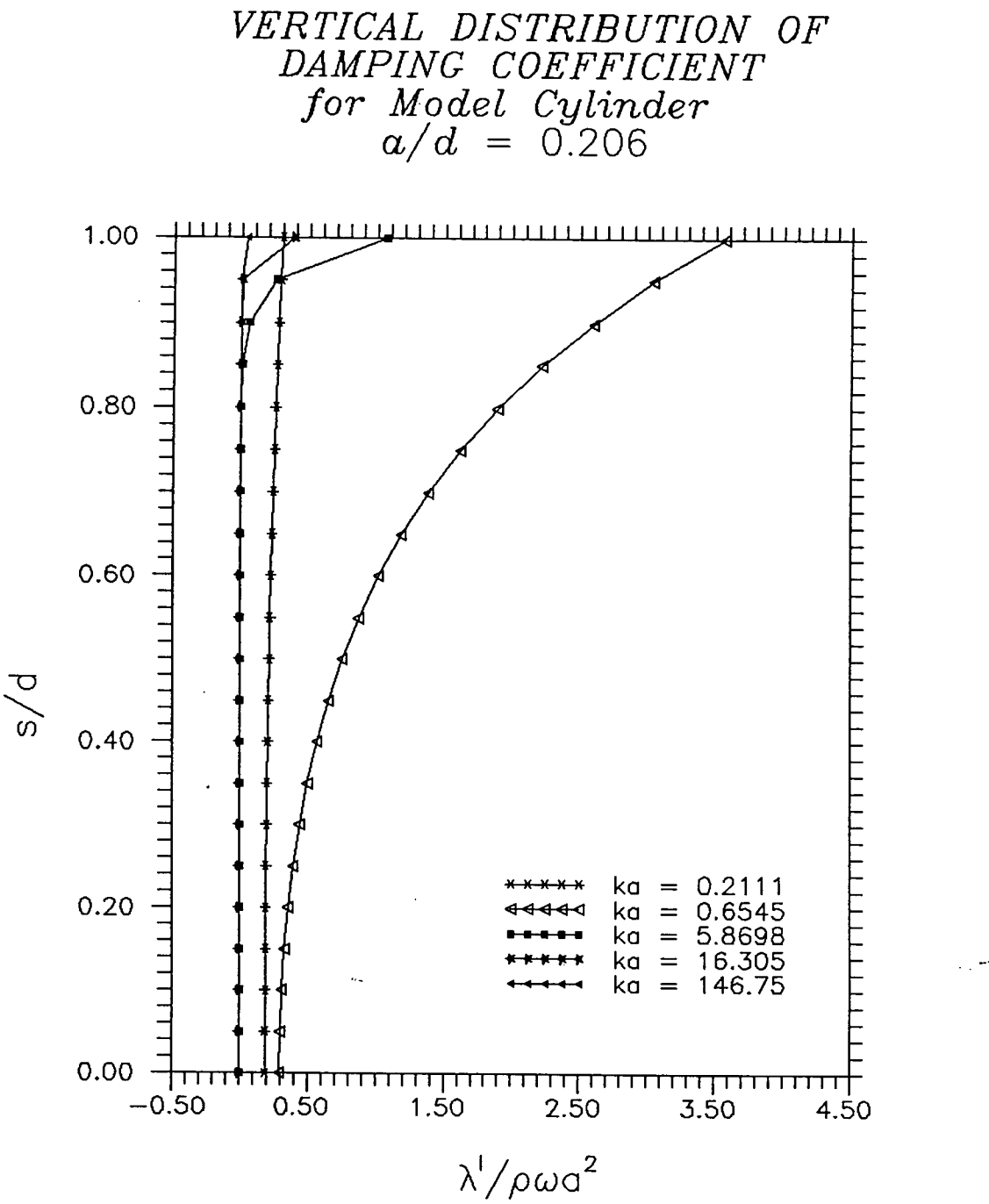

Figure 5.2(b) Vertical Distribution of Damping for Model

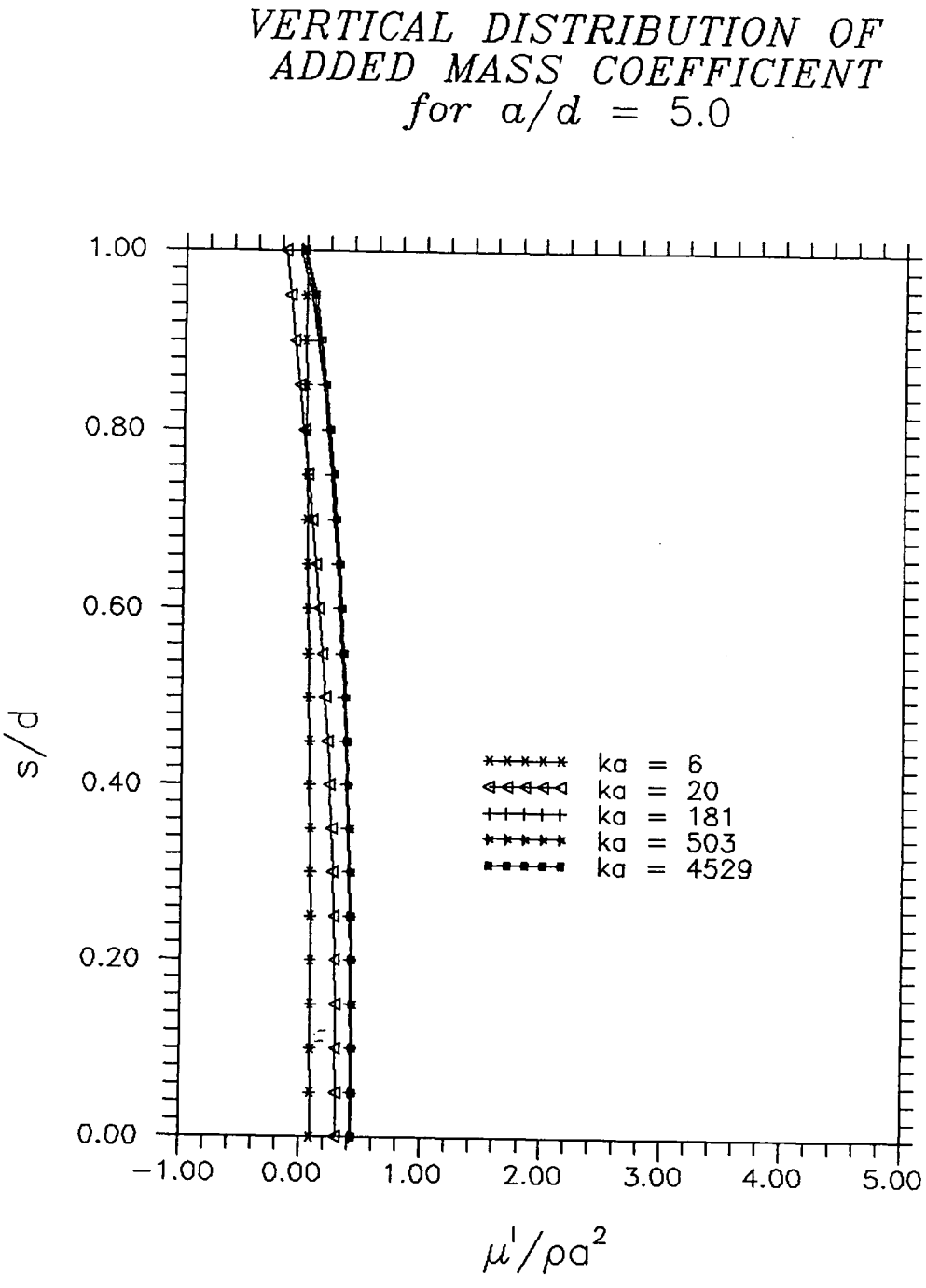

Figure 5.3(a) Vertical Distribution of Added Mass for a/d = 5

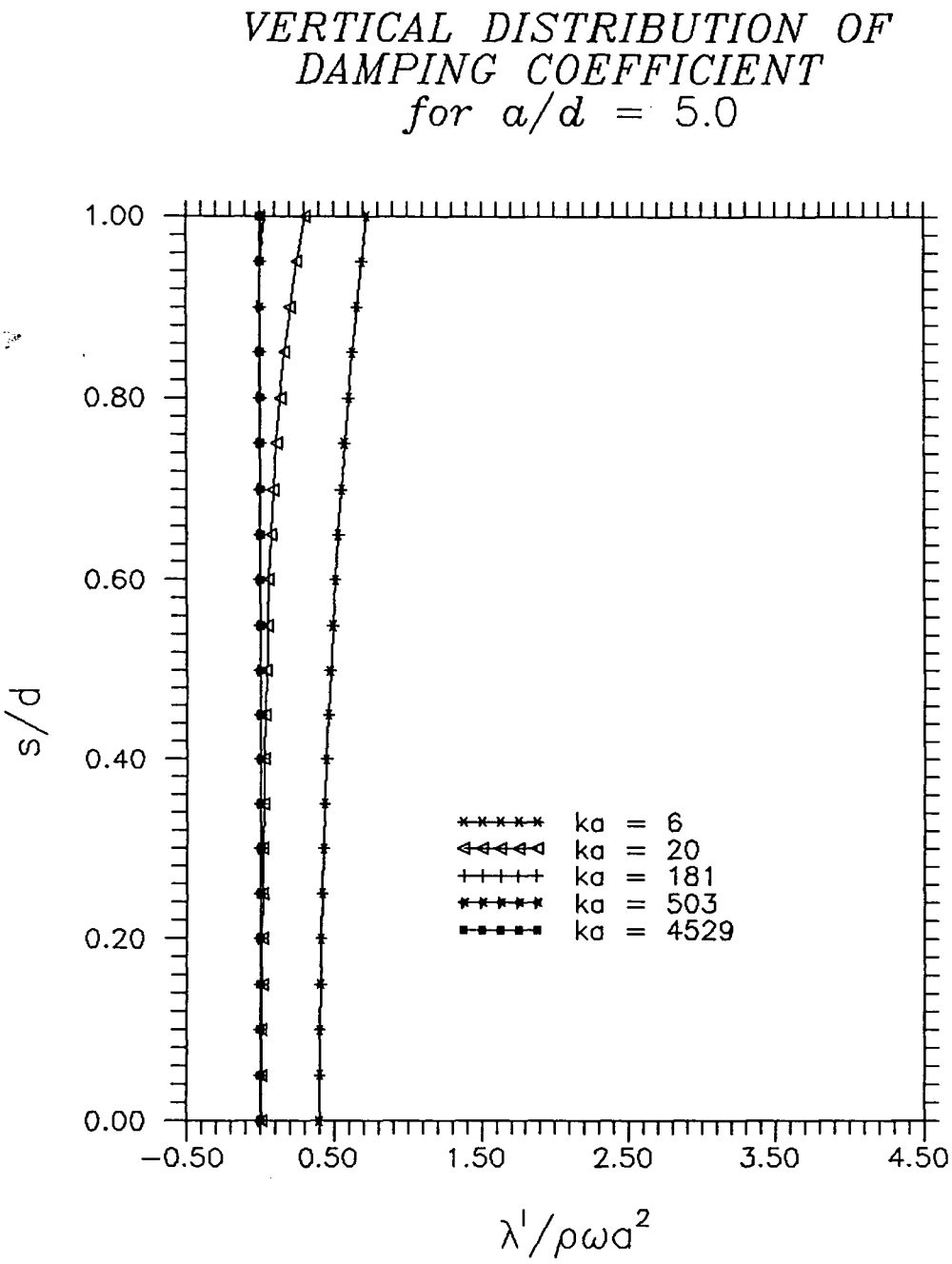

Figure 5.3(b) Vertical Distribution of Damping for a/d = 5

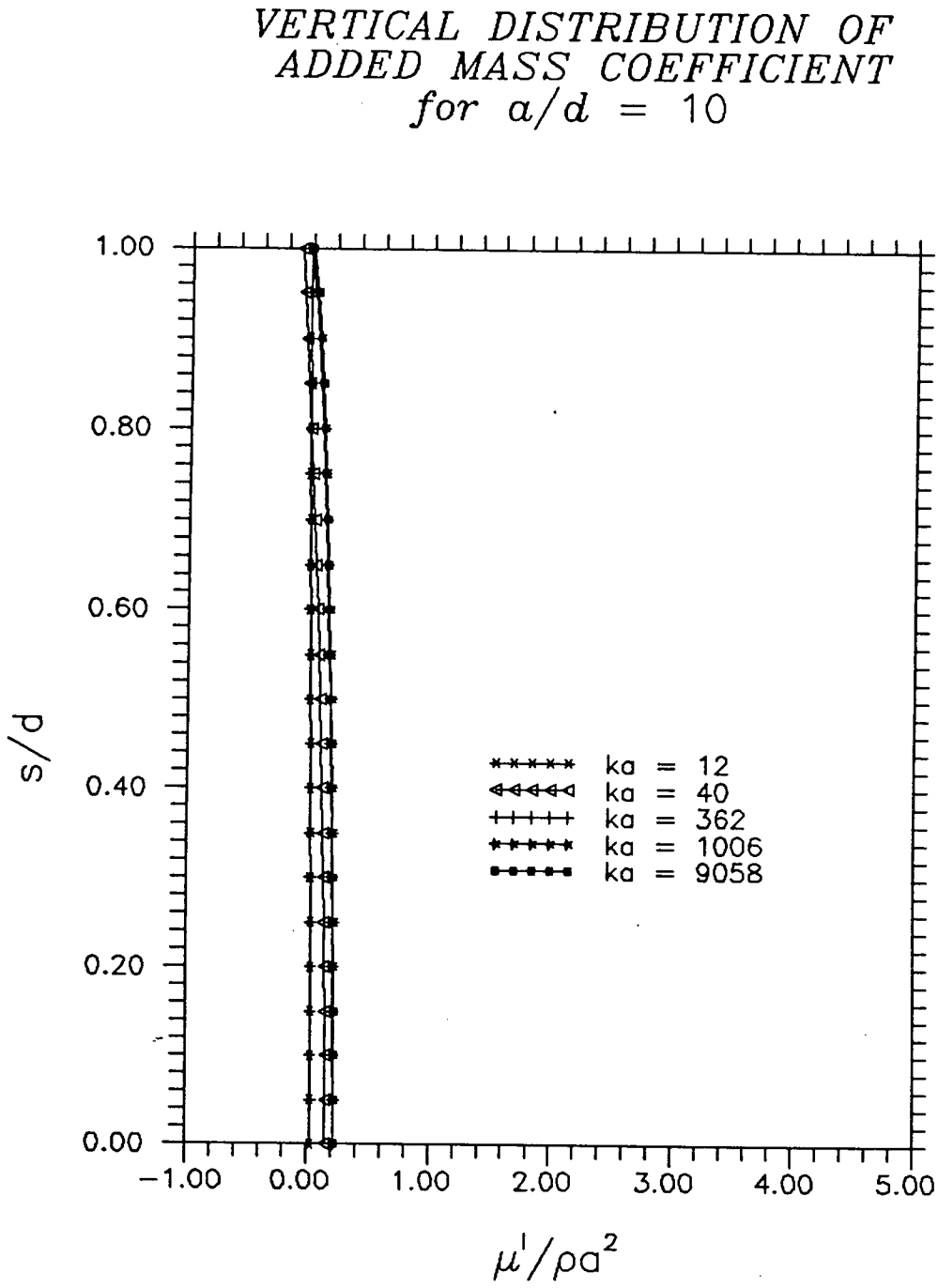

Figure 5.4(a) Vertical Distribution of Added Mass for a/d = 10

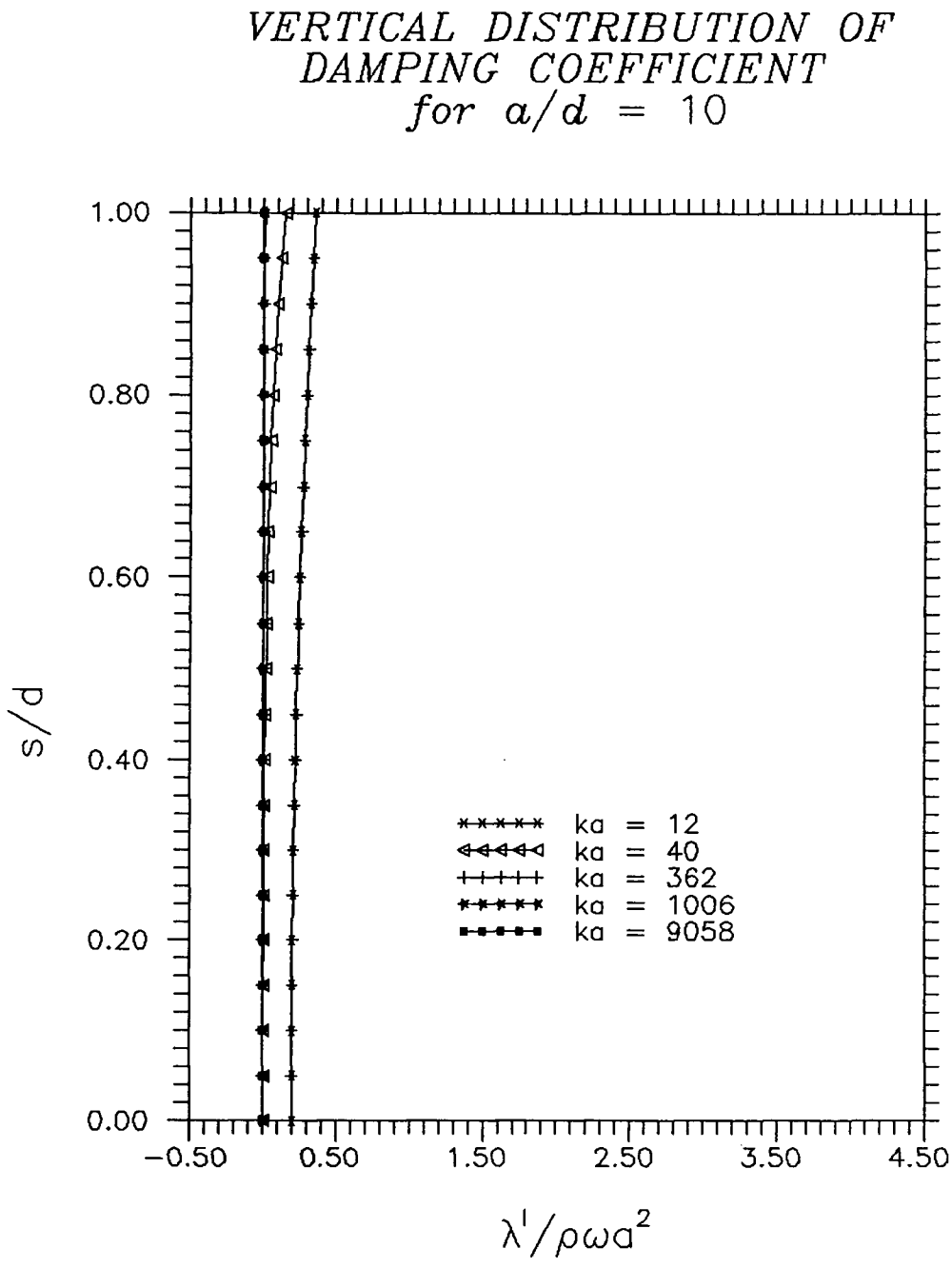

Figure 5.4(b) Vertical Distribution of Damping for a/d = 10

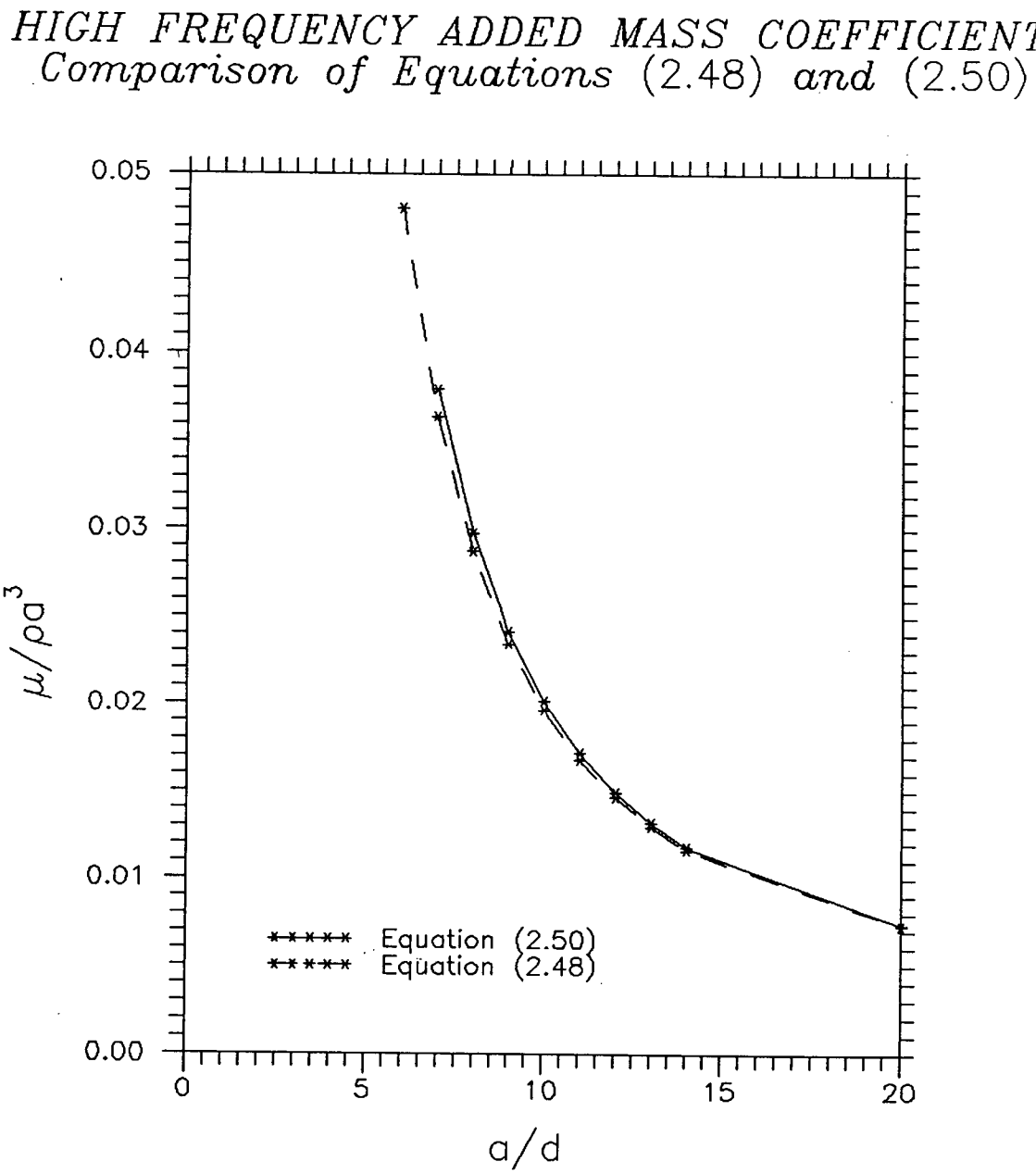

Figure 5.5 Comparison of Equations (2.48) and (2.50)

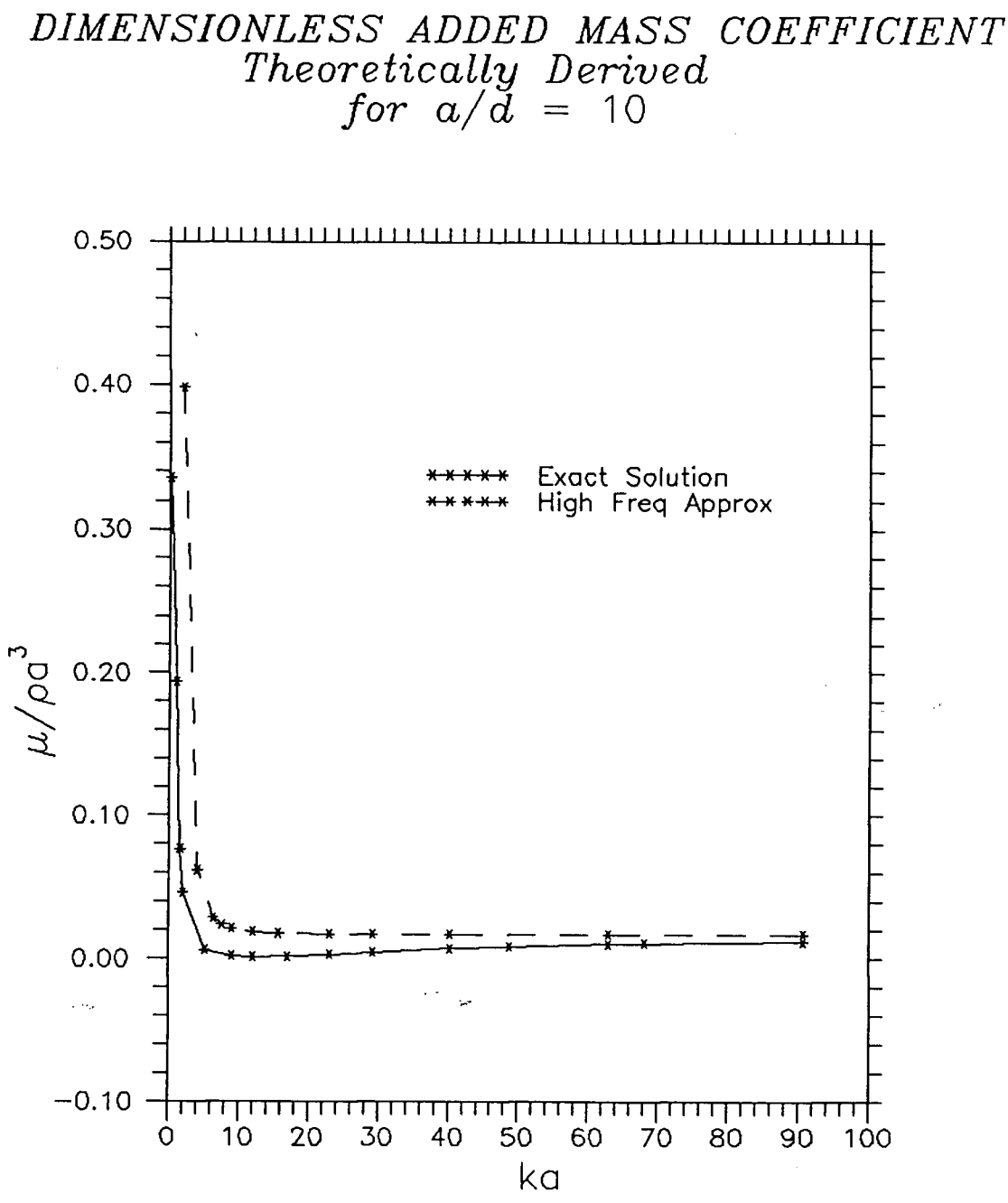

Figure 5.6(a) High Frequency Approximation of Added Mass for a/d = 10

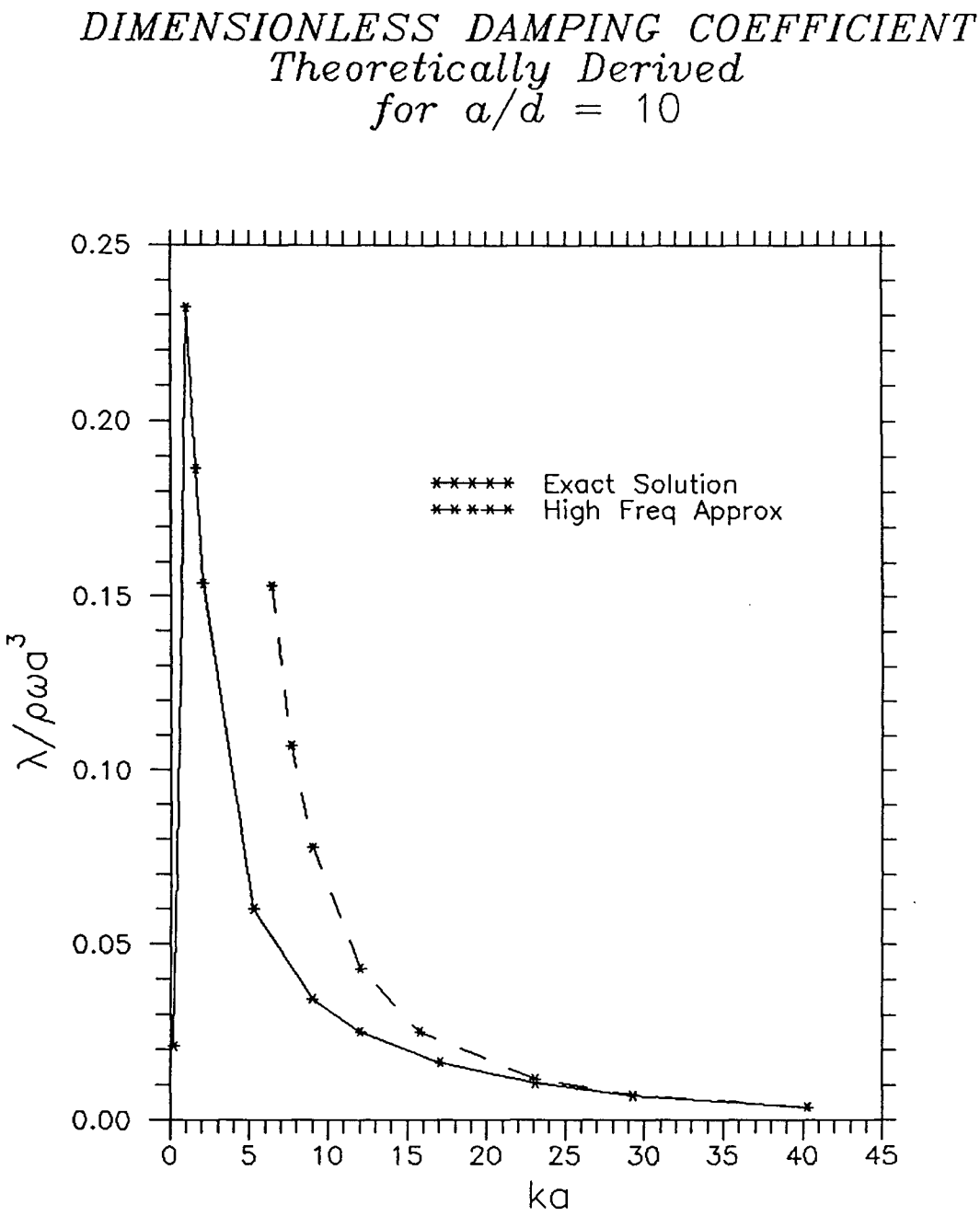

Figure 5.6(b) High Frequency Approximation of Damping for a/d = 10

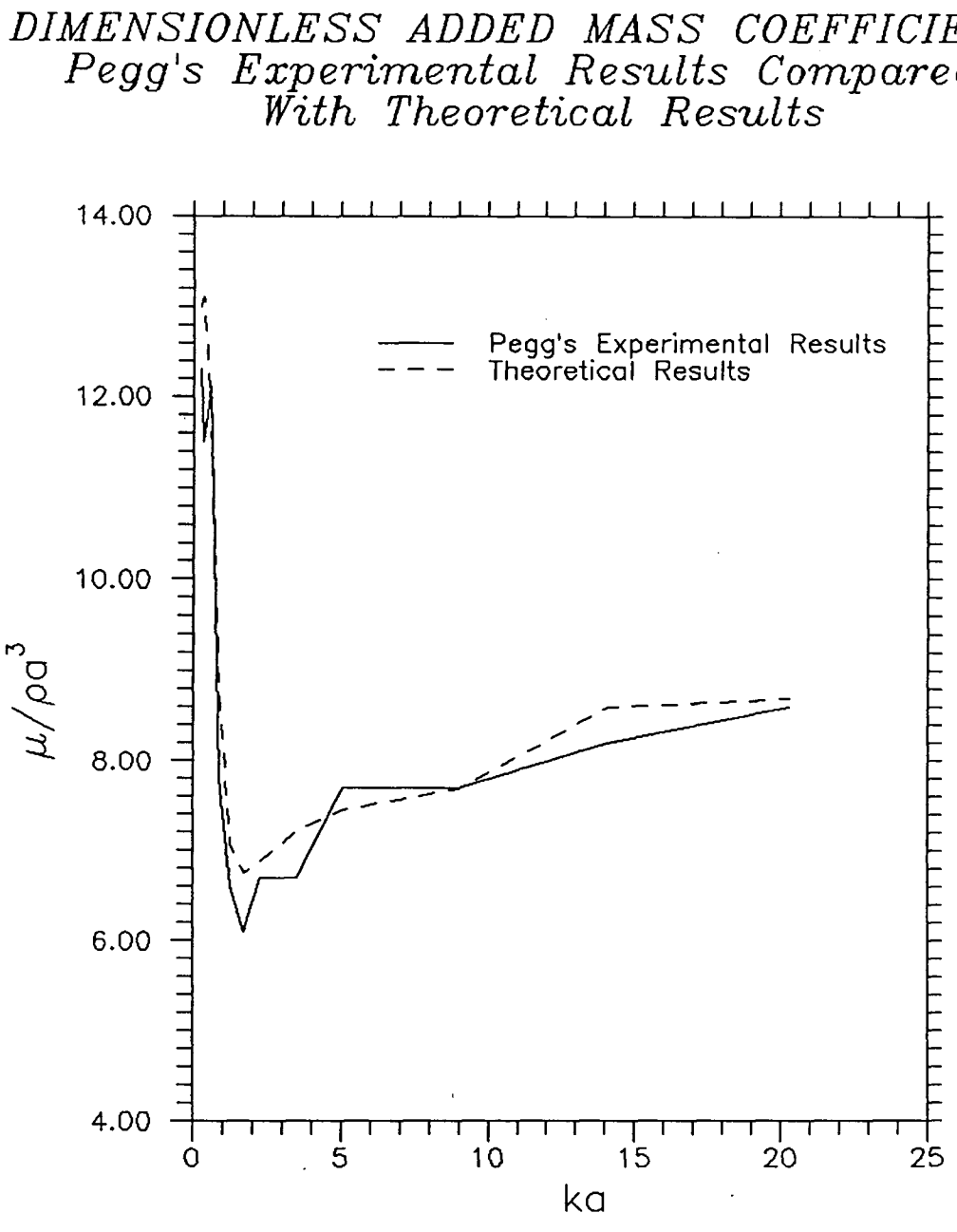

Figure 5.7(a) Comparison of Theoretical Added Mass with Pegg's Experimental Added Mass Results

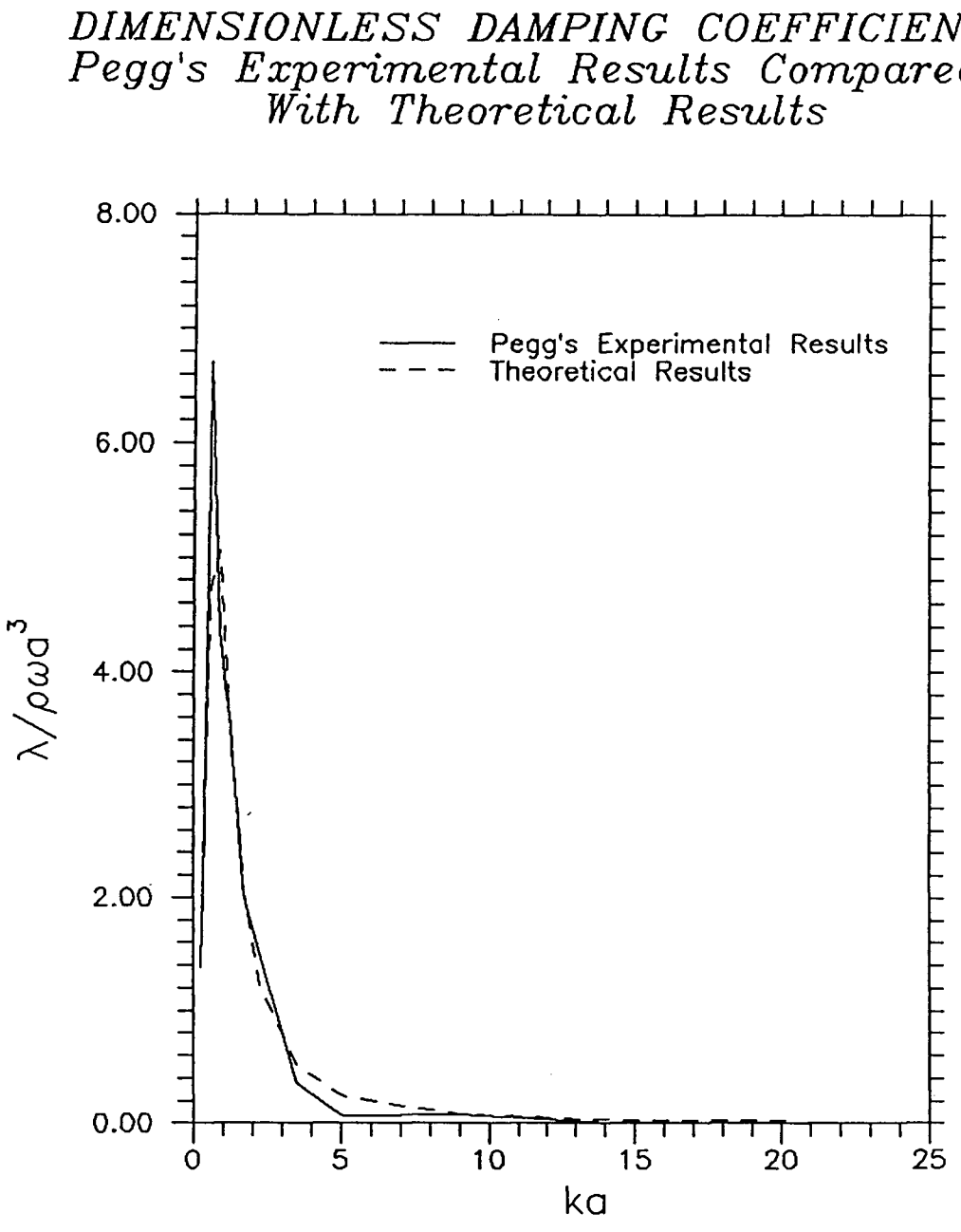

Figure 5.7(b) Comparison of Theoretical Damping with Pegg's Experimental Damping Results

PHOTOGRAPHS

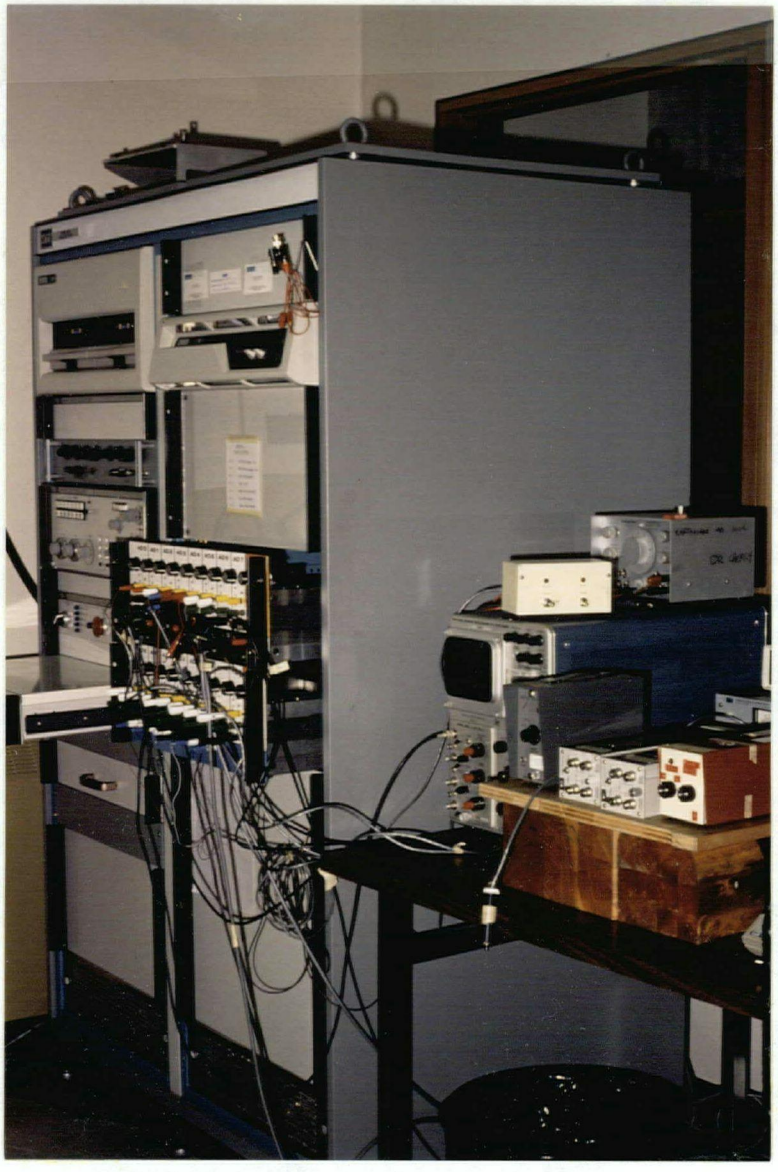

Photo 3.1 Physical Arrangement of Data Acquisition System

Photo 3.2 Shaking Table

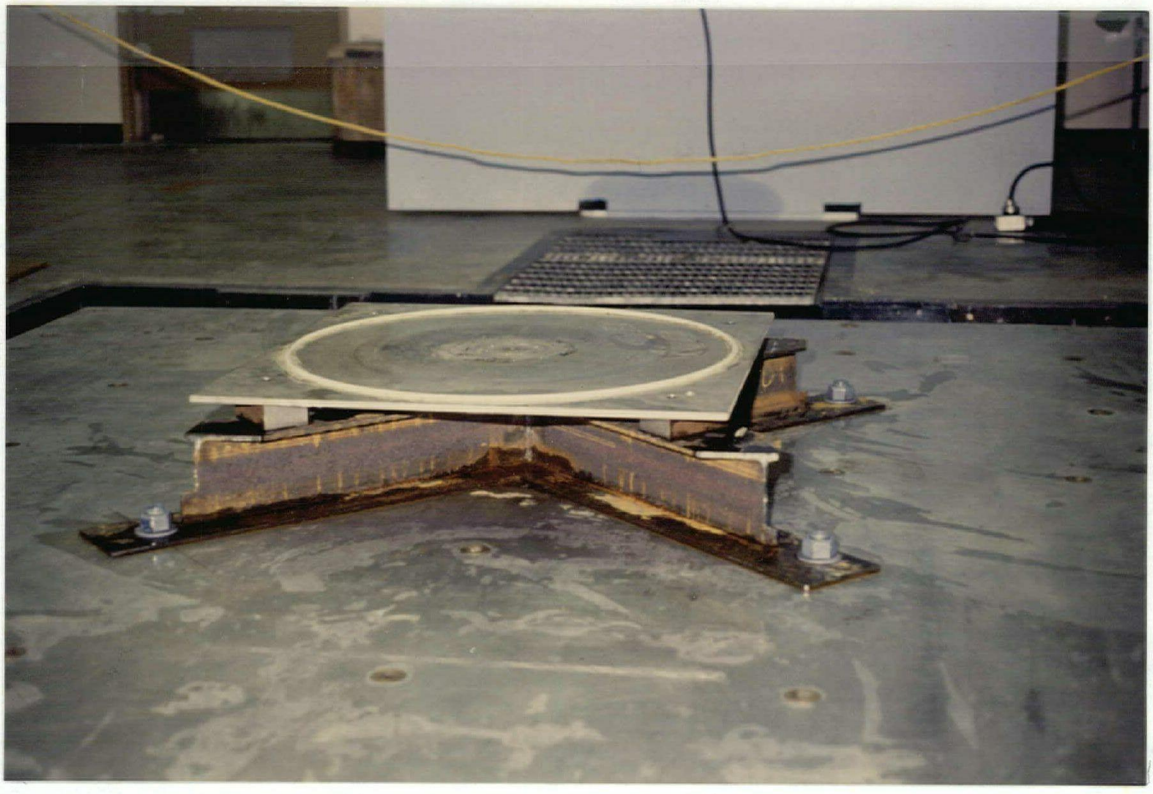

Photo 3.3 Base Support for Model

Photo 3.4 Model Cylinder

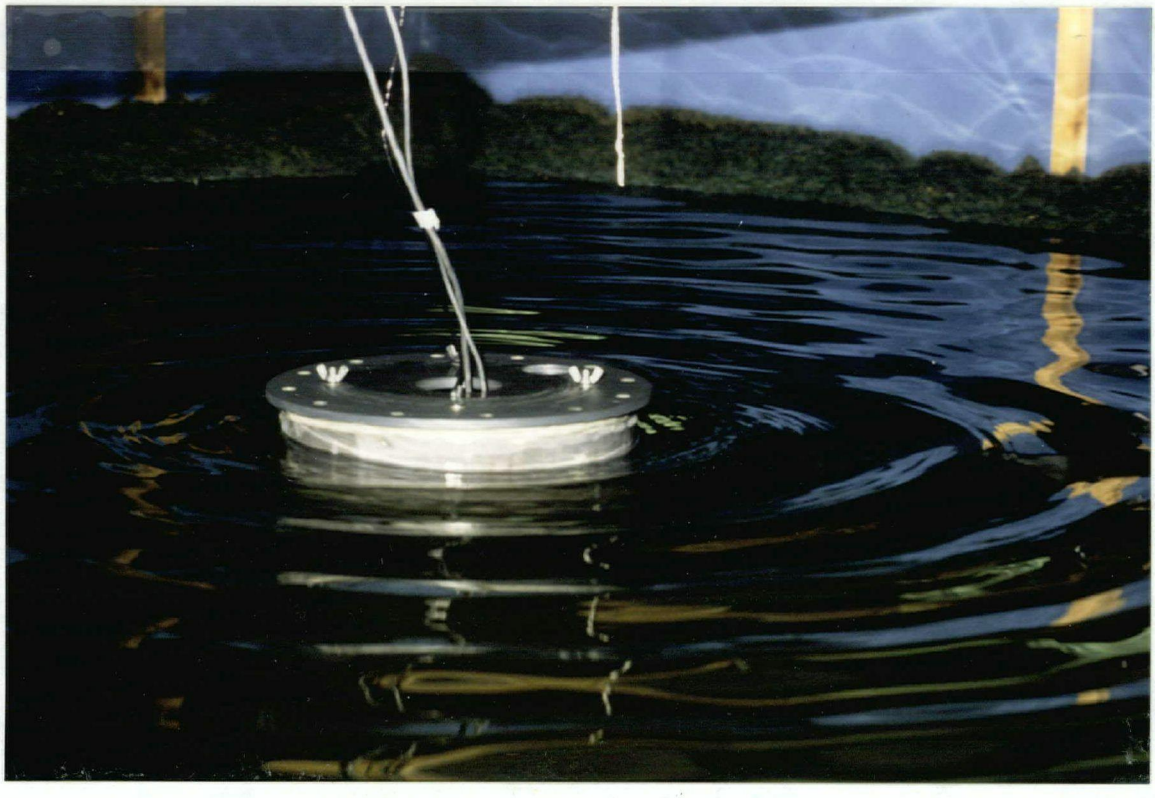

Photo 3.5 Sinusoidal Test : f = 3 Hz

TABLES

Section Level 1

Test Frequency (Hz)	Displacement Amplitude (mm)	Dimensionless Added Mass ($\mu'/\rho a^3$)	Dimensionless Damping ($\lambda'/\rho\omega a^3$)
1.0	7.40	12.80	7.67
1.0	5.72	12.51	9.93
1.0	4.34	12.54	10.99
3.0	2.85	4.46	6.31
5.0	0.88	1.79	-1.02
5.0	0.28	2.50	8.11
11.0	0.19	1.99	7.54
15.0	0.08	5.48	4.61

ρ = water density (kg/m^3) a = cylinder radius (m)

ω = frequency (rads/sec) μ' = added mass (kg)

λ' = damping (kg/s)

Table 5.1 Experimental Results for s/d = 0.9048
(Section Level 1)

Section Level 2

Test Frequency (Hz)	Displacement Amplitude (mm)	Dimensionless Added Mass ($\mu'/\rho a^3$)	Dimensionless Damping ($\lambda'/\rho\omega a^3$)
1.0	7.26	2.78	1.89
1.0	5.62	2.81	2.22
1.0	4.28	2.86	2.14
3.0	2.84	0.87	1.42
5.0	0.87	-0.18	2.94
5.0	0.28	4.68	1.56
11.0	0.18	0.55	0.47
15.0	0.08	0.21	0.46

ρ = water density (kg/m^3) a = cylinder radius (m)

ω = frequency (rads/s) μ' = added mass (kg)

λ' = damping (kg/s)

Table 5.2 Experimental Results for s/d = 0.6482
(Section Level 2)

Test Frequency (Hz)	Total Displacement (cm)	Pegg's Experiments Dimensionless Added Mass ($\mu/\rho a^3$)	Pegg's Experiments Dimensionless Damping ($\lambda/\rho\omega a^3$)	Theoretical Dimensionless Added Mass ($\mu/\rho a^3$)	Theoretical Dimensionless Damping ($\lambda/\rho\omega a^3$)
0.60	1.75	11.2	1.43	13.0	1.38
		2.31	12.3	0.63	
		1.38	11.24	1.43	
1.00	2.37	11.4	6.0	11.9	4.73
		1.30	11.6	5.5	
		0.614	12.1	5.8	
		1.09	11.7	6.7	
		1.54	11.5	6.6	
2.00	0.416	6.5	1.2	7.3	1.23
		0.859	6.3	1.4	
		0.26	6.3	1.1	
		1.21	6.7	1.5	
		0.665	6.5	1.3	
5.00	0.23	8.2	0.12	8.6	0.03
		0.236	7.9	0.0	
		0.209	8.0	0.0	
		0.120	8.2	0.0	
6.00	0.105	8.6	0.0	8.7	0.02
		0.106	8.1	0.1	

ρ = water density (kg/m^3) $\quad$ a = cylinder radius (m)

ω = frequency (rads/s) $\quad$ μ = added mass (kg)

λ = damping (kg/s)

Table 5.3 Comparison of Theoretical Results with Pegg's Experimental Results (Pegg, 1983)

APPENDICES

A: Dimensional Analysis of Hydrodynamic Force
B: Measurement and Analysis of Data
C: Instrument Calibration and Typical Data
D: Description of Computer Programs

Appendix A

DIMENSIONAL ANALYSIS OF HYDRODYNAMIC FORCE

A dimensional analysis can be used to plan the experimental part of the study most efficiently. The symbols F, L, and T are used to denote the dimensions of force, length, and time respectively. The added mass μ (which has the basic dimensions $[F{\cdot}L^{-1}{\cdot}T^2]$) and the fluid damping coefficient λ $[F{\cdot}L^{-1}{\cdot}T]$ are considered to be the dependent variables in the investigation. These quantities are assumed to depend on the following list of independent variables:

(i) ρ, the density of the fluid $[F\,T^2\,L^{-4}]$;
(ii) ν, the kinematic viscosity of the fluid $[L^2\,T^{-1}]$;
(iii) a, the radius of the cylinder [L] ;
(iv) ε, the mean height of surface protrusions (a measure of surface roughness)[L] ;
(v) ω, the angular frequency of excitation $[T^{-1}]$;
(vi) ξ, the amplitude of the oscillation [L] ;
(vii) E, the modulus of elasticity of the cylinder $[F\,L^{-2}]$;
(viii) d, the water depth [L] ; and
(ix) g, the gravitational acceleration $[L{\cdot}T^{-2}]$.

The added mass and damping coefficients may be expressed in a general form as

$$\mu = f_1(\rho, \nu, a, \xi, \varepsilon, \omega, E, d, g) \qquad (A1)$$

and

$$\lambda = f_2(\rho, \nu, a, \xi, \varepsilon, \omega, E, d, g) \ . \qquad (A2)$$

Application of the Buckingham Pi theorem gives

$$\pi_1 = F_1(\pi_2, \pi_3, \pi_4, \pi_5, \pi_6, \pi_7) \tag{A3}$$

and

$$\pi_7 = F_2(\pi_2, \pi_3, \pi_4, \pi_5, \pi_6, \pi_7) \tag{A4}$$

where

$$\pi_1 = \frac{\mu}{\rho a^3}\ ,\quad \pi_2 = \frac{\omega a^2}{\nu} = S\ ,\quad \pi_3 = \frac{a}{d}\ ,\quad \pi_4 = \frac{a}{\xi}\ ,$$

$$\pi_5 = \frac{\varepsilon}{a}\ ,\quad \pi_6 = \frac{\rho a^2 \omega^2}{E}\ ,\quad \pi_7 = \frac{\omega^2 a}{g} \text{ or } ka\ , \tag{A5}$$

$$\text{and}\quad \pi_8 = \frac{\lambda}{\rho a^3 \omega}\ .$$

In view of the discussion concerning flow separation effects, the characteristic Stokes number, S, may generally be omitted. In addition, linearity of the problem implies that π_4 is omitted. Also, π_5 is not important since the cylinder surface is assumed to be smooth. When the structure is rigid, as is the case in this investigation, the variable E is not required; thus π_6 is not included. The dimensionless equations (A3) and (A4), therefore, reduce to

$$\frac{\mu}{\rho a^3} = F_1\left(\frac{a}{d}, ka\right) \tag{A6}$$

and

$$\frac{\lambda}{\rho a^3 \omega} = F_2\left(\frac{a}{d}, ka\right) \tag{A7}$$

in which F_1 and F_2 are unknown functions, determined from theory or experiment. The hydrodynamic coefficients per unit length depend on an additional dimensionless term, s/d. The numerical results presented in this thesis are intended to clarify the nature of these relationships.

Appendix B

MEASUREMENT AND ANALYSIS OF EXPERIMENTAL DATA

B.1 Instrumentation

Sensors which were mounted on the test specimen and those which are permanently to the shaking table were used to measure the response of the model cylinder to sinusoidal excitation.

B.1.1 Acceleration

The actual table acceleration is measured by a Kistler MD 305A 50g accelerometer which is permanently attached to the shaking table. This device was used in conjunction with a servo-amplifier to measure the base acceleration of the cylinder for a given test frequency.

A dynamic analysis of the active part of the model cylinder revealed that the natural frequency of this component in water was within the range of test frequencies. Resonant effects were, therefore, expected to occur, whereby the cylinder would undergo a rocking mode of motion rather than a pure translational mode. For this reason, a Stratham 20g accelerometer was attached to the aluminum flange at the level of the central aluminum shaft tip aligned in the direction of table motion. Any amplification in the acceleration of the shaft tip relative to that of the base would appear upon examination of the acceleration records and could thus be accounted for in the final analysis, as shown in a later section.

B.1.2 Displacement

The hydraulic actuator for the earthquake simulation system is supplied with an internally mounted LVDT. The LVDT requires A.C. excitation and provides an A.C. output . The amplitude of the output varies in direct proportion to the amount of

displacement of the LVDT core. The LVDT transducer is attached to the base of the actuator and the moveable core is positioned by the actuator's piston. When the piston is at mid-stroke, output of the LVDT is zero. Output voltage increases from zero as the piston is displaced from mid-stroke. The table displacement, hence that of the cylinder base, is measured and used to check the base acceleration record for the same frequency, according to the relation

$$a = - \omega^2 \cdot X \ . \qquad (B1)$$

B.1.3 Shear Force

The shear force component developed at the base of the cylinder's aluminum shaft due to the sectional fluid force was calculated from strain data obtained by 350-ohm aluminum-compatible strain gauges. Half-bridge circuits were utilized so that only bending strains were measured; two dummy gauges completed the Wheatstone bridge arrangement. The aluminum shaft was instrumented with two sets of four strain gauges, positioned according to Figure B.1. The shear component due to the fluid force acting on the 2-inch cylinder section was subsequently determined for the given test frequency.

B.2 Data Acquisition

The data acquisition system is controlled by the PDP-11/04 minicomputer with 32K word memory. An AR-11 real time module is used to perform Analog-Digital conversion and to support real time clock functions. The data is stored digitally on floppy disks and can be transferred to the U.B.C. mainframe Amdahl computer or to the AST 286 Premium microcomputer. For purposes of this experimental study, the AST was used; the program PROCOMM establishes the communication link between the PDP-11 and the AST and allows file transfer from the PDP-11 to the AST.

At present, 16 channels of data may be acquired with individual signal conditioning, including variable gain and frequencies. Current acquisition rates are about 2 kHz continuously and up to 35 kHz in burst mode. All channels of data are conditioned by a variable gain buffer and a variable cut-off filter to provide optimal control over signal levels

and reliability of acquired data. Data can be recorded in analog or digital form with the capability for analog to digital conversion. The 16-channel multiplexer and 10-bit A-D converter of the AR-11 board are used for sampling analog signals. Scope channel X (a 10-bit D-A converter) is used for driving the shaking table; whereas, channel Y is used for previewing the earthquake to be simulated or for examining the input signals on an oscilloscope. Most of the software for data acquisition and table command is written in Fortran. The software controls the external devices (e.g. table's hydraulic system, D-A and A-D converters, transducers) and performs data formatting, plotting, and statistical and spectral analyses.

Before one can proceed with an actual experiment, the D-A and A-D converters must be calibrated, using the program CALIB, which allows verification of the accuracy of the A-D and D-A cards and monitors the calibration of the transducers, strain gauges, and so on. Actual creation of experiments and recording of data are performed by the program ACQUIR, which permits the digitization of up to 16 analog signals by means of the 16 A-D converter channels while simultaneously driving the shaking table with some input waveform. Various test parameters, such as sampling rates and durations, are chosen at this stage. Once data have been recorded in binary form, they are processed by the program OMFORM, which assigns actual engineering values to the original data and performs some arithmetic operations and time-history plotting. The program EDSPEC allows plotting of the Fourier and power spectra of both earthquake and formatted data files from OMFORM. Generated spectral values may be Hanned and can be stored in a formatted file for later use.

By rule of thumb, the channel sampling rate is usually taken to be ten times the test frequency. That is, for a frequency of 1.0 Hz it is recommended that each channel be sampled every 0.1 seconds (or 10 Hz). For this experimental study, a sampling period of 0.01 seconds was used for test frequencies 1.0 to 5.0 Hz, 0.005 seconds for 11.0 and 15.0 Hz. Dip switch settings (which govern the resolution of the data acquisition) for each channel varied according to the test frequency and table displacement, usually 5 for the top strain channel and 2 for the table displacement channel. A description of how to use the dip switch (among other things) is given in the Earthquake Laboratory's resident data acquisition system operation manual.

B.3 Data Analysis

For purposes of this thesis, the Fortran program ANALYS was written to quickly compute the hydrodynamic coefficients from recorded strain and displacement data for each test frequency ω and section elevation s above the tank floor. The section below describes in certain detail the analysis.

B.3.1 Strain Gauge Data Analysis

Figure B.1 is a definition sketch of the problem. The base displacement is described by

$$X_g(t) = \mathbf{X} \cos(\omega t) \tag{B2}$$

and the base acceleration by

$$\ddot{X} = -\omega^2 \mathbf{X} \cos(\omega t) \ . \tag{B3}$$

The strain signal obtained from either the top or the bottom of the shaft with the cylinder being surrounded by either air or water can be represented by the following expression:

$$\varepsilon_n^{(m)}(t) = A_n^{(m)} \cos(\omega t - \delta_n^{(m)}) \tag{B4}$$

where ε is the strain, A is the amplitude of the signal, ω is the excitation frequency (in radians), δ is the phase difference between the base displacement record and the strain signal, superscript-m denotes the medium in which the cylinder is immersed (i.e. "A" for air and "W" for water), and subscript-n distinguishes between the two strain gauge Wheatstone bridge arrangements (i.e. "1" for the top strain and "2" for the bottom strain).

The strain-moment relationship for beams in elastic bending is given by

$$\varepsilon = \frac{My}{EI} \tag{B5}$$

which gives strain on a cross-section subjected to a bending moment M, at any point that is located a distance y from the neutral axis (which passes through the centroid of the shaft's cross-sectional area). For the current model design and loading, Equation (B5) is expressed in the form

$$V^{(m)} = \Delta\varepsilon^{(m)} \frac{2EI}{DH} \tag{B6}$$

where $\Delta\varepsilon$ is the difference between the average strain at the top of the aluminum shaft (ε_1) and that at the bottom of the shaft (ε_2), V is the sectional base shear, and EI is the shaft stiffness which is determined from a static load deflection test, such that

$$EI = \frac{PL^3}{\Delta}\ ; \tag{B7}$$

the aluminum shaft, encircled by the aluminum can, was supported horizontally as a cantilever, and a known mass was hung from its free end. The vertical deflection was measured and EI then calculated. It was discovered that this value for EI matched very closely the value found using E = 70 GPa (for aluminum) and $I = \frac{\pi}{64} D^4$.

Subtraction of Equation (B6) when m is "A" from Equation (B6) when m is "W" yields

$$F_z(t) = \frac{2EI}{DH} \left[\Delta\varepsilon^{(W)} - \Delta\varepsilon^{(A)}\right] \tag{B8}$$

where $F_z(t)$ is the fluid force acting on the 2-inch section, D is the shaft diameter, and H is the distance between the centres of the strain gauge sets. Upon expansion of Equation (B4) for both top and bottom strains and both air and water and substitution of the resulting expressions into Equation (B8), one obtains

$$\begin{aligned} F_z(t) = \frac{2EI}{DH} \Big\{ \cos\omega t \Big[& A_2^{(W)} \cos(\delta_2^{(W)}) - A_1^{(W)} \cos(\delta_1^{(W)}) \\ & + A_1^{(A)} \cos(\delta_1^{(A)}) - A_2^{(A)} \cos(\delta_2^{(A)}) \Big] \\ + \sin\omega t \Big[& A_2^{(W)} \sin(\delta_2^{(W)}) - A_1^{(W)} \sin(\delta_1^{(W)}) \\ & + A_1^{(A)} \sin(\delta_1^{(A)}) - A_2^{(A)} \sin(\delta_2^{(A)}) \Big] \Big\} \end{aligned} \tag{B9}$$

when the bottom strain is assumed to be greater than the top strain. One can now recall Equation (2.60) and expand it to get

$$F_z(t) = \mu' [\omega^2 \mathbf{X} \cos(\omega t)] + \lambda' [\omega \mathbf{X} \sin(\omega t)] \ . \qquad \text{(B10)}$$

By equating Equations (B10) and (B9), one can solve for the sectional added mass and damping coefficients:

$$\mu' = \frac{\left[A_2^{(W)}\cos(\delta_2^{(W)}) - A_1^{(W)}\cos(\delta_1^{(W)}) + A_1^{(A)}\cos(\delta_1^{(A)}) - A_2^{(A)}\cos(\delta_2^{(A)})\right]}{\omega^2 \mathbf{X}} \qquad \text{(B11)}$$

$$\lambda' = \frac{\left[A_2^{(W)}\sin(\delta_2^{(W)}) - A_1^{(W)}\sin(\delta_1^{(W)}) + A_1^{(A)}\sin(\delta_1^{(A)}) - A_2^{(A)}\sin(\delta_2^{(A)})\right]}{\omega \mathbf{X}} \qquad \text{(B12)}$$

The units of the coefficients are kg and kg/s respectively when EI has units of N·mm^2, D and H are in millimetres, ω in radians per second, $\mathbf{X}$ in metres, δ in radians, and A in millimetres. The amplitude $A^{(m)}$ of a given strain signal and $\mathbf{X}$ of the corresponding table displacement signal were measured directly from the signals. The phase shift $\delta^{(m)}$ was obtained in the following way. A reference point of t = 1.0 sec was arbitrarily chosen. The time at which the first peak occurred after this reference point was noted for the displacement signal and for the strain signal under consideration. The phase shift is then the difference in these times multiplied by 2π. For example, for a water test conducted at a frequency of 1.0 Hz for Section Level 1, the first peak after 1.0 sec in the displacement signal was found to occur at 1.985 sec and in the bottom strain signal at 2.065 sec. The phase shift was thus calculated to be 0.5027 radians.

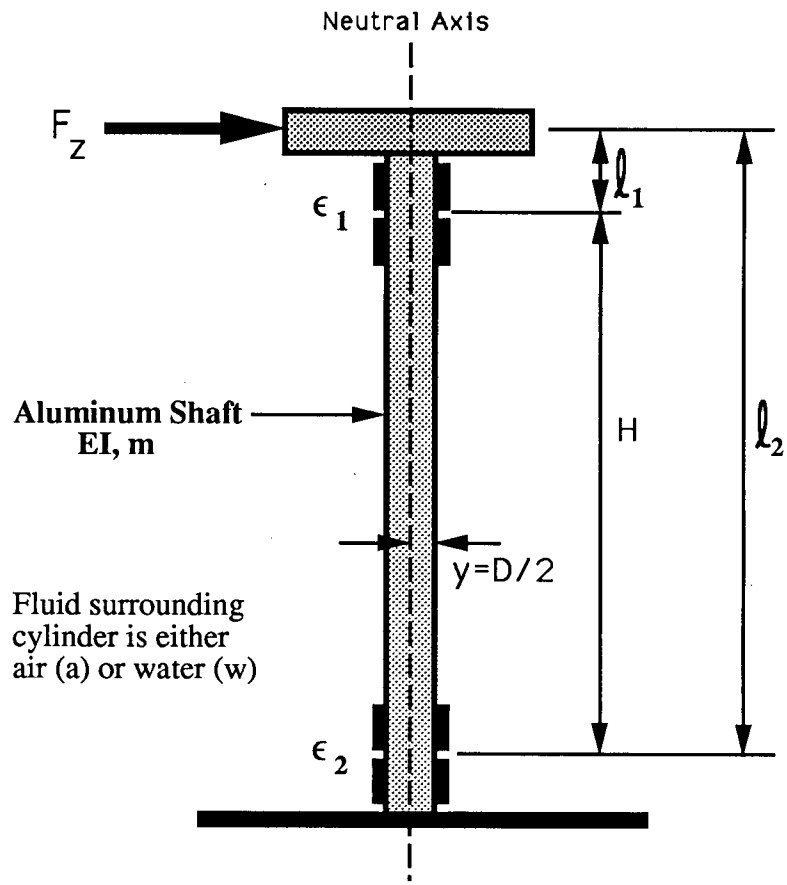

$$F_z = \text{cnst}\,[\,\Delta\epsilon^{(w)} - \Delta\epsilon^{(a)}\,]$$

where

$$\text{cnst} = \frac{EI}{yH}$$

$$\Delta\epsilon = \epsilon_2 - \epsilon_1$$

Figure B.1 Schematic of Strain Gauge Setup

Appendix C

INSTRUMENT CALIBRATION AND TYPICAL DATA

Instruments were periodically calibrated to ensure that experimental results were reliably obtained. Initially, the shaking table was calibrated for a preset maximum-amplitude range (in this case, Range 2 which corresponds to a peak amplitude of ±2.5 inches). A digital gauge measured the actual displacement of the table from its equilibrium position, each measurement corresponding to a particular voltage recorded by the table LVDT. A calibration factor of 4.00 Volts per inch was confirmed, where a positive value indicates motion towards the control room in the laboratory. It was then necessary to calibrate the table's SPAN control with excitation frequency, a reason being to avoid "spiking the table" unexpectedly. It was noted, for example, that an oscillation amplitude of 0.5 inches at a frequency of 0.1 Hz was obtained when the SPAN was set to a value of about 208. Of course, the given calibration factors are unique to this study; the various structural elements sitting directly on the shaking table affect its motion. A calibration factor for the shaft tip accelerometer was also determined. The output voltages measured by the accelerometer in the upward, horizontal, and downward orientations were noted alongside the corresponding acceleration. That is, the acceleration is ±1.0 g when aligned in the vertical direction and 0 g when horizontal, and there are corresponding voltages for these conditions. Static load tests were the means by which the strain gauges were calibrated. The aluminum shaft was supported horizontally at its base end and known masses were hung from its free end. For each known applied load, from which the strain may be calculated, there was a corresponding output voltage for the top strain gauges and for the bottom ones. Calibration curves of voltage versus micro-strain were then drawn and slopes calculated.

Figure C.1 illustrates the data which was typical of low-frequency sinusoidal testing. The computer software DADiSP was used to process each of the signals generated in a

given frequency test. Smoothing of all but the table displacement signals was necessary, especially for those recorded when $f \geq 3.0$ Hz.

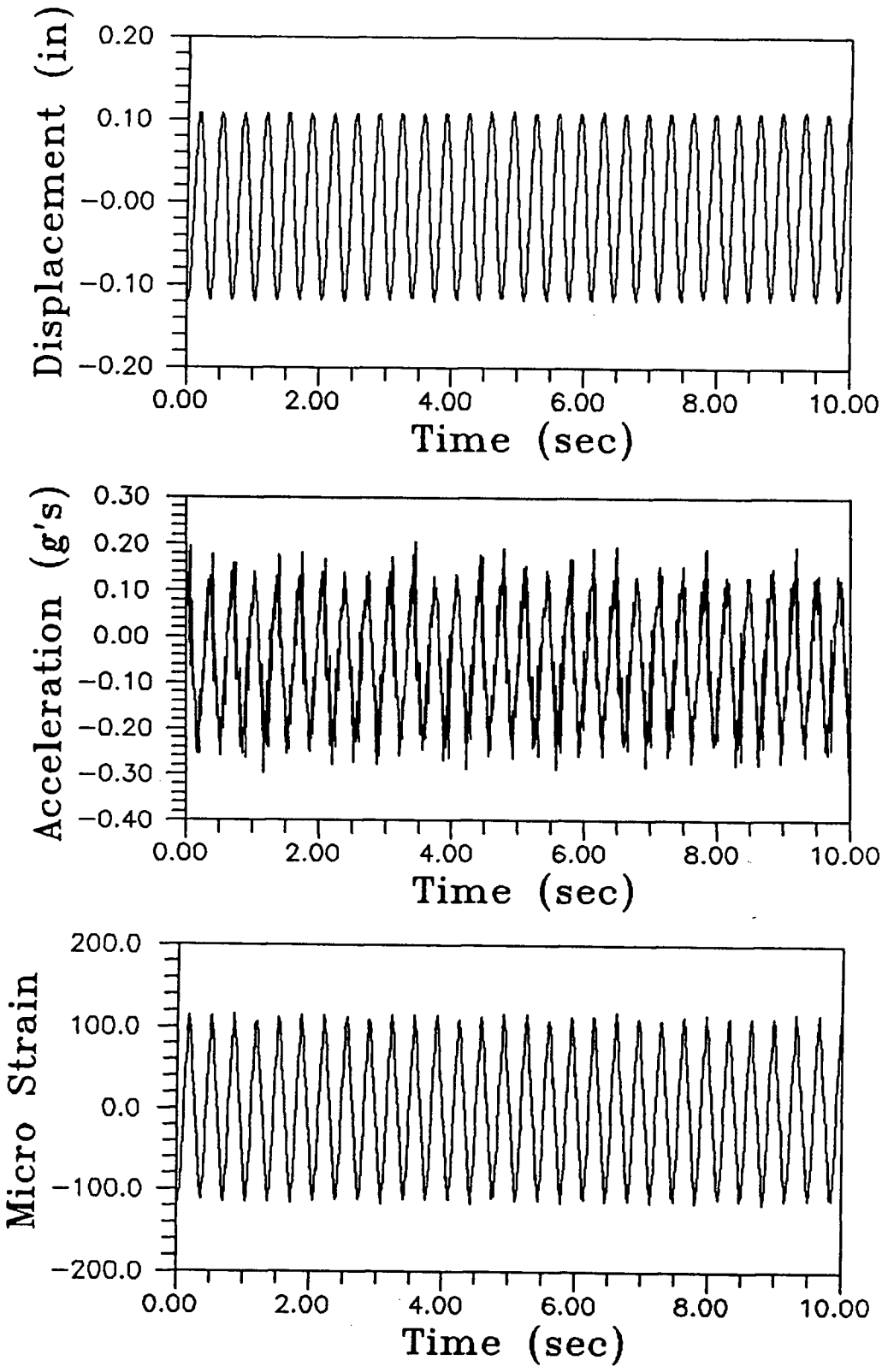

Figure C.1 Typical Data : Table Displacement, Shaft Tip Acceleration, Bottom Shaft Strain : f = 3 Hz : Water

Appendix D

DESCRIPTION OF COMPUTER PROGRAMS

D.1 Program *COEFFICIENTS*

A Fortran-77 computer program called *Coefficients* , the mathematical basis for which has been presented in Chapter Two, was written to numerically evaluate the added mass and damping coefficients for an isolated vertical surface-piercing circular cylinder subjected to horizontal uni-directional external excitation (i.e. earthquake, ice loading) using Equations (2.35), (2.36), (2.34), and (2.33c). The vertical distribution of the hydrodynamic coefficients is also computed.

The user must provide an input data file which contains the structure's radius, water depth and density, and desired excitation frequencies. The data are read from logical input unit 5, and the resulting output is sent to unit 6. For example, to run the compiled version of the program on the mainframe computer, called *Coeff*, with a data file named *Data* and an output file named *Results*, the following command is issued:

```
$RUN COEFF 5=DATA 6=RESULTS
```

The file *Data* must contain the information described below in the same order as shown. The characters in parentheses following the variable names refer to the format requirements of the data.

Line 1

A (F10.3): radius of structure, in metres

D (F10.3): water depth, in metres

RHO (F10.3): water density, in kg/m^3

Line 2

NP (I3): number of runs requested; NP is equal to the number of FREQ(I) values for which the hydrodynamic coefficients are required

Line 3 to NP

FREQ(I) (F5.1): excitation frequency, in Hz

Line (NP+1)

FLAG (I3): if FLAG = 0 then s (elevation above the seabed) is computed; otherwise, various s values must be read in from the input file, as shown below

if FLAG ≠ 0 then the following lines are included...

Line (NP+2)

NS (I3): number of s values requested for determination of vertical distribution

Lines (NP+3) to [NS+(NP+3)]

ELEV(I) (F7.4): elevation above the seabed, s, in metres

A listing of the program *Coefficients* and sample output file are provided in this appendix, as well as the listing files for *High* and *Analys*.

D.2 Program *HIGH*

Equations (2.44b) and (2.50) were programmed for numerical evaluation on the AST-286 Premium microcomputer. The program *High* computes the high-frequency approximations for the added mass and damping coefficients for a vertical surface-piercing circular cylinder subjected to horizontal unidirectional ground excitation.

To run the compiled version of the program, there must be an existing output file and the data file must contain the following information.

Line 1

NC (I3): number of structure radius-to-water depth ratios for which the high-frequency approximations are required

Lines 2 to (NC+1)

RADIUS(I) (F10.3): radius of structure, in metres

DEPTH(I) (F10.3): water depth, in metres

Line (NC+2)

RHO (F10.3): water density, in kg/m^3

Line (NC+3)

NP (I3): number of excitation frequencies

Lines (NC+4) to [NP+(NC+3)]

FREQ(I) (F5.2): excitation frequency, in Hz

D.3 Program *ANALYS*

A Fortran-77 computer program called *Analys* calculates the hydrodynamic coefficients for a given cylinder section subjected to ground excitation at a given test frequency. *Analys* is a data analysis program which utilizes the equations derived in Appendix B.

The program has been compiled by Professional Fortran Compiler (PROFORT). The input data file must contain the information described below.

Line 1

LEVEL (I2): Section Level designation number, where 1 denotes the topmost level and 4 denotes the bottom level

NUM (I3): number of test frequencies in analysis

Line 2

D (F8.2): diameter of aluminum shaft, in mm

L (F8.2): effective length of aluminum shaft, in mm
RAD (F8.4): cylinder's outer radius, in metres
EI (E15.4): shaft stiffness, in $N \cdot mm^2$
RHO (F7.1): water density, in kg/m^3

Line 3

S1 (F8.2): distance from centre of top strain gauge Wheatstone bridge arrangement to centre of aluminum flange at shaft tip, in mm
S2 (F8.2): distance from centre of bottom strain gauge Wheatstone bridge arrangement to centre of aluminum flange at shaft tip, in mm

Lines 4 to 6 are repeated NUM times...

Line 4

FREQ (F6.2): excitation frequency, in Hz
XAMP (F8.2): oxcillation amplitude, in mm

Line 5

A1W, A1A, A2W, A2A (4E15.4): amplitude of either the top [1] or bottom [2] strain signal for shaking in either air [A] or water [W]

Line 6

TP1W, TP1A, TP2W, TP2A, TP3W, TP3A (6F7.3): time of first downward zero-crossing which occurs after first positive peak after the 1.0-second mark in the response signal [1-top strain; 2-bottom strain] for shaking in either air [A] or water [W]

```
C*************************************************************
C
C     Program COEFFICIENTS
C         Last Update:  September 2, 1988
C
C     This program calculates the added mass and damping
C     coefficients for an isolated vertical surface-
C     piercing circular cylinder.  Their vertical distri-
C     bution is included in the computations.
C
C     The mathematical formulation is based on the
C     theory (potential flow) developed for the purposes
C     of this thesis.
C
C*************************************************************
C
      IMPLICIT REAL*4 (A-H,O-Z)
      INTEGER FLAG,COUNT
      DIMENSION ELEV(10)
      COMPLEX BH,BHP,BF,AI,TEM,AMZ(50)
      COMMON/BLK1/A,D,RHO,NP,FREQ(50)
      COMMON/BLK2/FR,WL,AKD,AKA
      COMMON/BLK3/AMZP,AMZA,ADZP,ADZA
      COMMON/BLK4/AMP,AM,ADP,AD
C
      PI=3.141592654
      G=9.806
      AI=CMPLX(0.,1.)
      CALL INPUT(FLAG)
      IF (FLAG .EQ. 0) GOTO 18
C
      READ (5,5) NS
 5    FORMAT (I3)
      DO 15 I=1,NS
          READ (5,10) ELEV(I)
 10       FORMAT (F7.4)
 15    CONTINUE
C
 18   A3=A**3
C
      DO 100 I = 1,NP
        FR = FREQ(I)
        W = 2.*PI*FR
        DGT2 = FR*FR*D/G
        CALL MIAKD(AKD,DGT2)
        WL = 2.*PI*D/AKD
        AKA=AKD*A/D
        AK=AKA/A
        CALL PARA
        FKD = 2.
```

```
      IF(AKD.LE.10.) THEN
        FKD = 2.*TANH(AKD)/(1.+2.*AKD/SINH(2.*AKD))
       ENDIF
      BJ0 = BESJ0(AKA,IND)
      BJ1 = BESJ1(AKA,IND)
      BY0 = BESY0(AKA,IND)
      BY1 = BESY1(AKA,IND)
      BJ1P = BJ0 - BJ1/AKA
      BY1P = BY0 - BY1/AKA
      BH = BJ1 + AI*BY1
      BHP = BJ1P + AI*BY1P
      BF = (BH/BHP)*FKD/(AKA**2)
      ADP = -PI*AIMAG(BF)
C
      SHR = 0.
      IF (AKD.LE.10.) SHR = 2.*AKD/SINH(2.*AKD)
      TEM = (BH/BHP)*2./(AKD*(1.+ SHR))
C
      IF (FLAG .EQ. 0) GOTO 19
      DO 22 IZ=1,NS
        S=ELEV(IZ)
        AKS = AK*S
        IF (AKD .GE. 174.) CHR = EXP(AKS-AKD)
        IF (AKD .LT. 174.) CHR = COSH(AKS)/COSH(AKD)
 22     AMZ(IZ) = TEM*CHR
        GOTO 24
C
 19   IZZ=21
      DIV1=21.
      DIV2=0.
      DO 23 IZ = 1,IZZ
        DIV2=DIV2+1.
        S = D*(DIV1 - DIV2)/(DIV1 - 1.)
C
        AKS = AK*S
        IF (AKD .GE. 174.) CHR = EXP(AKS-AKD)
        IF (AKD .LT. 174.) CHR = COSH(AKS)/COSH(AKD)
 23     AMZ(IZ) = TEM*CHR
 24     SUM = 0.
        DO 4 N = 1,30
          CALL MAKN(N,AKD,AKND)
          ARG = AKND*A/D
          BK0 = BSEK0(ARG,IND)
          BK1 = BSEK1(ARG,IND)
          BKP = -(BK0+BK1/ARG)
          FN = 4.*SIN(AKND)**2/(2.*AKND + SIN(2.*AKND))
          SUM = SUM + (BK1/BKP)*FN/(ARG**2)
C
          TEM = (BK1/BKP)*4.*SIN(AKND)/(AKND*(2.*AKND +
     &          SIN(2.*AKND)))
```

```
C
            IF (FLAG .EQ. 0) GOTO 28
            DO 26 IZ=1,NS
                S=ELEV(IZ)
                AKNS = AKND*S/D
   26           AMZ(IZ) = AMZ(IZ) + TEM*COS(AKNS)
                GOTO 55
C
   28       DIV2=0.
            DO 25 IZ = 1,IZZ
              DIV2=DIV2+1.
              S = D*(DIV1 - DIV2)/(DIV1 - 1.)
C
              AKNS = AKND*S/D
   25         AMZ(IZ) = AMZ(IZ) + TEM*COS(AKNS)
    4       CONTINUE
C
   55      IF (FLAG .EQ. 0) GOTO 33
           WRITE (8,73) FR
   73      FORMAT (' FREQUENCY (HZ):',F6.2)
           DO 43 IZ=1,NS
               S=ELEV(IZ)
             AMZP = -REAL(AMZ(IZ))*PI*D/A
             AMZA = -REAL(AMZ(IZ))*RHO*PI*A*D
             ADZP = -AIMAG(AMZ(IZ))*PI*D/A
             ADZA = -AIMAG(AMZ(IZ))*RHO*W*A*PI*D
             CALL DISTRN(S)
   43       CONTINUE
              GOTO 50
C
   33      DIV2=0.
           WRITE (8,73) FR
           DO 36 IZ = 1, IZZ
             DIV2=DIV2+1.
             S = D*(DIV1 - DIV2)/(DIV1 - 1.)
C
             AMZP = -REAL(AMZ(IZ))*PI*D/A
             AMZA = -REAL(AMZ(IZ))*RHO*PI*A*D
             ADZP = -AIMAG(AMZ(IZ))*PI*D/A
             ADZA = -AIMAG(AMZ(IZ))*RHO*W*A*PI*D
             CALL DISTRN(S,D)
   36       CONTINUE
C
   50      BF = BF + SUM
           AMP = -PI*REAL(BF)
           AD = ADP*W*A3*RHO
           AM = AMP*A3*RHO
           CALL TOTAL
  100   CONTINUE
        STOP
```

```
      END
C
C
      FUNCTION FN(X,C)
      FN= TAN(X)*X + C
      RETURN
      END
C
C
      SUBROUTINE MAKN(N,AKD,AKND)
C ** Calculates kn*d for Specified n and AKD
C ** Solution of AKND*TAN(AKND) = C
C
      PI = 3.141592654
      C = AKD*TANH(AKD)
      XL = (N-0.5)*PI + 0.0001
      XR = N*PI
      FR = FN(XR,C)
1     X = 0.5*(XL + XR)
      U = 0.5*ABS(XR - XL)
      IF (U.LE.0.001) GO TO 3
      F = FN(X,C)
      IF (F*FR.LT.0.) GO TO 2
      XR = X
      FR = F
      GO TO 1
2     XL = X
      GO TO 1
3     AKND = X
      RETURN
      END
C
      SUBROUTINE MIAKD(AKD, DGT2)
C ** Calculates  AKD  from  DGT2
C
      PI = 3.141592654
      C = 4. * PI * PI * DGT2
      X = SQRT(C)
      IF (C - 0.1) 30, 30, 10
   10 Y = C / TANH(X)
      IF (ABS(X - Y) - 0.0001) 80, 80, 20
   20 X = Y
      GO TO 10
   30 Y = X + 0.006
   40 Z = (X + Y) / 2.
      W = (X*TANH(X) - C) * (Z*TANH(Z) - C)
      IF (W) 50, 80, 60
   50 Y = Z
      GO TO 70
   60 X = Z
```

```
   70 IF (ABS(X - Y) - 0.0001) 80, 80, 40
   80 AKD = Y
      RETURN
      END
C
C
      SUBROUTINE INPUT(FLAG)
C ** Printing Program Headings; Input of Data
C
      IMPLICIT REAL*4 (A-H,O-Z)
      COMMON/BLK1/A,D,RHO,NP,FREQ(50)
      INTEGER FLAG
      READ (5,10) A,D,RHO
10    FORMAT (3F10.3)
      READ (5,20) NP
20    FORMAT (I3)
      DO 40 I=1,NP
        READ (5,30) FREQ(I)
30      FORMAT (F6.2)
40     CONTINUE
      READ (5,45) FLAG
45    FORMAT (I3)
      WRITE (6,50)
50    FORMAT (///,5X,'HYDRODYNAMIC COEFFICIENTS ',
     &'FOR A VERTICAL',/,
     &5X,'SURFACE-PIERCING CIRCULAR CYLINDER',/,5X,
     &'--------------------------------------')
      WRITE (6,60) A,D,RHO
60    FORMAT (//,8X,'CYLINDER RADIUS (M) =',F10.3,/,8X,
     &'WATER DEPTH (M) =',F10.3,/,8X,
     &'WATER DENSITY (KG/M3) =',F7.1)
      RETURN
      END
C
C
      SUBROUTINE PARA
C ** Printing Table Headings and Wave Parameters
C
      IMPLICIT REAL*4 (A-H,O-Z)
      COMMON/BLK2/FR,WL,AKD,AKA
      WRITE (6,5)
5     FORMAT(//,4X,'*****************',
     &'*****************************')
      WRITE (6,10) FR,WL,AKD,AKA
10    FORMAT(//,8X,'FREQUENCY (HZ) =',F6.2,/,8X,
     &'WAVELENGTH (M) =',
     &F12.4,/,8X,'KD =',F12.4,/,8X,'KA =',F12.4)
      WRITE (6,15)
15    FORMAT(//,5X,'DISTRIBUTION OF COEFFICIENTS ',
     &'OVER DEPTH',/,5X,
```

```
     &'-------------------------------------')
      WRITE (6,20)
20    FORMAT(/,3X,'(COEFFICIENTS GIVEN BELOW ',
     &'ARE DIMENIONLESS)')
      WRITE (6,30)
30    FORMAT(//,6X,' S/D ',9X,'ADDED MASS',7X,
     &'DAMPING',/)
      RETURN
      END
C
C
      SUBROUTINE DISTRN(S,D)
C ** Printing Results for Vertical Distribution
C
      IMPLICIT REAL*4 (A-H,O-Z)
      COMMON/BLK3/AMZP,AMZA,ADZP,ADZA
      E=S/D
      WRITE (6,10) E,AMZP,ADZP
      WRITE (8,10) E,AMZP,ADZP
10    FORMAT(4X,F7.4,2X,2(2X,E14.4))
      RETURN
      END
C
C
      SUBROUTINE TOTAL
C ** Printing Total Coefficient Values
C
      IMPLICIT REAL*4 (A-H,O-Z)
      COMMON/BLK2/FR,WL,AKD,AKA
      COMMON/BLK4/AMP,AM,ADP,AD
      WRITE (6,10) AMP,ADP,AM,AD
10    FORMAT(/,5X,'TOTAL HYDRODYNAMIC COEFFICIENTS:',/,
     &5X,'-------------------------------',//,4X,
     &'DIMENSIONLESS ADDED MASS =',E12.4,/,11X,
     &'AND DAMPING =',
     &E12.4,//,4X,'ADDED MASS (KG) =',E12.4,/,4X,
     &'DAMPING (KG/S) =',E12.4)
      WRITE (7,20) AKA,AMP,ADP
20    FORMAT (F12.4,E12.4,E12.4)
      RETURN
      END
```

HYDRODYNAMIC COEFFICIENTS FOR A VERTICAL
SURFACE-PIERCING CIRCULAR CYLINDER

CYLINDER RADIUS (M) = 0.140
WATER DEPTH (M) = 0.533
WATER DENSITY (KG/M3) = 1000.0

****

FREQUENCY (HZ) = 0.60
WAVELENGTH (M) = 3.3184
KD = 1.0092
KA = 0.2651

DISTRIBUTION OF COEFFICIENTS OVER DEPTH

(COEFFICIENTS GIVEN BELOW ARE DIMENIONLESS)

S/D	ADDED MASS	DAMPING
1.000	0.3954E+01	0.4763E+00
0.950	0.3825E+01	0.4585E+00
0.900	0.3726E+01	0.4418E+00
0.850	0.3645E+01	0.4263E+00
0.800	0.3578E+01	0.4119E+00
0.750	0.3521E+01	0.3985E+00
0.700	0.3473E+01	0.3862E+00
0.650	0.3432E+01	0.3748E+00
0.600	0.3397E+01	0.3644E+00
0.550	0.3367E+01	0.3549E+00
0.500	0.3341E+01	0.3463E+00
0.450	0.3319E+01	0.3386E+00
0.400	0.3300E+01	0.3318E+00
0.350	0.3284E+01	0.3258E+00
0.300	0.3270E+01	0.3206E+00
0.250	0.3259E+01	0.3163E+00
0.200	0.3250E+01	0.3127E+00
0.150	0.3243E+01	0.3100E+00
0.100	0.3239E+01	0.3080E+00
0.050	0.3236E+01	0.3069E+00
0.0	0.3235E+01	0.3065E+00

TOTAL HYDRODYNAMIC COEFFICIENTS:

```
DIMENSIONLESS ADDED MASS =  0.1300E+02
      AND DAMPING =  0.1375E+01

ADDED MASS (KG) =  0.3567E+02
DAMPING (KG/S) =  0.1423E+02

**********************************************

    FREQUENCY (HZ) =  1.00
    WAVELENGTH (M) =      1.5228
    KD =      2.1993
    KA =      0.5777

 DISTRIBUTION OF COEFFICIENTS OVER DEPTH
 ---------------------------------------

(COEFFICIENTS GIVEN BELOW ARE DIMENIONLESS)

   S/D          ADDED MASS       DAMPING

  1.000         0.4581E+01      0.2798E+01
  0.950         0.4172E+01      0.2515E+01
  0.900         0.3867E+01      0.2261E+01
  0.850         0.3631E+01      0.2035E+01
  0.800         0.3446E+01      0.1833E+01
  0.750         0.3299E+01      0.1654E+01
  0.700         0.3182E+01      0.1495E+01
  0.650         0.3088E+01      0.1354E+01
  0.600         0.3013E+01      0.1229E+01
  0.550         0.2954E+01      0.1119E+01
  0.500         0.2906E+01      0.1023E+01
  0.450         0.2868E+01      0.9387E+00
  0.400         0.2838E+01      0.8660E+00
  0.350         0.2815E+01      0.8039E+00
  0.300         0.2796E+01      0.7514E+00
  0.250         0.2782E+01      0.7081E+00
  0.200         0.2771E+01      0.6734E+00
  0.150         0.2764E+01      0.6468E+00
  0.100         0.2758E+01      0.6280E+00
  0.050         0.2755E+01      0.6168E+00
  0.0           0.2754E+01      0.6131E+00

 TOTAL HYDRODYNAMIC COEFFICIENTS:
 --------------------------------

DIMENSIONLESS ADDED MASS =  0.1187E+02
```

```
       AND DAMPING =  0.4727E+01

ADDED MASS (KG) =  0.3256E+02
DAMPING (KG/S) =  0.8150E+02

**********************************************

    FREQUENCY (HZ) =  2.00
    WAVELENGTH (M) =      0.3902
    KD =      8.5833
    KA =      2.2545

 DISTRIBUTION OF COEFFICIENTS OVER DEPTH
 ---------------------------------------

(COEFFICIENTS GIVEN BELOW ARE DIMENIONLESS)

   S/D          ADDED MASS       DAMPING

  1.000        -0.5183E+00      0.2777E+01
  0.950        -0.1325E+00      0.1808E+01
  0.900         0.3319E+00      0.1177E+01
  0.850         0.7643E+00      0.7664E+00
  0.800         0.1138E+01      0.4990E+00
  0.750         0.1449E+01      0.3249E+00
  0.700         0.1705E+01      0.2115E+00
  0.650         0.1912E+01      0.1377E+00
  0.600         0.2080E+01      0.8965E-01
  0.550         0.2217E+01      0.5837E-01
  0.500         0.2327E+01      0.3801E-01
  0.450         0.2416E+01      0.2475E-01
  0.400         0.2488E+01      0.1612E-01
  0.350         0.2546E+01      0.1051E-01
  0.300         0.2592E+01      0.6867E-02
  0.250         0.2629E+01      0.4506E-02
  0.200         0.2657E+01      0.2987E-02
  0.150         0.2678E+01      0.2027E-02
  0.100         0.2693E+01      0.1447E-02
  0.050         0.2701E+01      0.1137E-02
  0.0           0.2704E+01      0.1040E-02

 TOTAL HYDRODYNAMIC COEFFICIENTS:
 --------------------------------

DIMENSIONLESS ADDED MASS =  0.7291E+01
       AND DAMPING =  0.1232E+01
```

```
ADDED MASS (KG) =  0.2001E+02
DAMPING (KG/S) =  0.4248E+02

**********************************************

    FREQUENCY (HZ) =  5.00
    WAVELENGTH (M) =      0.0624
    KD =      53.6457
    KA =      14.0908

 DISTRIBUTION OF COEFFICIENTS OVER DEPTH
 ---------------------------------------

(COEFFICIENTS GIVEN BELOW ARE DIMENIONLESS)

   S/D          ADDED MASS        DAMPING

  1.000        -0.3924E+00       0.4462E+00
  0.950         0.6553E+00       0.3052E-01
  0.900         0.1233E+01       0.2088E-02
  0.850         0.1596E+01       0.1428E-03
  0.800         0.1855E+01       0.9770E-05
  0.750         0.2052E+01       0.6683E-06
  0.700         0.2201E+01       0.4572E-07
  0.650         0.2318E+01       0.3127E-08
  0.600         0.2414E+01       0.2139E-09
  0.550         0.2493E+01       0.1463E-10
  0.500         0.2557E+01       0.1001E-11
  0.450         0.2607E+01       0.6848E-13
  0.400         0.2650E+01       0.4685E-14
  0.350         0.2686E+01       0.3205E-15
  0.300         0.2715E+01       0.2192E-16
  0.250         0.2737E+01       0.1500E-17
  0.200         0.2754E+01       0.1026E-18
  0.150         0.2769E+01       0.7017E-20
  0.100         0.2778E+01       0.4800E-21
  0.050         0.2783E+01       0.3299E-22
  0.0           0.2785E+01       0.4493E-23

 TOTAL HYDRODYNAMIC COEFFICIENTS:
 --------------------------------

DIMENSIONLESS ADDED MASS =  0.8593E+01
       AND DAMPING =  0.3166E-01
```

```
ADDED MASS (KG) =  0.2358E+02
DAMPING (KG/S) =  0.2730E+01

**********************************************

    FREQUENCY (HZ) =  6.00
    WAVELENGTH (M) =      0.0434
    KD =      77.2498
    KA =      20.2907

 DISTRIBUTION OF COEFFICIENTS OVER DEPTH
 ---------------------------------------

(COEFFICIENTS GIVEN BELOW ARE DIMENIONLESS)

    S/D          ADDED MASS       DAMPING

   1.000        -0.2992E+00      0.3097E+00
   0.950         0.7608E+00      0.6509E-02
   0.900         0.1293E+01      0.1368E-03
   0.850         0.1634E+01      0.2875E-05
   0.800         0.1883E+01      0.6042E-07
   0.750         0.2073E+01      0.1270E-08
   0.700         0.2218E+01      0.2668E-10
   0.650         0.2332E+01      0.5608E-12
   0.600         0.2424E+01      0.1179E-13
   0.550         0.2502E+01      0.2477E-15
   0.500         0.2564E+01      0.5205E-17
   0.450         0.2614E+01      0.1094E-18
   0.400         0.2656E+01      0.2299E-20
   0.350         0.2691E+01      0.4831E-22
   0.300         0.2720E+01      0.1015E-23
   0.250         0.2741E+01      0.2134E-25
   0.200         0.2758E+01      0.4484E-27
   0.150         0.2772E+01      0.9424E-29
   0.100         0.2782E+01      0.1981E-30
   0.050         0.2787E+01      0.4164E-32
   0.0           0.2788E+01      0.1749E-33

 TOTAL HYDRODYNAMIC COEFFICIENTS:
 --------------------------------

DIMENSIONLESS ADDED MASS =  0.8671E+01
       AND DAMPING =  0.1527E-01

ADDED MASS (KG) =  0.2379E+02
```

```
DAMPING (KG/S) =  0.1579E+01
```

```
C***********************************************
C
C  HIGH Frequency Approximation Program
C       last update: October 13, 1988
C
C  This program calculates the high-frequency
C  approximations for the added mass and
C  damping coefficients for a vertical
C  surface-piercing circular cylinder subjected
C  to horizontal unidirectional ground ex-
C  citation.
C
C  Executable on IBM-PC microcomputer
C
C***********************************************
C
      REAL G,PI,RHO,A,D,A3,FR,W,DGT2,AD,AM
      INTEGER NC,I,NP
      DIMENSION RADIUS(10),DEPTH(10),FREQ(50)
C
      PI=3.141592654
      G=9.806
C
      OPEN (UNIT=5,FILE='HIGH.DAT',STATUS='OLD')
      OPEN (UNIT=6,FILE='HIGH.OUT',STATUS='OLD')
C
      READ (5,10) NC
10    FORMAT (I3)
      DO 20 I=1,NC
          READ (5,15) RADIUS(I),DEPTH(I)
15        FORMAT (2F10.3)
20     CONTINUE
      READ (5,25) RHO
25    FORMAT (F10.3)
      READ (5,30) NP
30    FORMAT (I3)
      DO 40 I=1,NP
          READ (5,35) FREQ(I)
35        FORMAT (F5.2)
40     CONTINUE
C
      WRITE (6,50)
50    FORMAT (//,5X,'HIGH-FREQUENCY',
     &' APPROXIMATION',/,5X,'--------------',
     &'--------------')
C
      DO 1000 I=1,NC
          A=RADIUS(I)
          D=DEPTH(I)
          A3=A**3
```

```
          WRITE (6,55)
55        FORMAT (//,8X,'**********************')
          WRITE (6,60) A,D,RHO
60        FORMAT (//,8X,'RADIUS (M):',F10.3,/,8X,
     &'DEPTH (M):',F10.3,/,8X,'DENSITY (KG/M3):',
     &F7.1,//)
          WRITE (6,65)
65        FORMAT (' FREQ (HZ)',6X,'KA',4X,'AMP (/M)',4X,
     &'ADP (/M)',4X,'AM (KG)',5X,'AD (KG/S)',/)
          DO 500 J=1,NP
              FR=FREQ(J)
              W=2.*PI*FR
              DGT2=FR*FR*D/G
              CALL MIAKD (AKD,DGT2)
              AKA=AKD*A/D
C
          AMP=0.542751371*PI*(D/A)**2.+(PI/(AKA)**3.)
          ADP=2.*PI/(AKA)**2.
          AM=RHO*A3*AMP
          AD=RHO*A3*W*ADP
C
              WRITE (6,70) FR,AKA,AMP,ADP,AM,AD
70            FORMAT (F7.2,F12.2,4E12.4)
500        CONTINUE
1000    CONTINUE
C
      STOP
      END
C
      SUBROUTINE MIAKD(AKD,DGT2)
C
C  Subroutine to calculate ka
C  from d/gT2
C
      PI=3.141592654
      C=4.*PI*PI*DGT2
      X=SQRT(C)
      IF (C-0.1) 30,30,10
10    Y=C/TANH(X)
      IF (ABS(X-Y)-0.0001) 80,80,20
20    X=Y
      GOTO 10
30    Y=X+0.006
40    Z=(X+Y)/2.
      W=(X*TANH(X)-C)*(Z*TANH(Z)-C)
      IF (W) 50,80,60
50    Y=Z
      GO TO 70
60    X=Z
70    IF (ABS(X-Y)-0.0001) 80,80,40
```

```
80      AKD=Y
        RETURN
        END
```

```
C************************************************
C
C   Experimental Data ANALYSis Program
C      last update: January 19, 1989
C
C   This program calculates the fluid force and
C   hydrodynamic coefficients acting on the vertical
C   circular cylinder for given test frequencies
C   at a given section level above the tank floor.
C
C   The experimental data has been acquired
C   by the E/Q laboratory's PDP-11/04 mini-
C   computer and subsequently formatted by
C   the program OMFORM and transferred to the
C   AST-286 Premium microcomputer in the E/Q
C   laboratory.
C
C************************************************
C
      INTEGER WHICH
      WHICH=0
C
      WRITE (*,5)
   5  FORMAT (///' EXPERIMENTAL STUDY : DATA ANALYSIS'/
     .' ---------------------------------'//)
  10  WRITE (*,15)
  15  FORMAT (3X,'Analysis of Data Obtained from:'/,6X,
     .'[1] Strain Gauges',/,6X,
     .'[2] End Program',//)
  20  WRITE (*,25)
  25  FORMAT (3X,'SELECT ONE OF THE ABOVE:')
      READ (*,26) WHICH
  26  FORMAT (I2)
C
      IN=0.0
      IF (WHICH .EQ. 1) GOTO 50
      IF (WHICH .EQ. 2) GOTO 30
      GOTO 20
C
  50  CALL STRAIN (IN,OUT)
      GOTO 10
C
  30  STOP
      END
C
C ** Strain Gauge Data Analysis
C
      SUBROUTINE STRAIN (IN,OUT)
C
        INTEGER LEVEL,NUM,ANSWER
```

```
      REAL D,L,EI,MASS,FREQ,XAMP,A1W,A1A,A2W,A2A
      REAL TP1W,TP1A,TP2W,TP2A,TP3W,TP3A,H,S2,S1,W,CNST
      REAL SUM1,SUM2,AM,AD,AMP,ADP,RAD,RHO
      CHARACTER*20 INPUT,OUTPUT
C
      PI=3.141592654
      WRITE (*,100)
 100  FORMAT (' Input Data Filename? (STATUS is OLD)',/)
      READ (*,110) INPUT
 110  FORMAT (A20)
      OPEN (UNIT=7,FILE=INPUT,STATUS='OLD')
      WRITE (*,150)
 150  FORMAT (' Output Data Filename? (STATUS is UNKNOWN)',/)
      READ (*,160) OUTPUT
 160  FORMAT (A20)
      OPEN (UNIT=8,FILE=OUTPUT,STATUS='UNKNOWN')
C
C  Data is read in from the input file
C          D - shaft diameter, in mm
C          L - shaft length, in mm
C        RAD - cylinder radius, in m
C         EI - shaft stiffness, in N-mm2
C        RHO - water density, in kg/m3
C      S1,S2 - gauge distances, in mm
C
      READ (7,112) LEVEL,NUM
 112  FORMAT (I2,I3)
      READ (7,120) D,L,RAD,EI,RHO
 120  FORMAT (2F8.2,F8.4,E15.4,F7.1)
      READ (7,130) S1,S2
 130  FORMAT (2F8.2)
C
      H = S2-S1
      CNST = 2.0*EI/(D*H)
C
      WRITE (8,170)
 170  FORMAT (' STRAIN GAUGE DATA ANALYSIS',/,
     . ' -------------------------',/)
      WRITE (8,171) LEVEL
 171  FORMAT (' Section Level:',I2,/)
      WRITE (8,180) D,L,EI
 180  FORMAT (' Diameter D (mm):',F8.2,/,
     . ' Cantilever Length L (mm):',
     . F8.2,/,' Stiffness EI (N-mm2):',E15.4,/)
      WRITE (8,190) S1,S2
 190  FORMAT (' Distance from Gauge Set to Shaft Tip (mm):',/,
     . '    Top [CH 1] =',F8.2,/,
     . '    Bottom [CH 3] =',F8.2,//,
     . '************************',/)
C
```

```
C  Determining the dimensionless force coefficients for each
C  test frequency (in Hz) and displacement amplitude (in mm)
C          A1W - amplitude of top strain signal (1), in mm/mm,
C                obtained when cylinder is in water (W)
C          A2A - amplitude of bottom strain signal (2), in mm/mm,
C                obtained when cylinder is in air (A)
C          D1W - phase shift between displacement signal and
C                top strain signal (1), in radians, in water (W)
C         TP3A - time of the first downward zero-crossing, which
C                occurs after the first positive peak after the
C                1.0-second mark, in the displacement signal (3)
C                for shaking in air (A)
C         TP2W - same as for TP3A, except signal is that of the
C                bottom strain (2) for shaking in water (W)
C
      DO 1000 K=1,NUM,1

        READ (7,115) FREQ, XAMP
 115    FORMAT (F6.2,F8.2)
        READ (7,135) A1W,A1A,A2W,A2A
 135    FORMAT (4E15.4)
        READ (7,136) TP1W,TP1A,TP2W,TP2A,TP3W,TP3A
 136    FORMAT (6F7.3)
C
        PI = 3.141592654
        W = 2.0*PI*FREQ
C
        D1W = W*ABS(TP3W-TP1W)
        D1A = W*ABS(TP3A-TP1A)
        D2W = W*ABS(TP3W-TP2W)
        D2A = W*ABS(TP3A-TP2A)
C
        SUM1=(A1W*COS(D1W))-(A2W*COS(D2W))
     .       +(A2A*COS(D2A))-(A1A*COS(D1A))
        SUM2=(A1W*SIN(D1W))-(A2W*SIN(D2W))
     .       +(A2A*SIN(D2A))-(A1A*SIN(D1A))
C
C  Note that XAMP is initially in millimetres...hence multiplied
C  by 0.001 to get it into metres
C
        AM = (-1.0)*CNST*SUM1/(W*W*XAMP*0.001)
        AD = (-1.0)*CNST*SUM2/(W*XAMP*0.001)
C
C  The force coefficients are made dimensionless here
C
        AMZ = AM/(RHO*RAD**3)
        ADZ = AD/(RHO*W*RAD**3)
C
        WRITE (8,175) FREQ,XAMP
 175    FORMAT (' FREQUENCY: ',F6.2,' Hz'/
```

```
     .  ' X-AMPLITUDE: ',F8.2,' mm'/)
C
        WRITE (8,222) AMZ,ADZ
 222    FORMAT ('  Dimensionless Added Mass Coefficient :  ',
     .  E15.4,/,'  Dimensionless Damping Coefficient :  ',
     .  E15.4,//,'************************',/)
C
 1000 CONTINUE
C
        OUT=IN
        RETURN
        END
```